FLOW ASSURANCE PROBLEMS IN THE GEO-ENERGY INDUSTRY: MICROBIAL INFLUENCED CORROSION, AND PRECIPITATION OF CLAYS IN RESERVOIR ACID STIMULATION

Makungu Marco Madirisha

FLOW ASSURANCE PROBLEMS IN THE GEO-ENERGY INDUSTRY: MICROBIAL INFLUENCED CORROSION, AND PRECIPITATION OF CLAYS IN RESERVOIR ACID STIMULATION

DISSERTATION

to obtain
the degree of doctor at the University of Twente,
on the authority of the rector magnificus,
Prof.dr.ir. A. Veldkamp
on account of the decision of the Doctorate Board,
to be publicly defended
on 22nd of June 2022 at 1245 hrs

by

Makungu Marco Madirisha
born on the 5th of February 1979
Magu, United Republic of Tanzania

This thesis has been approved by:
Prof. dr. F. D. van der Meer (Supervisor)
Dr. H.R.G.K. Hack (Supervisor)

ITC dissertation number 413
ITC, P.O. Box 217, 7500 AE Enschede, The Netherlands

ISBN: 978-90-365-5398-8
DOI: https://doi.org/10.3990/1.9789036553988

Cover designed by: Job Duim

Printed by: CTRL-P Hengelo

Financially made possible by NUFFIC as component of the NICHE Tanzania-Dutch Energy Capacity Building (TDECB) project

Graduation committee:

Chair/Secretary: Dean of the Faculty

Supervisors:

Prof. dr. F.D. van der Meer
University of Twente

Dr. H.R.G.K. Hack
University of Twente

Committee members:

Prof. dr. V.G. Jetten
University of Twente

Prof. dr. G. van der Steenhoven
University of Twente and KNMI

Prof. dr. A. K. Skidmore
University of Twente

Prof. dr. J.D.A.M. van Wees
University of Utrechtand TNO

Dr. K. F. Kilulya
University of Dar es Salaam

To my wife, Nakaniwa Amini Mrikaria

Acknowledgments

I sincerely praise the almighty God for His graces, power, nourishment, and above all, His faithfulness and love during my PhD trajectory. Furthermore, I am thankful to various people, organizations, and institutions whose assistance during undertaking my PhD study has been invaluable. In particular, I am extremely grateful to express my deepest gratitude to my Promotors, Prof. dr. F.D. van der Meer and Dr. H.R.G.K. Hack of the Department of Applied Earth Science (AES), by the then Department of Earth System Analysis (ESA), University of Twente, who made this work possible. Without their friendly guidance, mentoring, constructive criticisms, patience, and encouragement throughout all stages of the work, this PhD would not have been achievable.

I highly acknowledge the Netherlands Initiative for Capacity Development in Higher Education (NICHE-NUFFIC) for providing the funding for this research through the Tanzania – Dutch Energy Capacity Building project (TDECB) (OFI93936314). I am also sincerely indebted to the project manager of TDECB, Dr. Dinand Alkema of the Department of Applied Earth Science (AES) for valuable support in approving various budget issues related to my PhD study. Moreover, the Government Chemist Laboratory Authority, Nelson Mandela Institute of Science and Technology, Arusha Technical College, and University of Dar es Salaam, Tanzania are acknowledged for allowing to use of their laboratories for analyses. The Geoscience laboratory of the Faculty of Geo-Information Science and Earth Observation, University of Twente is also acknowledged for the ICP-OES and XRD analyses. Rick Veenstra from Saxion University of Applied Sciences and Zacharia E. Mabala from the Institute of Resource Assessment of the University of Dar es Salaam are acknowledged for the SEM-EDS analyses and the map sketch, respectively. The Tanzania Petroleum Development Corporation (TPDC) is acknowledged for providing the carbon steel API 5L X70M HFW.

My acknowledgments are also extended to the academic, technical, and administrative staff of the Faculty of Geo-Information Science and Earth Observation-University of Twente, College of Natural and Applied Sciences

(Department of Chemistry and Department of Geology)-University of Dar es Salaam, and Department of Geoscience and Engineering-TU Delft (especially Ing. Wim Verwaal) for their kind cooperation, encouragement, and various support during my research. In addition, special thanks are extended to the management of the University of Dar es Salaam (UDSM) for giving me the study leave. Lastly, my deepest appreciation goes to my beloved parents, wife, children, and brothers for their moral support, prayers, and great patience during the whole time of my PhD.

Waiver

The outbreak of coronavirus disease (COVID-19) has adversely affected research activities at Universities. In particular, COVID-19 has caused problems in the logistics of the research described in this thesis. However, some measures were taken to ensure that the research could be completed successfully and on an acceptable good level. The measures taken are:

- A large part of the laboratory work was shifted from laboratories in the Netherlands to those in Tanzania because laboratories in the Netherlands in as well Twente and Delft universities were closed for long periods; longer than in Tanzania.
- The mode of supervision was changed from face-to-face to digital i.e to a diverse array of communication platforms such as Microsoft Teams, Zoom, email, and telephone. These online meetings and alternative communication platforms were effective and sufficient although more time-consuming than face-to-face communication.
- The University of Twente, University of Dar es Salaam and NUFFIC-NICHE agreed to extend my PhD registration, study leave, and scholarship, respectively.

Table of contents

List of figures

List of tables

1 General introduction

Geo-energy resources such as oil, gas, and geothermal energy are the most important sources of energy for billions of people around the world (Liu and Ramirez, 2017; Theyab, 2018; TU-Delft, 2018). The resources for and processes in energy production of geothermal energy, oil, and gas are to a certain extent similar. For example, the fluids, mostly water in geothermal energy, oil, and gas, circulate through or are present in the subsurface of the Earth in the pores and channels between pores in rocks and soils, such as sandstone and sand, and in natural fracture systems (Field et al., 2018). Furthermore, non-volcanic geothermal energy, oil, and gas reservoirs are all found in sedimentary basins (Ziabakhsh-Ganji et al., 2018). The exploitation of geothermal resources requires either extraction of warm or hot fluids, normally water, from the subsurface or injection of fluids, normally also water in a suitable rock or soil layer in the subsurface in which the water will be heated whereafter it is pumped back to surface. The returned warm or hot water can be used for heating or power generation depending on the temperature of the water arriving at the surface (Kagel et al., 2005). Oil and gas exploitation extract oil or gas from the sedimentary subsurface layers. The rocks and soils for all energy sources should be porous and permeable to allow for the fluids and gases to be pumped in or extracted. As the rocks and soils in the various geo-energy resources are similar, such are the installations, consisting of boreholes and various process installations at the surface. Most of the boreholes and installations are made of metals; mainly steel. The similarity implies that problems experienced in oil and gas exploitation are to a certain extent similar to the problems experienced in geothermal energy production and that a possible solution is often applied to all geo-energy sources.

The oil, gas, and geothermal energy industry are often encountered so-called “flow assurance problems” which means that the flow of fluids and gas are hampered. Swelling and migration of fines, in particular, clay particles and clay precipitation in the reservoir may be such flow assurance problems. Corrosion of metal casings, pipelines, or installations is another. Swelling and migration of fine materials and clay precipitation may hamper or block the flow through the rocks, soils, and installations whereas corrosion of metals may cause leakages and failure of boreholes, pipelines (Fig.1.1), and installations (Ahmad et al., 2018; Pearce et al., 2018; Theyab, 2018). Flow assurance problems depend on an interrelated combination of factors involving the chemistry of the fluid (i.e. mineral content, water, oil, gas, and microbes), flow dynamics, and operating conditions (pressure and temperature) (He et al., 2012; Xiao et al., 2017). Localized corrosion mainly caused by microbes, also known as Microbial Influenced Corrosion (MIC) is reported to be the major cause of metal pipe and installation leakage and contributing to 20% of the total annual corrosion cost in the geo-energy (Alabbas and Mishra, 2013; Clarke and Aguilera, 2001). The most important species in MIC are Sulfate Reducing Bacteria (SRB). MIC is often difficult to understand in detail because the type and the capability of microbial metabolites that are causing the corrosion are difficult to identify (Little et al., 2020; Riskin and Khentov, 2019). The industry also uses plastic or other non-metal materials for pipelines and installations or metallic parts are covered by a layer of non-metal (mostly also some form of plastic) to avoid contact between the metal and a corrosive environment. These non-metal materials are not part of this research.

Fig. 1.1: Corrosion of carbon steel piping[1]

Acid stimulation by the introduction of an acid in a reservoir that dissolves acid-soluble minerals is often used to improve the permeability (Fig.1.2) and hence the flow of fluids and gases in reservoirs. However, often acid stimulation result in swelling and migration of fine materials and clay precipitation also denoted as “formation damage”, that reduce reservoir porosity and permeability (clog pores and interconnecting pore channels) and consequently hinder the flow of fluids and gases in or from the reservoir (Wilson et al., 2014).

The flow of fluids and gases may also be hampered by another mechanism. Fluids used in acid stimulation, i.e. acids, may react with clay minerals acting as cement in the grain skeleton. This may cause the dissolution of particles

---

[1] *https://www.corrosionpedia.com/21-types-of-pipe-corrosion-failure/2/1484*

from the grain skeleton, cause the collapse of the grain skeleton and reduce permeability (Madirisha et al., 2019). For these reasons chelating agents such as aminopolycarboxylic acids (APCAs) are used as these have limited reactions with the clay minerals while also reducing the rates of secondary and tertiary reactions such as precipitation (Aldakkan et al., 2018; Hassan and Al-Hashim, 2016). A poor understanding of the geochemistry and hydrochemistry of the reservoir before acid stimulation is often likely the reason. In this research, the geochemical interactions between acid and clays are investigated as it is likely that these determine the dissolution and precipitation of clay minerals (Rose et al., 2010).

Fig. 1.2: Microscopic image indicating treated dolomite rock samples with the chelating agent

This study investigates two flow assurance problems, that is, bio-corrosion, and precipitation of clays as a consequence of acid stimulation to enhance reservoir permeability. For bio-corrosion, the role of biofilm and acid organic metabolites on the corrosion of metals is investigated. For precipitation of clays, the interaction (dissolution-precipitation) between dozing chemicals (Biodegradable Chelating Agents (BCA's)) as typical examples for dozing chemicals used in reservoir chemical stimulation) and clay minerals are investigated.

1.1 Flow assurance problems

Flow assurance refers to the free flow of fluids and gases from the reservoir up to processing and transportation facilities (Theyab 2018). Flow assurance addresses broad aspects of the problems of flow distortion such as corrosion, hydrates, wax, asphaltenes, slugging, naphthenates, emulsion, scales, and formation of solids (sediments, fines, clays, and sands)(Bai and Bai, 2005; Khanna and Patwardhan, 2019). A general overview of geo-energy resources (geothermal energy, oil, and natural gas) is presented in section 1.2 and section 1.3, and a review of the literature on flow assurance (bio-corrosion, and precipitation of clay during acid stimulation) is discussed in Chapter 2.

1.2 Oil and natural gas

Oil in a subsurface reservoir is a complex mixture of hydrocarbons that occur in sedimentary rocks in the form of gases (petroleum gases), liquids (e.g. crude oil), semisolids (e.g. bitumen), solids (e.g. wax or asphaltite), and/or water (Curley, 2011; Riazi, 2005). Oil is generated by the thermal degradation of kerogen in the source beds. Kerogen refers to the dispersed and insoluble organic matter in rock including coal and mineral oil deposits (Vandenbroucke, 2003; von Bloh et al., 2008). Kerogen is made from organic matter of either terrestrial higher plants or aquatic lower plants and bacteria (Welte and Tissot, 1984). Kerogen is divided into three parts, namely labile, refractory and inert (Mackenzie and Quigley, 1988). With increasing burial, the temperature in these rocks rises and around 80-150 ^{o}C, the chemically labile portion of the kerogen begins to transform into oil and the formed oil migrate to its place of accumulation in the reservoir traps (Mackenzie and Quigley, 1988).

Natural gas (NG) originates from coal beds (the so-called “mother rock”) which is a particular variety of kerogen. With increasing burial and temperature greater than 150 ^{o}C, the chemically labile and refractory kerogen portions of the kerogen begin to transform into a gas. As in oil migration, the formed gas migrates to and is trapped in a porous rock layer (so-called “reservoir rock") under an impermeable layer (a so-called “cap rock” or “cap-layer”), Fig. 1.3 (Curley, 2011). Often also, water is present in oil and natural gas reservoirs. Oil and natural gas reservoirs are found in sedimentary basins with temperatures in the range of 50-150 ^{o}C (Gunnlaugsson et al., 2014b; Junrong et al., 2015; Xiao et al., 2016a; Yang, 2011). Reservoir rocks are mainly sandstones, limestone, and dolomite.

Oil and gas reservoirs are characterized by low oxygen levels that might be attributed to oxygen reactivity with rock in water-rock reactions. In addition, a conversion of organic matter into kerogen followed by kerogen thermal maturation during the formation of oil or natural gas is another reason for the low oxygen levels. Low oxygen content implies that oil and gas originate from sediments in an anaerobic environment (Craddock et al., 2018).

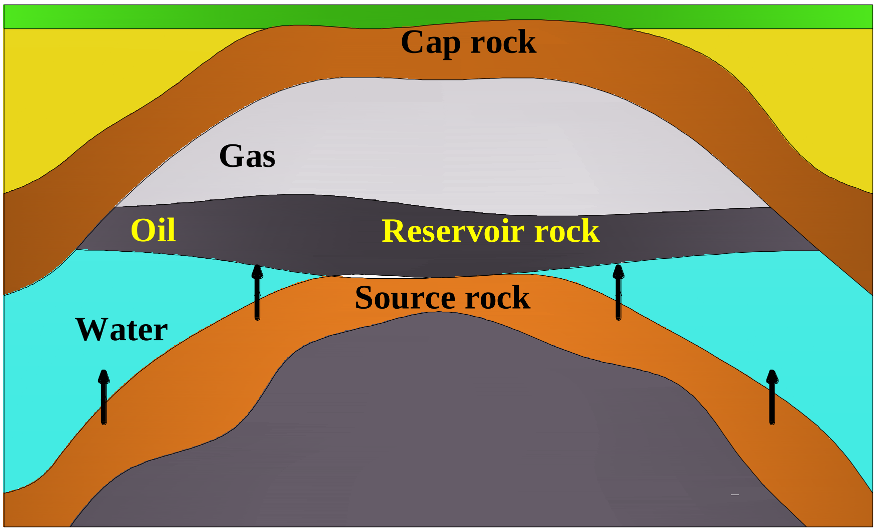

Fig. 1.3: A porous rock layer (reservoir rock) under an impermeable layer (cap rock or cap layer)

Oil and natural gas are transported from the well to a refinery or gas plant, then to a terminal, and eventually over possible long distances to end-users or consumers using pipelines, purpose-built ships, or other transport means. Steel borehole (also "wellbore") pipes and pipelines play a key role throughout the world as the main part of the network for oil and gas transportation (Ngwira and Pulkkinen, 2018; Saeed and Ronagh, 2015). However, oil and gas installations such as pipelines contain also produced water that either is generated from underground reservoirs (Fig.1.4) or originates from secondary or tertiary activities that use water for enhancing recovery rates and safety operations in wells (Neff et al., 2011).

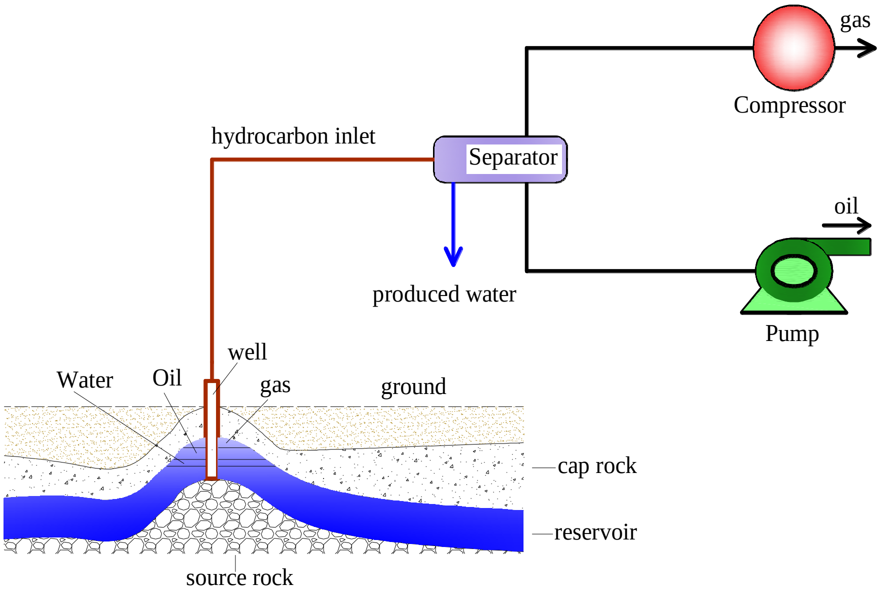

Fig. 1.4: Production of water during oil and gas exploitation

Produced water contains dissolved and dispersed oil components, dissolved formation minerals including radionuclides, production chemicals (chemicals to ease production), dissolved gases, and/or produced solids (Bahadori, 2017). These are grouped normally in five groups: hydrocarbons, salts, metals, radionuclides, and production chemicals (Hansen and Davies, 1994). The salts are mainly chlorides, carbonates, and sulfides of Ca, Mg, and Na (Dresel and Rose, 2010). The amount of chlorides in produced water is mostly far higher compared to chlorides contained in seawater (Sumi, 2005). According to Magot et al. (Magot et al., 1997), the presence of SO_4^{2-} and CO_3^{2-} in water is evidence for the existence of microbes with metabolic processes. Sulfate is widely distributed in many water systems and therefore its presence is evidence for troublesome species of corrosion namely, sulfate-reducing bacteria (SRB) and sulfate-reducing archaea (SRA) (Li et al., 2018).

1.2.1 Oil and natural gas in Tanzania

Tanzania has sedimentary basins with considerable energy reserves due to its geological and structural composition (Muhongo, 2013). There are four main categories of sedimentary basins which are recognizable as the potential for hydrocarbons in Tanzania: inland rift basins, coastal basins, shelf, and shallow offshore basins, and deep offshore basins (Rachel Angelo et al., 2019). In these sedimentary basins, the presence of petroleum systems has been evidenced by seismic data and oil seeps at the surface (Muhongo, 2013). To date, natural gas discoveries had been made at Songo Songo (Fig 1.5), Mnazi Bay, Kiliwani, Mkuranga, and Ruvuma and Ruvu basins (Dailynews, 2020). A total of 96 wells are drilled both offshore and onshore. However, natural gas is currently produced both offshore and onshore at Songo Songo and Kiliwani (from Songo Songo island), and Mnazi Bay (Dailynews, 2020). Natural gas from Songo Songo Island and Mnazi Bay is transported through pipelines to the capital of Dar es Salaam to generate power. With the presence of vast sedimentary basins, exploration continues and more hydrocarbon discoveries are anticipated from onshore and shallow waters, deep offshore, and inland rift basins.

Fig. 1.5: Songo Songo natural gas field in Tanzania[2]

1.3 Geothermal energy

Geothermal energy is energy produced from the heat energy stored in the Earth's interior that originates mainly due to the decay of radioactive isotopes, such as potassium-40, uranium-238, and thorium-232 (Barbier, 2002; Earle, 2019; Lund, 2018). In addition, a small portion of the core's heat comes from the friction generated along the margins of continental plates and the redistribution of materials within Earth by gravitational forces. Geothermal energy provides long-term energy with a lower carbon footprint and maintenance costs than other renewable energy (Junrong et al., 2015). Geothermal energy (Fig. 1.6) can be utilized for power generation, heating, cooling, and could effectively replace fossil fuels (Wang et al., 2016a). Geothermal effects can be present on the surface. Depending on reservoir temperature and discharge rates, the surface manifestations are seeps of

---

[2] *https://hawilti.com/energy/naturalgas/tanzania-orca-energy-submits-50m-capex-plan-for-songo-songo-development-next-year/*

warm and hot water, fumaroles, hot springs, boiling springs and pool, geysers, silica sinter terrace, phreatic explosion craters, and zones of acid alteration (Cody, 2007; Gunnlaugsson et al., 2014b).

Fig.1.6: A geothermal power plant in the Netherlands[3]

The classification of geothermal systems is not very well defined (Breede et al., 2015). Various classifications are used such as classification based on the geological settings or enthalpy of the geothermal fluids. Classification of geothermal systems based on geological settings classifies geothermal systems as hot dry rock, enhanced or engineered geothermal systems, hot wet rock, hot fractured rock, and hot sedimentary aquifer systems. According to Breede et al. (2015) and Gupta & Roy (2006), geothermal systems are

---

[3] *https://dutchfiltration.com/geothermal-energy/*

classified as hydrothermal (convective), hot sedimentary aquifers (deep aquifers), and petrothermal (conductive) based on their geological settings (Fig 1.7).

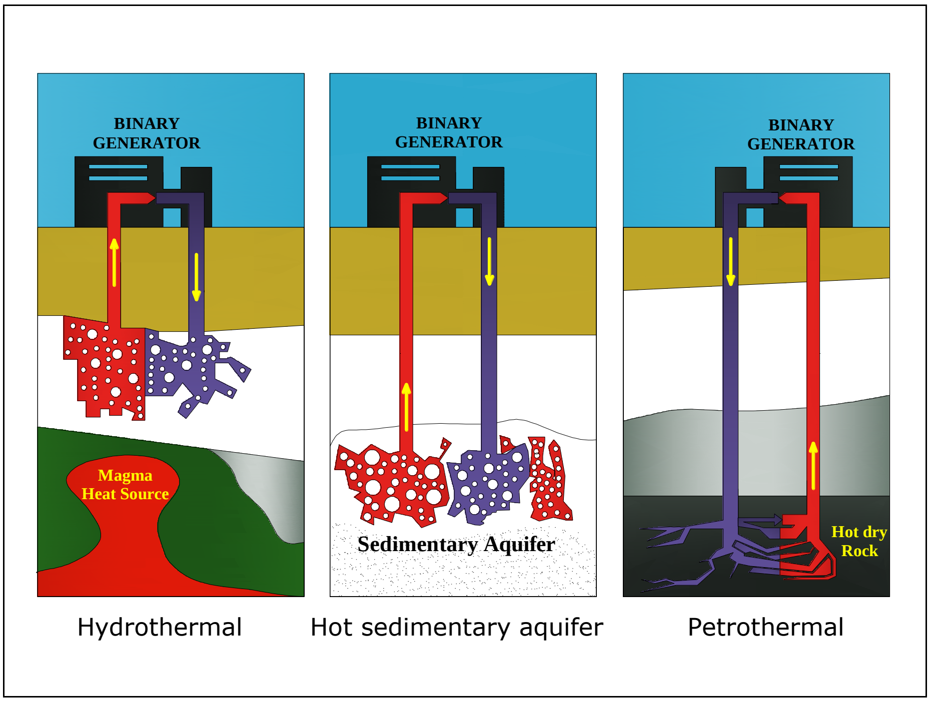

Fig. 1.7: Classification of geothermal systems

Hydrothermal systems (HSs) are geothermal systems found in areas of heat sustained by tectonic activity or associated with volcanic centers and magma reservoirs (Gehringer and Loksha, 2012; Saemundsson et al., 2009). HSs are classified as common and conventional. Both common and conventional HSs are convective systems where the former is dominated by liquid while the latter with vapor at a high geothermal gradient. Both HSs are characterized by sufficient reservoir permeability and water supply (Bertani, 2016). HSs contain all three components naturally i.e. a heat source, a heat sink (reservoir), and a heat exchanger (fluid). For sustainability of HSs, re-injection of the produced water in a second well is necessary to maintain sufficient pressure in the reservoir. In addition, re-injection is also necessary to avoid environmental pollution(Bertani, 2016).

For hot sedimentary aquifer systems, the systems are similar to common and conventional hydrothermal systems with the difference being that the systems are characterized by lack of a localized magmatic heat source and heat supply is conduction dominated (Breede et al., 2015; Gupta and Roy, 2006). The reservoir rock types of hot sedimentary aquifer systems are typically sedimentary, such as sandstone and limestone. A large portion of the world's geothermal reserves is contained in sedimentary formations mainly sandstone and carbonate. Often sandstone formations contain clay minerals such as montmorillonite, kaolinite, or illite (Fulignati, 2020).

Petrothermal systems (PSs) are geothermal systems that do have not enough water in the subsurface thus water has to be supplied and re-injected after geothermal production (Breede et al., 2015). The fluid permeability of most PSs is too low and therefore stimulation techniques such as hydraulic fracturing have to be applied to create an artificial reservoir. PSs indicate a conduction-dominated heat source.

Classification of geothermal systems based on the enthalpy of the geothermal fluids is often used, thus reservoirs are classified as low, medium, and high enthalpy (or temperature) reservoirs (Cody, 2007; Gunnlaugsson et al., 2014b). High-temperature reservoirs are found in volcanic regions, and in many deep reservoirs (2 – 4 km depth) of sedimentary basins depending on the local temperature gradient (Cody, 2007; Moore and Allis, 2017). Medium and low-temperature reservoirs are found in sedimentary basins where the water heats up to the temperatures (50-150°C) (Edenhofer et al., 2011; Gunnlaugsson et al., 2014b; Junrong et al., 2015). Produced water from low to medium temperature geothermal reservoirs often contains dissolved solids and inorganic/organic gas while that from high temperature geothermal reservoirs often contain solids, steam and inorganic/organic gas. The steam and inorganic/organic gas are found separately in the reservoir but also sometimes together in liquid phase (Saemundsson et al., 2009). Geothermal water in medium and high enthalpy reservoirs is characterized by a very low concentration of oxygen. This is due to either oxygen solubility in water that decreases rapidly with temperature or due to oxygen reactivity with hydrogen sulfide, or with rock minerals in water-rock reactions (Gunnlaugsson et al., 2014b; Vitaller et al., 2020).

Production of geothermal energy is done by producing hot water and steam from the subsurface or by pumping water into the subsurface which is then extracted after heating (Toth and Bobok, 2016). Different technologies depending on temperature, depth, and heat are employed for the exploitation of geothermal energy. The two most common technologies of geothermal exploitation are flash steam and binary technology (Lund, 2008; Ouali et al., 2015). The flash steam technology is used for high-temperature geothermal resources. This technique extracts steam which generates electricity via turbines. Binary technology (Fig. 1.8) is used in medium and low-temperature geothermal resources. In binary technology, hot water from the subsurface transfers heat to another fluid (working fluid) when moving through a heat exchanger, before being cooled and returned to the ground through an injection well. In a heat exchanger, the working fluid vaporizes, and then drives the turbines. This working fluid is characterized by a lower boiling point and passes through the condenser and the cycle keeps repeating. Therefore, the production of electricity with binary power plants has been made possible from geothermal reservoirs with temperatures lower than 150 °C.

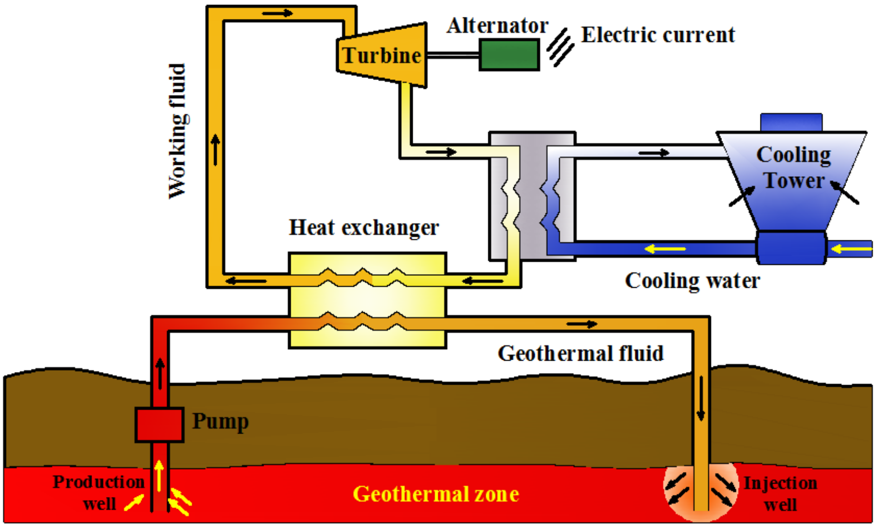

Fig. 1.8: Production of geothermal energy in low and medium-temperature geothermal energy (Lund, 2008)

1.3.1 Geothermal energy in Tanzania

Tanzania's geothermal resources especially medium and low temperature, are mainly found along the sedimentary basins and are characterized by surface manifestations, mainly hot springs. These include hot springs in the coastal basin, i.e south of Dar es Salaam (Luhoi, Kisaki and Utete), and to the north in the Tanga region (Amboni and Bombo), in the intra-cratonic basin i.e Mponde, Takwa, Hika, Gonga, Msule, Isanja, Ibadakuli, Balangida, Kondoa, Balangidalalu, Mnanka, Nyamosi and Maji moto-Mara., and in the western rift basin i.e Mtagata, Maji moto-Rukwa, Mapu, Ivuna and Rock of Hades (Kajugus et al., 2018; Mnjokava et al., 2012). Tanzania has also geothermal resources in volcanic regions. These are briefly mentioned to be complete, although the research is not particularly directed towards volcanic geothermal resources. Volcanic geothermal resources in Tanzania include the south-western volcanic province which includes geothermal systems such as Ngozi, Songwe, Kasimulu, Kiejo- Mbaka, Mbarali, and Daraja la Mungu. Another volcanic province is in the northern part of Tanzania which includes geothermal systems such as Eyasi, Natron, Manyara, Mount Meru, and Masware. Currently, there are numerous geothermal projects in Tanzania including Ngozi, Keijo-Mbaka, Songwe, Luhoi, and Natron for which the detailed surface studies for the first three geothermal fields are completed (Kajugus et al., 2018). In March 2021, the Tanzania Geothermal Development Company (TGDC) successfully drilled the first geothermal well (KMB-1) at Keijo-Mbaka (Fig.1.9).

Fig. 1.9: Spudding-in of the first geothermal well in Tanzania[4]

1.4 Research gap

Flow assurance problems in the geo-energy industry such as bio-corrosion of wells and surface installation, and precipitation of clays in the reservoir cause several problems such as material loss and flow path blockages (Fig.1.10). Though poorly understood and challenging to mitigate, Microbial Influenced Corrosion (MIC) is appreciated as the major cause of deterioration of well (75%) and surface installation (50%) (Khan et al., 2021). MIC is more difficult to forecast than abiotic corrosion because it is a complex type of corrosion that involves more than one process. MIC does not have a specific form and in addition, the type and capability of microbial metabolites that are causing corrosion are often uncertain too (Riskin and Khentov, 2019). The most

---

[4] *https://www.esi-africa.com/industry-sectors/generation/spudding-in-marks-progress-for-tanzanias-geothermal-aspirations/*

important species in MIC are Sulfate Reducing Bacteria (SRB) that utilize sulfate ions as electron acceptors and produce H_2S indirectly. Research on SRB is limited to simulate the effects of H_2S as the only SRB metabolic product and ignore dissimilatory respiration of SRB and the presence of biofilm (Bao et al., 2012; Fatah and Ismail, 2013; Fatah et al., 2011; Fatah et al., 2013; Feng et al., 2006; Liu et al., 2017; Newman et al., 1992; Sherar et al., 2011). CO_2 from SRB dissimilatory sulfate reduction, and a biofilm which is a diverse structure stabilized by the Extracellular Polymeric Substrate (EPS) have an important role in corrosion. Furthermore, the existing research often ignores the heterogeneity of the microbial environment. For example, different microbial species can share a living space, for example, SRB with methanogens, SRB with acetogenic, and SRB with fermentative bacteria (acid-producing bacteria). Different interacting species of microbes produce different metabolites such as organic acids which in turn result in metabolic heterogeneity within bacterial communities (Kim et al., 2015; Wong et al., 2021) Combinations of different metabolites in one microbial habitat are likely to have a particular kinetic effect on corrosion that is specific for the combination of metabolites (Kip and Van Veen, 2015). Therefore, MIC is now a prime area of research in terms of understanding the SRB species, their interactions with metals and other microorganisms.

Acid stimulation in reservoirs to improve permeability which is recognized as a cheap technique sometimes fails because of poor compatibility of the acid chosen and the clay minerals present in the reservoir (Kamal et al., 2019; Portier et al., 2009). This failure is known to cause several problems including precipitation of clay. Clay precipitates hinder the production of economic volumes of fluid or gas from the reservoir (Portier et al., 2007). Generally, precipitation of clay minerals also denoted as formation damage, often are envisioned to form the majority of fluid- or gas flow barriers in the reservoir (Farrell et al., 2021). Clay minerals precipitate within pore spaces and channels between pores and consequently decrease pore connectivity and permeability (Chagneau et al., 2015; Farrell et al., 2021). Prior knowledge of understanding the interaction between clays and the stimulating agent is therefore required.

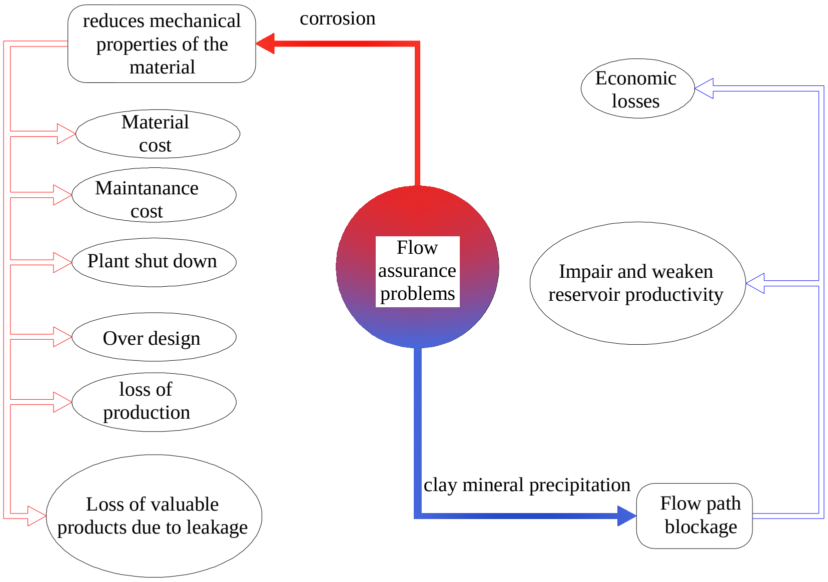

Fig. 1.10: Effects of flow assurance problems in the geo-energy industry

1.5 Research Questions

Based on the research gaps, this study aimed to focus on the following three research questions:

i. What is the role of biofilm in corrosion due to Sulfate Reducing Bacteria (SRB)?

ii. What is the role of organic acid metabolites in SRB corrosion?

iii. What is the influence of biodegradable chelating agents in the precipitation of clay minerals responsible resulting for the decrease of reservoir permeability?

1.6 The objective of the study

The research aims towards understanding bio-corrosion and precipitation of clay minerals during acid stimulation as flow assurance problems in the geo-energy industry. Precisely, the research aims at understanding the role of biofilm and organic acid metabolites in corrosion induced by SRB. In addition, the research aims at understanding the influence of biodegradable chelating agents (BCA1, BCA2, and BCA3) in the precipitation of clays (kaolinite-natural (KN) and montmorillonite-K10 (MM)), responsible for the reduction of permeability. To attain the general objective, the following specific objectives are set:

i. To determine the electrochemical parameters and amount of dissolved metal ions in solution due to the influence of biofilm, acetic, and L-ascorbic on SRB corrosion

ii. To characterize the surface chemical composition of the metal test coupons due to the influence of biofilm, acetic, and L-ascorbic on SRB corrosion

iii. To characterize changes in surface properties of the clay minerals due to their interaction with biodegradable chelating agents

iv. To determine the amount of dissolved metal ions in solution due to the interaction of clay minerals and biodegradable chelating agents

For bio-corrosion, the research takes into account the temperature, exposure time, pH, depleted O_2 environment, and the surface of the test coupons to obtain data on electrochemical parameters, chemical composition on the surface of test coupons, and dissolved metal ions in solution. For the influence of biodegradable chelating agents toward precipitation of clays, the research takes into account the pressure, temperature, brine (pH, salinity, and conductivity), and depleted O_2 environment to obtain information on changes in surface properties of the clay minerals, and dissolved metal ions in solution. Furthermore, inferential statistics mainly multiple linear regression and t-test are employed for data analysis.

1.7 Significance of the study

The obtained results on the role of microbial metabolites on SRB corrosion (chapter 3 and 4) and the influence of biodegradable chelating agents on precipitation of clay minerals of geothermal reservoir formations (Chapter 5) have major applications in flow assurance problems. For example, the results on the role of biofilm and organic acid metabolites have an impact on geo-energy material design and corrosion mitigation strategies. Also, it is useful for quantifying the severity of MIC threat and the relative vulnerability of different materials to MIC and optimizing production in the geo-energy industry.

Furthermore, the knowledge on the influence of biodegradable chelating agents in the precipitation of clays in the reservoir (chapter 5) will help in overcoming problems such as clay precipitation and migration during acid stimulation. This in turn will enable have a smooth flow of fluid and gas from the reservoir and thus optimize production.

1.8 Dissertation structure

This dissertation consists of seven chapters. Three of the chapters corresponding to the objectives of the study are already published papers (Madirisha et al., 2022a, b, c). The following is a summary of each chapter of the thesis.

Chapter 1 provides the general introduction on the geo-energy (Natural gas, petroleum, and geothermal), research gaps and questions, objectives, and significance of the study. In this chapter, the flow assurance problems associated with geo-energy are introduced.

Chapter 2 provides a critical literature survey based on which the objectives and significance of this study have been stated. The two selected flow assurance problems namely, bio-corrosion and precipitation of clays during acid stimulation are discussed thoroughly.

Chapter 3 describes the role of biofilm in the bio- corrosion of carbon steel in Sulfate Reducing Bacteria (SRB) in oil and gas exploitation and geothermal installations. This chapter is published as *Madirisha, M., Hack, R., & Van der Meer, F. (2022). Simulated microbial corrosion in oil, gas and non-volcanic geothermal energy installations: The role of biofilm on pipeline corrosion. Energy Reports, 8, 2964-2975*.

Chapter 4 describes the role of simulated organic acid metabolites on pipeline corrosion in sulfate reducing bacteria environment. This chapter is accepted for publication and is referenced as *Madirisha, M., Hack, R., & Van der Meer, F. (2022). The role of organic acid metabolites in geo-energy pipeline corrosion in a sulfate reducing bacteria environment. Heliyon, 8, e09420*

Chapter 5 describes the influence of biodegradable chelating agents (BCA1, BCA2, and BCA3) on clays in geothermal reservoir formations to acquire details on the precipitation of clays during reservoir acid stimulation. This chapter is published as *Madirisha, M., Hack, R., & Van der Meer, F. (2022). The influence of chelating agents on clays in geothermal reservoir formations: Implications to reservoir acid stimulation. Geothermics, 99, 102305*.

Chapter 6 provides a synthesis of the thesis i.e examines different literature sources and identifies their relationship to the thesis.

Chapter 7 provides conclusions and recommendations for further research.

2 Literature Review

2.1 Corrosion

Corrosion is either the chemical or the electrochemical destructive attack on material by its environment (Revie and Uhlig, 2008). Corrosion is a natural potential hazard in oil and gas exploitation, and geothermal energy production (Popoola et al., 2013; Veldkamp, 2016) The geo-energy industry today relies mostly on metallic materials as the primary backbone and skeleton for casings and pipelines. Metallic materials include metals such as ferrous (carbon steel, stainless steel, nickel alloys, galvanized steel pipes) and non-ferrous (copper, bronze, and aluminum pipes). The performance of these materials is governed by corrosion medium parameters (Fig. 2.1).

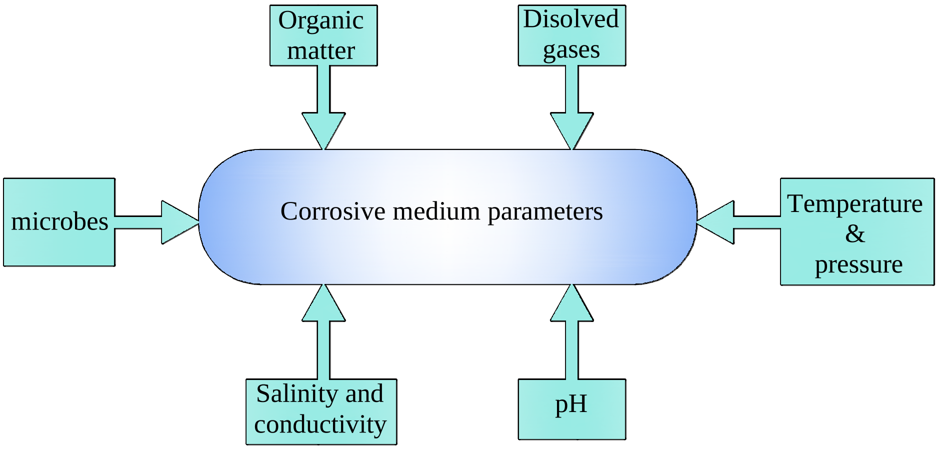

Fig. 2.1: Corrosion medium parameters

Carbon steels are suitable in harsh media, are low cost, have high mechanical strength, and are therefore extensively used in geo-energy applications (Batis et al., 1997; Provoost et al., 2018). Carbon steels are iron alloys containing up to 2.1 wt. % carbon. Some other components may be added to iron during carbon steel production to enhance corrosion-resistance properties (Kisku, 2020). Carbon steel is classified into three types namely, low, medium, and high carbon steel. Low-carbon steel has a carbon content of less than 0.25 wt. % and it is the most extensively used form of carbon steel. Low-carbon steel is often used in the geo-energy industry for pipes and casings (ibid.). The carbon steel materials suffer from both abiotic and biotic-induced corrosion. The biotic-induced corrosion also known as Microbial Influence Corrosion (MIC) or bio-corrosion, is expensive to correct and dangerous to personal health. Moreover, the reaction mechanisms responsible for the corrosion are still poorly understood (Kostecki et al., 2016). Often multiple mechanisms or multiple species of microorganisms are involved. Different microorganisms may be found in one habit and therefore several metabolic products may be produced with reinforcing or opposing kinetics (Bao et al., 2012).

2.1.1 Microbial Influenced Corrosion (MIC)

The term Microbial Influenced Corrosion (MIC) refers to corrosion due to the presence and influence of microbes such as fungi, algae, bacteria, lichens, cyanobacteria, archaea, and all protozoa (Little and Lee, 2006). Microbes influence the kinetics of corrosion processes or shift the mechanism for corrosion with the aid of sessile cells which are embedded in biofilms with extracellular polymeric substances (EPS) (Jia et al., 2018). The whole process involves both physical, biological, and electrochemical mechanisms, Fig. 2.2 (Videla and Herrera, 2004; Videla and Characklis, 1992).

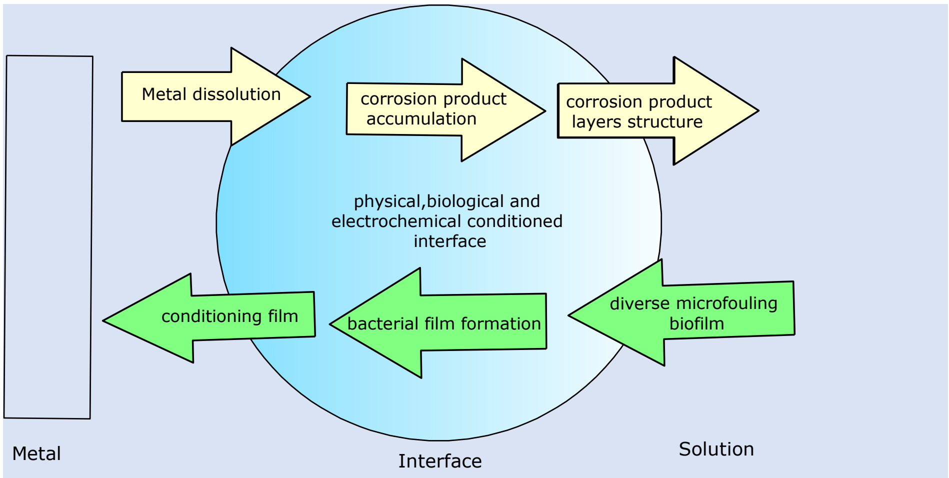

Fig. 2.2: Sequence of physical, biological, and electrochemical processes at metal/solution interface (Videla and Herrera, 2004).

From a chemistry perspective, MIC is electrochemical corrosion whereby microbes initiate, facilitate or accelerate a deterioration reaction on a material surface owing to the presence of the biofilms (Beech and Sunner, 2004; Parthipan et al., 2017). Electrochemical corrosion (Fig. 2.3) involves a shift of an electron from a free metal atom to an external electron acceptor, resulting in the formation of metal cations into the surrounding medium and deterioration of the material (Beech and Sunner, 2004). MIC is estimated to contribute 20% of the total cost of corrosion damage of metallic materials (Jia et al., 2018; Yuan et al., 2013). MIC is a major problem in several sectors such as energy (oil, gas, geothermal), marine transport, and cooling water systems (Little et al., 2020; Vigneron et al., 2018).

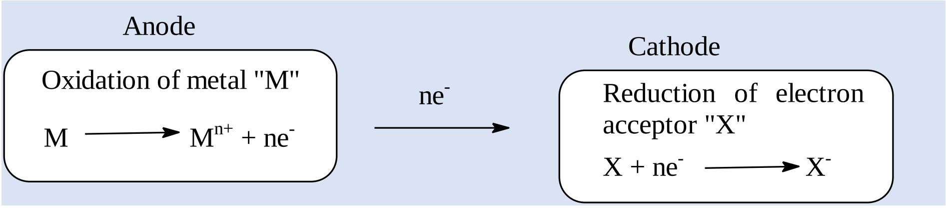

Fig. 2.3: Electrochemical corrosion on a metal surface involving free metal atom and external electron acceptor

2.1.1.1 Source of microbes in the geo-energy industry

The presence of microbes in geothermal energy, oil, and gas is associated with the produced water in these industries. Water reinjection systems upstream (e.g. drilling, well preparation, extraction, and production) and downstream activities (e.g. refining, processing, and purifying in petroleum and with microbes-contaminated pipes and heat exchangers in geothermal) are examples of where microbes can be introduced in petroleum and geothermal systems. Other sources of microbes may be associated with water re-injected into the subsurface geothermal reservoir after it has been used for energy production, to have a closed water system, or to avoid environmental pollution in a non-closed system (Kagel et al., 2005; Morozova et al., 2011). Water from other sources such as from surface rivers likely contaminated by microbes may be pumped into reservoirs to maintain a constant pressure or volume of water in the reservoir (Kagel, 2008). Similarly, water is injected into reservoirs in the oil and gas industry during enhanced oil and gas recovery. Water is known to create an excellent environment for microbes to grow and flourish (Neff et al., 2011; Sand, 2003). Water with dissolved minerals and elements provides all the essentials for microbial life such as carbon source, energy source, electron donors, and electron acceptors. Hence, microbes are widely present in many petroleum and geothermal industry systems on the surface and the subsurface.

2.1.1.2 Classification of microbes

Microbes are known to survive in both normal-growth conditions and abnormal growth at deviated conditions (i.e., extreme conditions). The classification of microbes in Table 2.1 is based on optimum growth temperatures (Javed et al., 2012; Kristjansson, 1991; Pavlov et al., 2007).

Table 2.1: Classification of microbes based on optimum growth temperatures (Javed et al., 2012; Kristjansson, 1991; Pavlov et al., 2007)

Terms	**Temperature Ranges**
Psychro- or kryophiles	< 0 °C up to 20 °C
Psychrotrophs	°C to 30 °C
Mesophiles	10 °C to 40 °C
Moderate thermophiles	35 °C to 55 °C
Thermophiles	50 °C to 85 °C
Extreme thermophiles	75 °C to 95 °C
Hyperthermophiles	> 90 °C

Microbes can subsist in either presence or absence of oxygen. The microbes that are capable to subsist in the presence of oxygen are referred to as “aerobes” while those subsisting in absence of oxygen are referred to as “obligate anaerobes”. However, some microbes may subsist in both presence or absence of oxygen and these are referred to as “facultative anaerobes” (Parthipan et al., 2017). In the presence of oxygen, these derive energy when electrons are transferred to oxygen; the terminal electron acceptor, while in absence of oxygen, a variety of organic and inorganic compounds may be used as the terminal electron acceptor (Little et al., 2006). Based on these differences in environmental conditions, microbes undergo different metabolic pathways that result in different metabolic products (Dworkin, 2006; Little et al., 2006). Therefore, the types of respiration and electron acceptors serve as a basis to classify microbes on their influence on corrosion. Based on this classification, microbes are grouped as sulfate reducing, methanogens, acetogens, iron reducing, sulfur-oxidizing, nitrate-reducing, and acid-producing (Barton and Fauque, 2009; Parthipan et al., 2017).

2.1.1.3 Sulfate reducing bacteria

Sulfate reducing bacteria (SRB) are ubiquitous anaerobes which are the most studied corrosive microbes in the geo-energy industry. SRB require an electron donor and acceptor to provide energy for their metabolism. Low-molecular-weight organic compounds are used as electron donors where they provide energy and carbon for growth. However, hydrogen gas may be used as an alternative electron donor by hydrogenase-positive SRB. SRB usually use sulfate as the terminal electron acceptor, reducing it finally to HS^-. In addition, electron acceptors such as sulfite, thiosulfate, and elemental sulphur are also used. In addition to sulfate, some SRB can also use. In addition, some SRB strains may switch to nitrate or nitrite as the terminal electron acceptor.

According to Liu et al, (2018), the electrode potential of the CO_2 + low-molecular-weight organic compound is close to the couple of Fe^{2+}/Fe^0, elemental iron can serve also as the electron donor for SRB metabolism. The electrons released by elemental iron oxidation are transferred from outside the cells across the cell wall to the SRB cytoplasm where sulfate reduction takes place (Li et al., 2018). This phenomenon is referred to as Extracellular Electron

Transfer (EET). EET therefore is a cross-sell wall electron transfer required for microbial respiration using an insoluble substrate. Soluble electron shuttles such as H^+/H_2, riboflavin, and flavin adenine dinucleotide (FAD), which are redox-active chemicals are used during EET (Jia et al., 2018). To elaborate, oxidation of insoluble iron occurs outside SRB cells while sulfate reduction occurs inside SRB cells thus requiring EET (Fig. 2.4). In contrast, the electrons released by low molecular weight organic substrates do not need for EET because the reaction occurs intracellularly and in the same proximity with sulfate reduction (Fig. 2.5), (Li et al., 2018).

EET in SRB MIC of carbon steel relying on an electron transport chain inside SRB. When there is a lack of carbon sources (electron donor), SRB are reported to consume elemental iron as the electron donor to produce energy (Li et al., 2015a). There are two different electron transfer methods for EET from a metal surface to a cell’s outer surface. One is direct electron transfer (DET) and the other is mediated electron transfer (MET) (Gu et al., 2019b). SRB species such as *Desulfovibrio ferrophilus* have redox-active outer membrane-bound c-type cytochromes (OMCs), which are capable of utilizing soluble electron mediators as electron shuttles (Gu et al., 2019b). The literature claims that EET is the major contributor of SRB MIC near-neutral pH (Jia et al., 2018). Thus, this type of MIC based on the electron is referred to as EET-MIC. The second type of MIC is attributed to secreted corrosive metabolites such as H_2S, CO_2, and organic acids. This type of MIC can be called metabolite MIC (M-MIC)(Jia et al., 2018).

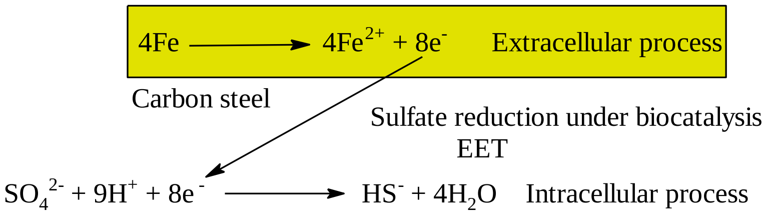

Fig 2.4: Oxidation and reduction reactions of SRB metabolism in the presence of elemental iron as an electron donor

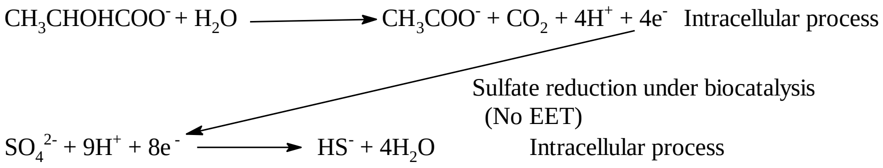

Fig 2.5: Oxidation and reduction reactions of SRB metabolism in the presence of low-molecular-weight organic compound as an electron donor

2.1.1.2 Microbial metabolites

The Microbial Influenced Corrosion (MIC) process starts when microbes begin to attach themselves to solid surfaces, colonize, flourish, and form biofilms. Biofilms are accumulations of mixed microbial communities within a complex matrix called “extra-cellular matrix” (Davey and O'toole, 2000). Generally, microbes may cause pitting, dealloying, enhanced erosion-corrosion, enhanced galvanic corrosion, stress corrosion cracking, and hydrogen embrittlement (Little and Lee, 2006). Microbes are capable of producing a variety of metabolites and may thrive at different levels of salt, temperatures, pressures, flow rates, and pH. Different species may thrive in one area and many metabolic products may be involved. Each of these may have its effect on the kinetics of corrosion. Microbes are reported to excrete a variety of metabolic products such as exopolymers, chelating agents, emulsifying compounds, exoenzymes, and organic acids (Fig. 2.6) (Marcus, 2011; Sand, 2003). These organic compounds may react with materials of natural and/or synthetic origin, causing swelling, total or partial dissolution, and, finally, deterioration. For example, organic acids are known to undergo reactions with materials by either the action of protons or chelation of metal ions and therefore promote corrosion by destroying the oxide layer formed on the material surface (Caneva et al., 2008).

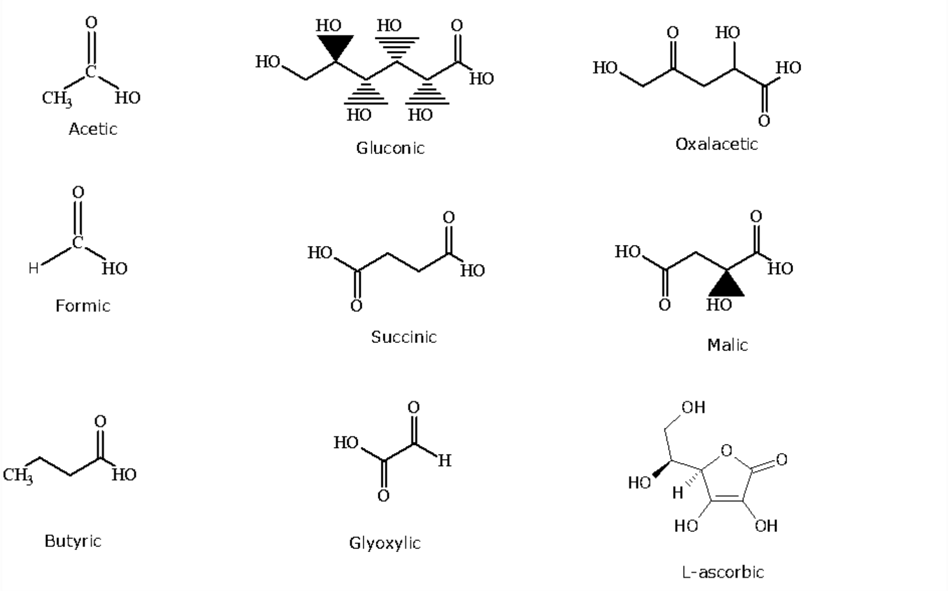

Fig. 2.6: Organic acid metabolites produced by microbes

2.2 Acid stimulation

Acid stimulation in the geo-energy is the predominantly used technique to ensure sufficient flow of fluid and is regarded as a cheaper solution compared to drilling and re-drill (Al-Arji et al., 2021; Aqui and Zarrouk, 2011a; Portier et al., 2009). Acid stimulation is a method where a certain volume of acid (or a mixture of acids) is injected into a reservoir. This improves or maintains well productivity. The improvement of the well is achieved by full or partial dissolution of minerals, mobilization of reservoir particles in fractures and pores, inhibition of secondary or tertiary reactions that result in sparingly soluble products, and controlling the reactivity of mineral surfaces (Lucas et al., 2020).

Acid stimulation increases the permeability by dissolving impairing material in the productive formation that is restricting flow. Acid stimulation can also dissolve formation rock itself to enhance primary flow paths, or to create secondary flow paths to the wellbore (Peksa et al., 2016). In geothermal systems, acid stimulation affects the zone around the injection well and further penetrates more deeply into the formation through fractures. When acid is injected into the porous matrix of the reservoir at a pressure below the fracture pressure of the formation, the process is known as "matrix acidizing" while that above fracture pressure is termed "fracture acidizing" (Nitters et al., 2016). The latter creates new or enlarges existing fractures. This provides conductive paths deeper into the formation (Aqui and Zarrouk, 2011a). This technique is more preferred compared to other techniques such as hydraulic fracturing because of a lesser demand on operational and safety resources. Furthermore, the high conductivity of an acid-etched fracture is another reason that makes this technique more suitable than other techniques such as thermal and hydraulic fracturing.

2.2.1 Interaction of acid and geothermal reservoir formation

Fluid and gas extraction, injection techniques, and reservoir management methods are quite similar for oil, gas, and geothermal systems (Portier et al., 2009). In both hydrocarbon and geothermal systems, formation damage should be minimized to optimize well performance. Formation damage is normally considered damage to the rock or soil that results in a reduction in reservoir characteristics such as porosity and permeability (Wilson et al., 2014). Formation damage can impair and reduce reservoir performance and consequently cause substantial economic losses. Formation damage is brought by several mechanisms such as solid invasion, and poor compatibility of either rock and fluid or fluid and fluid (Ngata et al., 2021). Formation damage begins immediately when drilling operations begins and continues during the productive life of the well. In general, impairment of the geo-energy reservoir mostly takes place during most field operations (Fig. 2.7).

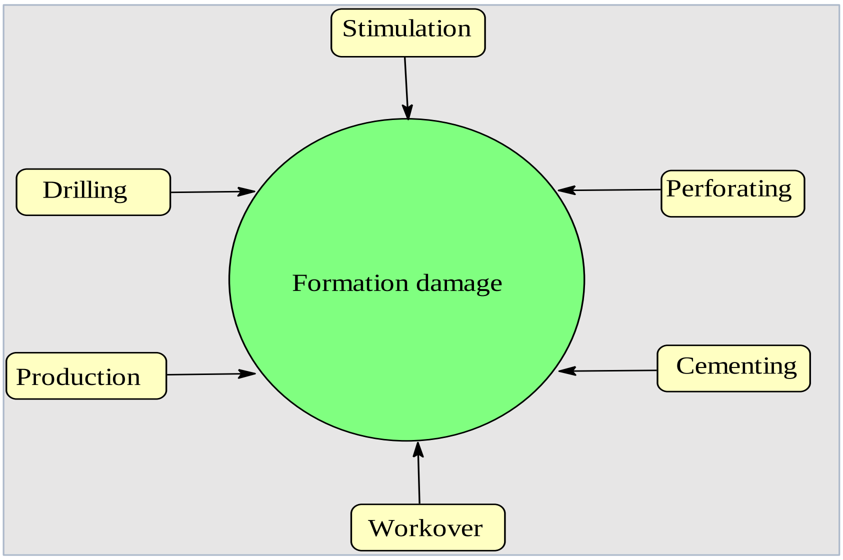

Fig.2.7: Source of formation damage in the geo-energy

Interaction of fluid/acid and reservoir formation affects the permeability in geothermal reservoirs. Injection of acid disturbs the existing equilibrium in the fluid-rock system and consequently, some minerals may dissolve while others may precipitate and this will modify the properties of the reservoir (Fritz et al., 2010; Xiao et al., 2017). Precipitation of secondary minerals within the matrix of the formation or in fractures reduces permeability. On the other hand, dissolution of existing minerals without precipitation can enhance reservoir quality and safeguard durable operations when proper selection of acid is made (Sanchez Roa et al., 2019). For example, re-injection of acid into the geothermal reservoir in geothermal systems causes a strong thermodynamic disequilibrium between the acid and the formation. This results in hydrothermal alterations that are often accompanied by dissolution-precipitation (Fritz et al., 2010; Ngo et al., 2016). Mineralogical transformations often have a significant impact on the fundamental properties of the reservoir and fluid pathways of the geothermal reservoir. On the other hand, mineralogical transformations may cause matrix un-consolidation due to part of the grain skeleton vanishing.

The selection of the acid injected in the reservoir is governed by many factors including the presence of formation fines (clay and non-clay minerals). Some clay minerals can react with acid and result in the formation of insoluble minerals. Prior knowledge on understanding various geochemical reactions with the reservoir formation especially the clays is required because such reactions give better information on clay dissolution capabilities and precipitate mitigation ability (Crundwell, 2014).

2.2.2 Precipitation of clay minerals in geothermal reservoir formations

The presence of clay minerals in the reservoir formation hampers the acid stimulation because clays are very sensitive to acids resulting in dissolution, precipitation, or migration (Higgs et al., 2015). The larger surface area of clays offers the clays a high reactivity (Ganor et al., 2003). Thus, clay minerals are often considered a major cause of water-sensitive formation damage (Nguyen et al., 2005; Wilson et al., 2014; Xiao et al., 2017). Water-sensitive formation damage is a function of the type and distribution of clay minerals within the pore space and fluid composition (Aksu et al., 2015). When evaluating the productive capacity of the geo-energy reservoir, the clay behavior in porous media has to be taken into account (Xiao et al., 2017). The most important types of clay minerals responsible for permeability reduction in reservoirs are kaolinite, montmorillonite, illite, chlorite, and fine-grained non-clay minerals (Ahmad et al., 2018). Clay minerals are a group of hydrous aluminum silicates with dimensions less than 0.005 mm (Marshall, 1994). Three clay minerals important in the geo-energy are kaolinite, montmorillonite, and illite (Anderson et al., 2010). Kaolinite and illite minerals are non-swelling clay minerals while montmorillonite is a swelling clay mineral. Both swelling and non-swelling clays can be allogenic or authigenic. Allogenic clays are tightly packed in the rock matrix and therefore are known to have less impact on formation damage than authigenic clays which have a direct vulnerability to pore fluids (Civan, 2007). Montmorillonite has both allogenic and authigenic characteristics while kaolinite has authigenic characteristics and mostly forms pore-filling flakes (Ali et al., 2010). Under favorable colloidal conditions, kaolinite like other non-swelling clay minerals are released from the pore surface and may undergo dissolution-precipitation reactions or migration. On the other hand, montmorillonite like other swelling clays expand first under favorable ionic conditions followed by disintegration and finally undergo dissolution-precipitation reactions or migration (Aksu et al., 2015; Sameni et al., 2015).

When acid interacts with aluminum phyllosilicates, i.e.clay minerals, water forms an activated complex[5] with the Al^{3+} sites, and H^+ ions form the activated complex with the $SiO_4{}^{4-}$ sites resulting in the dissolution of the clay minerals, Fig. 2.8 (Crundwell, 2014). The activated complexes formed can react with species in solution to form another species. For example, when mud acid (mixture of HF and HCl) enters a sandstone reservoir, the primary reaction begins which results in the formation of aluminum and silica fluorides (chemical reaction 2.1). This reaction results in the dissolution of the minerals without precipitation. The secondary reaction follows when the primary products are further reacted with other species in the solution(chemical reaction 2.2). This reaction results in the formation of a precipitate. Another reaction may happen as a tertiary reaction as the consequence of the formed product in reaction 2 to react with other species in solution (chemical reaction 2.3).

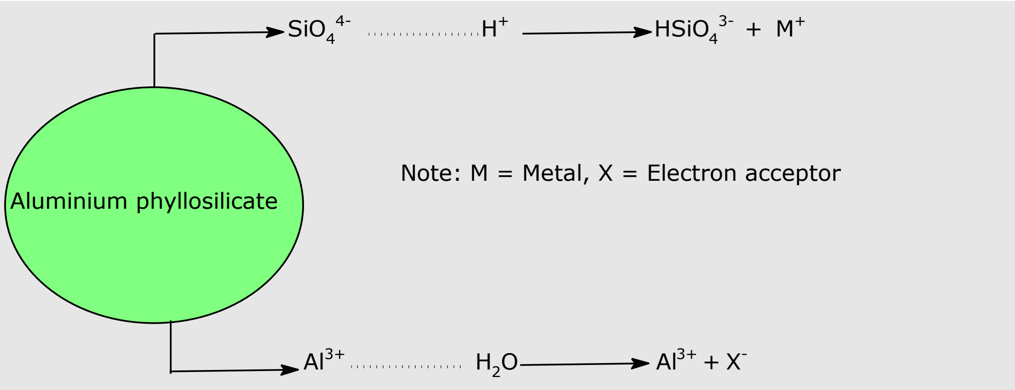

Fig. 2.8: Dissolution of hydrous aluminum phyllosilicates in acidic solutions

---

[5] *An **activated complex** is an unstable arrangement of atoms that is formed during the conversion of reactants into products.*

$$\text{HF + mineral + HCl} \longrightarrow \text{AlF}_y + \text{H}_2\text{SiF}_6 \qquad (2.1)$$

$$\text{H}_2\text{SiF}_6 \text{ + mineral + HCl} \longrightarrow \text{silica gel + AlF}_y \qquad (2.2)$$

$$\text{AlF}_y \text{ + mineral + HCl} \longrightarrow \text{AlF}_z\text{+ silica gel} \qquad (2.3)$$

2.2.2.1 The surface chemistry of clay minerals

The surface chemistry of clay minerals refers to the interaction of adsorbed molecules with the exchangeable cations, with the oxygen atoms, OH and OH_2^+ groups at the surface, and with the adsorbed water molecules (Tournassat et al., 2015). Clay minerals are made of layers where each layer consists of either one sheet of SiO_4 tetrahedra joined to one sheet of Al- or Mg-octahedra or one sheet of Al- or Mg-octahedra sandwiched between two sheets of Si-tetrahedra. The former are called 1:1 (Fig.2.9), the latter 2:1 (Fig. 2.10) clay minerals. Both 1:1 and 2:1 clay minerals have edges at which oxygen atoms and cations (Si^{4+}, $Al^{3+,}$ and Mg^{2+}) are exposed. The cations carry charges and react with molecules in the environment, usually water, to maintain charge neutrality and complete their coordination sphere. Thus, the edges consist of $–O^–$, -OH (Fig. 2.11), and $–OH_2^+$ (Fig.2.12)groups (Tournassat et al., 2015).

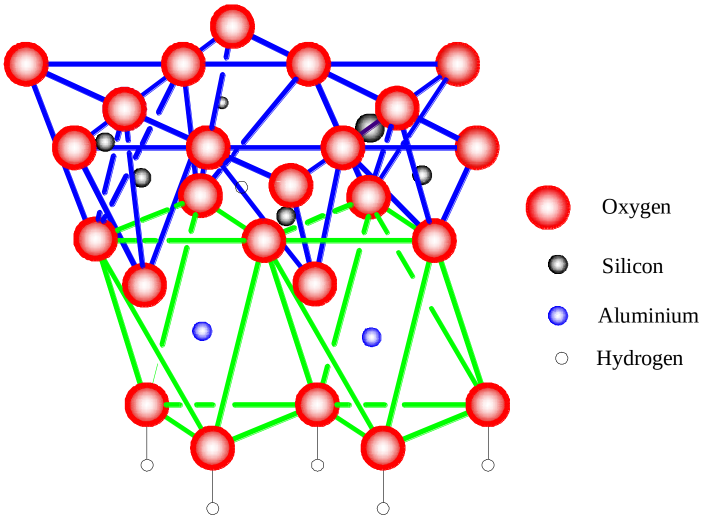

Fig. 2.9: Structure of 1:1 clay mineral

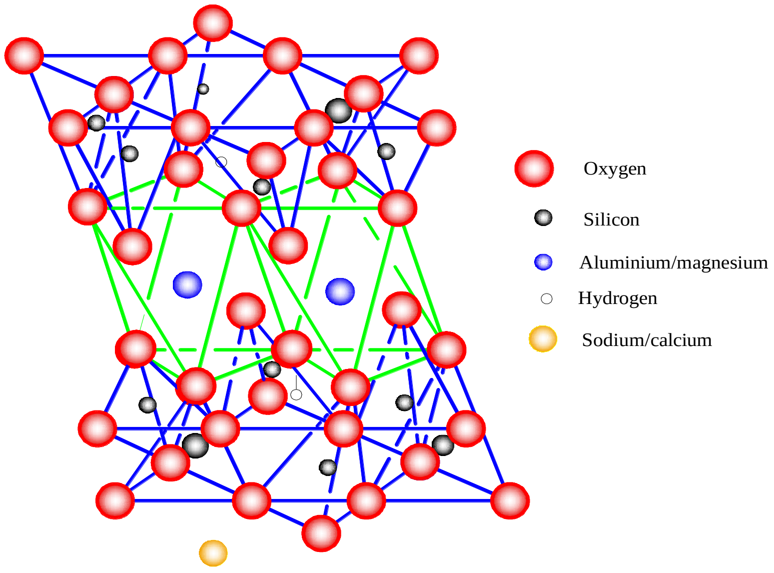

Fig. 2.10: Structure of 2.1 clay minerals

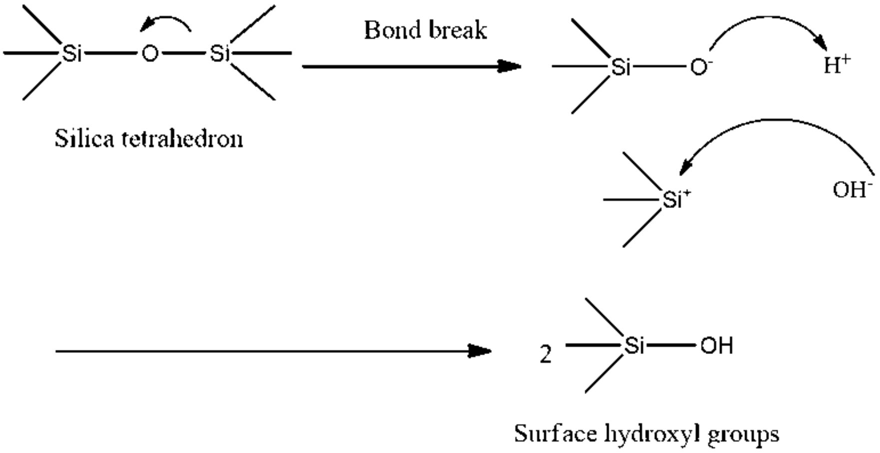

Fig.2.11: Surface hydroxyl groups generated on the edge of clay minerals during bond breaking on silica tetrahedron (A similar mechanism in alumina octahedral).

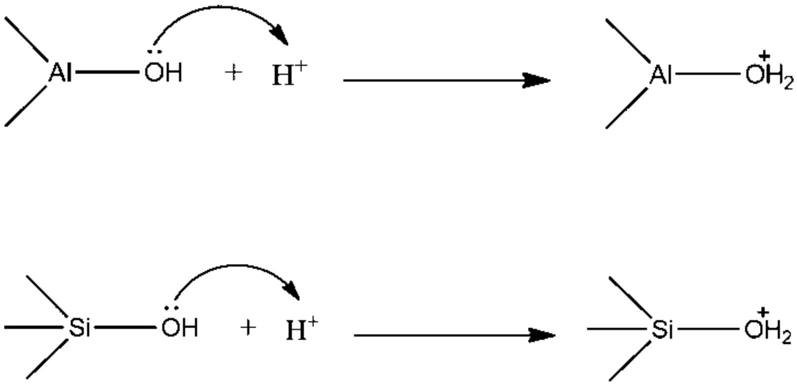

Fig.2.12: Reactions of surface hydroxyls with H^+ to make the surface of clay minerals electropositive.

Another primary source of both negative and positive charges in clay minerals is the dissociation of exchangeable cations. This refers to the substitution of

Si^{4+}, Al^{3+}, and Mg^{2+} with cations with comparable ionic radii in their respective tetrahedral and octahedral sheets. For example, Al^{3+} and Mg^{2+} in the octahedral may be replaced with cations such as $Fe^{3+/2+}$ and Zn^{2+}. The process of replacing one structural cation for another of similar size is referred to as isomorphous substitution However, replacement of a lower valence cation by one with a higher valence or vice versa is the key source of both negative and positive charges in clay minerals. For example, the substitution of one Al^{3+} for a Si^{4+} in the tetrahedron results in a gain of one negative charge. Alternatively, the replacement of a lower valence cation by one with a higher valence (Fe^{2+} by Fe^{3+}) results in a gain of one positive charge.

2.2.2.2 Kaolinite

One side of the crystal layer of kaolinite is composed of oxygen atoms only while the other side consists of hydroxyl groups. Hydrogen bonds and intermolecular forces join the crystal layers thus it is difficult for water to enter the crystal structure. This is the reason why isomorphous substitution occurs rarely in kaolinite and further the reason as to why very few exchangeable cations exist on its crystal surface.

2.2.2.3 Montmorillonite

In montmorillonite, all the top oxygen atoms in oxygen silicon tetrahedron point toward the alumina octahedron. silicon-oxygen tetrahedron sheets and alumina octahedron sheets bond with each other by sharing oxygen atoms. The interactions between crystal layers are intermolecular forces (no hydrogen bonds exist), so the crystal layers are loosely bonded and water can get into the structure easily. On the other hand, a considerable amount of lattice substitution exists, combining a large number of exchangeable cations in the crystal surface. When water gets into the crystal layer, these exchangeable cations dissociate in the water to form a diffusible electrical double layer. Thus, the surfaces of crystal layers are negatively charged, resulting in repulsion between layers and the clay expansion. The lattice substitution of montmorillonite occurs mainly in the alumina octahedron sheet, by replacing the aluminum atoms in the alumina octahedron with iron atoms or magnesium atoms. The silicon atoms in silicon-oxygen tetrahedron are rarely replaced.

2.2.3 Acids for reservoir stimulation

The injected acid for reservoir stimulation tends to enter the geothermal formation through the first fluid entry zone and dissolves the first-contacted minerals while leaving a large portion of the rest of the wellbore untreated (Lucas et al., 2020; Rose et al., 2010). The conventional acids currently in use are hydrochloric, hydrofluoric, acetic, formic, sulfamic, and chloroacetic (Portier et al., 2007). These acids differ in their chemical properties implying that their choice is dictated by the specific intention of the treatment and the underground reservoir characteristics. Hydrochloric acid (HCl), and a mixture of hydrofluoric acid (HF) and HCl (mud acid) are the most commonly used acids for reservoir stimulation. These acids are corrosive and reported to cause serious "pitting" corrosion that requires strong inhibitors for protection (Nitters et al., 2016). Furthermore, mineral acids are rapidly spending due to high reaction rates which results in undesirable results such as precipitation which is accompanied by secondary and tertiary reactions (Li, 2004). These undesirable results limit the application of mineral acids, especially at elevated temperatures. In general, the combination of problems of mineral acids such as precipitation, pitting corrosion, and poor compatibility with clay minerals limit the application of mineral acids(Portier et al., 2007). An alternative to mineral acid treatments is the use of chelating agents.

2.2.3.1 Chelating agents

Chelating agents are used nowadays as stand-alone stimulation fluids to improve reservoir permeability (Mahmoud et al., 2017). Chelating agents can chelate (or bind) metals and retard precipitation. Chelating agents have a lower dissolution rate thus take a more balanced path through the damaged or undamaged formation than the first fluid entry zone with mineral acids which leave the rest of the formation relatively untouched (Rose et al., 2010). Most types of chelating agents used in the geo-energy industry are aminopolycarboxylic acid chelating agents (APCAs) (Hassan and Al-Hashim, 2016). APCAs contain several carboxylate groups bound to one or more nitrogen atoms. These chemicals are derived from amino acids and like other chelates, they are capable of forming water-soluble complexes by coordinating metal ions and forming one or more heteroatomic rings (Bucheli-Witschel and Egli, 2001; Tariq et al., 2017a). For example, hydroxy ethylethylenediaminetriacetic acid (HEDTA), ethylenediaminetetraacetic acid (EDTA), and diethylenetriaminepentaacetic acid (DTPA) are shown in Fig. 2.13 (Mahmoud and Abdelgawad, 2015). Aminopolycarboxylic acid chelating agents like HEDTA, EDTA, and DTPA are non-biodegradable and therefore such property limits their application to the environment (Pinto et al., 2014). Replacement of synthetic APCs with natural APCs such as Nitrilotriacetic acid (NTA), ethylenediaminedisuccinic acid (EDDS), and iminodisuccinic acid (IDS) which are environmentally friendly is the promising alternative (Frenier et al., 2004; Pinto et al., 2014).

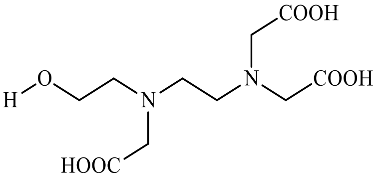

HEDTA

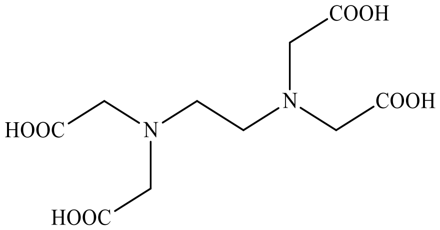

EDTA

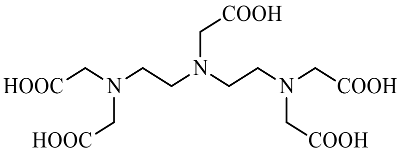

DTPA

Fig. 2.13: Aminopolycarboxylic acid chelating agents

The dissolution ability of minerals by organic ligands such as chelating agents can be explained by two competing theories, namely, indirect proton promoted dissolution mechanism or direct ligand promoted dissolution mechanism(Cama and Ganor, 2006). The major ions involved in mineral dissolution reactions are H^+, OH^-, H_2O, and ligands. The principal steps behind dissolution reactions are the attachment of solute species to surface cations that polarize, detachment of surficial cations, transport of these cations to the bulk solution, and the renewal of a surface site by protonation (Furrer and Stumm, 1986).

In a proton-promoted dissolution surface protonation of aluminosilicate minerals, acidic conditions enhance the dissolution rates because adsorbed protons polarize and weaken critical surface metal-oxygen bonds. This process facilitates the detachment of metal cations from the aluminosilicate mineral surface (Furrer and Stumm, 1986). In acidic conditions, adsorbed organic ligands are responsible to reduce the positive charge of mineral surfaces induced by the protonation of surface functional groups. As a result, more protons can accumulate at the mineral-water interface due to the reduced electrostatic repulsions and this can in turn increase the proton-promoted dissolution rates (Stumm, 1997). Organic ligands can form strong aqueous cation-ligand complexes with metal cations removed from the surface by dissolution. Generally, the overall dissolution rate in the acid condition can be represented as the sum of the proton promoted dissolution rate and the ligand promoted dissolution rate.

In a direct ligand promoted dissolution mechanism, chelating agent adsorbing on the surface sites of the clay mineral through a ligand exchange reaction promotes dissolution by facilitating the detachment of surface cations (Stumm, 1992). Adsorbed chelating ligands weaken the bonds of the metal-oxygen framework by shifting the electron density distribution towards the central metal ion and the ligands attached to it (coordination sphere). This results in a decrease of activation energy for hydrolysis and consequently increases the detachment of metal cations from the surface (Duckworth and Martin, 2001) Duckworth and Martin, 2001). Acidic conditions favor the ligand exchange adsorption mechanism because the increased electrostatic attraction between the ligand-acid functional groups and surface sites of the clay minerals allow ligand molecules to approach the surface and increase the possibility of ligand exchange (Feng et al., 2005).

3 Simulated microbial corrosion in oil, gas and non-volcanic geothermal energy installations: The role of biofilm on pipeline corrosion[6]

3.1 Introduction

An ongoing challenge in the oil, gas and geothermal industries is the design of materials for casings, pipes, and other installations that resist corrosion (Abadeh and Javidi, 2019; Faes et al., 2019; Ibrahim et al., 2018; Miranda-Herrera et al., 2010; NAM, 2015; Provoost et al., 2018; Veldkamp, 2016). Currently, carbon steel is the most widely used engineering material because the material is strong, easily available, and relatively cheap (Batis et al., 1997; Odusote et al., 2012; Provoost et al., 2018; Reinecker et al., 2019; Wang, 2018). However, carbon steel suffers from both abiotic and biotic corrosion damage (Daniilidis et al., 2020; Ibrahim et al., 2018). Biotic induced corrosion, commonly known as Microbial Influenced Corrosion, is difficult to forecast compared to abiotic corrosion since microbial, chemical, and physical processes occur together and interact, making the corrosion process very complex (Ibrahim et al., 2018; Kip and Van Veen, 2015; Little et al., 2020; Videla and Characklis, 1992; Yuan et al., 2013). In biotic-induced corrosion, the metabolic products of the microbes change the chemistry of the material-solution interface (Liang et al., 2014; Little et al., 2006; Parthipan et al., 2017). The chemical changes result in different effects such as induction of localized

---

[6] *This chapter is based on: Madirisha, M., Hack, R., & Van der Meer, F. (2022). Simulated microbial corrosion in oil, gas and non-volcanic geothermal energy installations: The role of biofilm on pipeline corrosion. Status: Accepted and it is the production section. Energy Reports, 8, 2964-2975*

corrosion, change in the rate of general corrosion, and corrosion inhibition (Videla and Herrera, 2005).

Microbes in oil, gas and low temperature (non-volcanic) geothermal wells subsist in the wide range of temperature that follows within the temperature range of oil, gas, and low temperature (non-volcanic) geothermal wells. Oil, gas and low temperature (non-volcanic) geothermal wells are of sedimentary origin and mostly have fluids with temperatures in the range 50 - 150 ^{o}C (Gunnlaugsson et al., 2014a; Wang et al., 2016b). On the other hand, the temperature of the fluids in installations outside the well decreases down to below 50 ^{o}C due to heat exchange with the outside environment and to a lesser degree due to Joule Thomson effects (Singer, 2017). This temperature also supports microbial life. The most important species in MIC are Sulfate Reducing Bacteria (SRB) that utilize sulfate ions as electron acceptors and produce H_2S indirectly (Fig. 3.1). This H_2S causes severe corrosion in the oil, gas, and geothermal industries and contributes to 50% of MIC (Ibrahim et al., 2018; Kip and Van Veen, 2015; Liu et al., 2019; Zhang et al., 2020). On the other hand, SRB oxidize organic substrate into CO_2 (Dissimilatory Sulfate Reduction, chemical equation 3.1) another source causing carbon steel corrosion (Kushkevych et al., 2021; Plugge et al., 2011; Tran et al., 2021). SRB are sensitive to environmental pH for growth, thus SRB are divided into three groups: acidophilic (pH of 2.9 to 6.5), alkaliphilic (pH of 6.9 to 9.9), and neutrophilic (pH of 6 to 8) (Tran et al., 2021).

$$SO_4^{2-} + 2CH_3CHOHCOO^- \longrightarrow 2CH_3COO^- + 2CO_2 + HS^- + OH^- + H_2O \qquad (3.1)$$

Recent research shows that the corrosion effects caused by SRB can be simulated by using abiotic sulfide (Bao et al., 2012; Fatah and Ismail, 2013;

Fatah et al., 2011; Fatah et al., 2013; Feng et al., 2006; Liu et al., 2017; Newman et al., 1992; Sherar et al., 2011). This research is limited to simulate the effects of H_2S as the only SRB metabolic product and ignore dissimilatory respiration of SRB and the presence of biofilm (Bao et al., 2012; Fatah and Ismail, 2013; Fatah et al., 2011; Fatah et al., 2013; Feng et al., 2006; Liu et al., 2017; Newman et al., 1992; Sherar et al., 2011). CO_2 from SRB dissimilatory sulfate reduction, and a biofilm which is a diverse structure stabilized by the Extracellular Polymeric Substrate (EPS) have an important role in corrosion (Blackwood, 2018; Procópio, 2019).

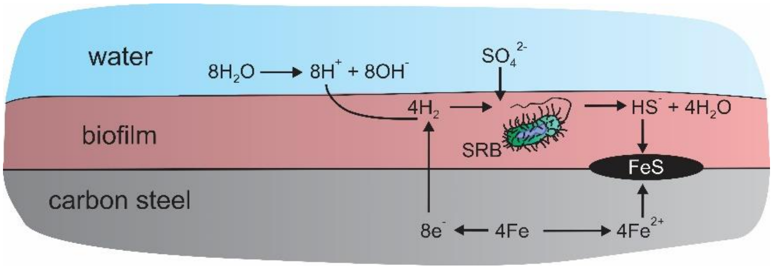

Fig.3.1:Carbon steel corrosion induced by SRB at the interface between carbon steel and water (Mori et al., 2010).

This article describes the research to the role of corrosion of a simulated biofilm in a simulated SRB environment i.e., in the presence of CO_2, $Na_2S.xH_2O$, and media (distilled water or brine solution). Experiments with distilled water are used as a reference to understand the role of biofilm in absence of chloride ions. The corrosion of carbon steel is simulated in an electrochemical cell, and Electrochemical Impedance Spectroscopy (EIS), and PotentioDynamic Polarization (PDP) techniques are used to monitor the electrochemical parameters of the carbon steel test coupons. Sodium alginate (3.0 wt%) and 0.004 M calcium chloride are used to simulate the biofilm while the experimental reactor is purged with CO_2 to create O_2 deprived conditions to reflect the SRB environment and at the same time to reflect the products produced by SRB under the dissimilatory sulfate reduction. Hydrated sodium sulfide (0.4 M $Na_2S.xH_2O$) is used as an indirect source of H_2S. The temperatures used are 30, 45 and 60 ^{o}C as most common strains of SRB exist in the temperature range of 25 to 60 ^{o}C (Cheng, 2013). The exposure time to establish the kinetics for the carbon steel corrosion is 60 and 120 minutes. The resulting electrochemical parameters are used to evaluate corrosion kinetic adsorption parameters. Metal ions dissolved in solution due to corrosion are measured with Inductive Coupled Plasma- Optical Emission Spectrometry (ICP – OES). The statistical T-test is used to compare the means of different variables and to find the extent that such differences are 'by chance'. Corrosion products formed on the surface of carbon steel test coupons and the reference materials are analyzed with a Scanning Electron Microscope coupled with an Energy Dispersive Spectrometer (SEM-EDS) and by X-Ray Diffraction (XRD). The results from surface analyses are used to support the electrochemical results.

3.2 The role of biofilm in corrosion

Microbial growth in closed environments (e.g. pipelines or other closed installations) is characterized by the formation of a biofilm (Kip and Van Veen, 2015; Little et al., 2020). The fundamental constituent of the biofilm is the Extracellular Polymeric Substrate (EPS). EPS, therefore, is an integral part of the biofilm matrix (Karygianni et al., 2020). The role of biofilm in corrosion is investigated and reported in the literature (Blackwood, 2018; Karn et al., 2017; Little et al., 2020; Procópio, 2019). Biofilm significantly influences the conditioning of the physicochemical properties of material surfaces and therefore it is associated with either inhibition or acceleration of aggressive and localized forms of corrosion (Bao et al., 2012; Li et al., 2013; Procópio, 2019). In particular, biofilms can locally change the concentrations of chemical species such as dissolved oxygen, chloride, and other ionic species as well as pH levels, all of which influence corrosion (Blackwood, 2018). Other literature reports that a biofilm binds metal cations and leads to the dissolution of metals and changes in the material (Beech and Sunner, 2004). Starkey (1985) suggests that heterogeneities on the material surface caused by biofilm are one of the factors responsible for anaerobic corrosion.

3.3 Materials and methods

The test materials used for the tests are prepared and controlled very carefully to resemble "real" situations. Artificial biofilms are used to investigate the effect of biofilm on carbon steel corrosion as real microbial biofilms are too complex to simulate and analyze. In this series of tests, calcium alginate is used to simulate biofilm because it is comparable to the structure and properties of biofilm in real situations as shown by various authors (Chang et al., 2010; Nassif et al., 2020). NaCl solution is used to simulate the salinity of brine present in the oil, gas, and non-volcanic geothermal installations. $Na_2S.xH_2O$ is used to mimic the source of H_2S while CO_2 is purged in the system to create an O_2 deprived environment and at the same time serve as SRB product through dissimilatory sulfate reduction (El Mendili et al., 2013; Sherar et al., 2011). SRB do not produce the H_2S directly as presented by reaction (3.2) and (3.3). With sodium sulfide, the H_2S is produced indirectly according to reactions (3.4) and (3.3).

$$SO_4^{2-} + 9H^+ + 8e^- \longrightarrow HS^- + 4H_2O \qquad (3.2)$$

$$HS^- + H^+ \rightleftharpoons H_2S \qquad (3.3)$$

$$Na_2S + H_2O \longrightarrow 2Na^+ + HS^- + OH^- \qquad (3.4)$$

3.3.1 Carbon steel coupons and chemicals to simulate SRB environment

A piece of steel pipe (carbon steel API 5L X70M HFW) of 2 m length is made available by the Tanzania Petroleum Development Corporation. The chemical composition is shown in Table 3.1. The pipe is cut into circular carbon steel coupons of 14 mm diameter and 1.5 mm thick to fit the dimensions required for the working electrode in the electrochemical cell. The carbon steel coupons function as the working electrode of the cell. The surfaces of the coupons are polished with silicon carbide abrasive paper of increasingly fine grit (graded 100, 200, 400, 600, 800, and 1000) to have smooth surfaces which do not influence the electrochemical behavior of the material (Chang et al., 2019; Nor Asma et al., 2011). The polished surfaces are further cleaned with distilled water, acetone, and ethanol, and again washed with distilled water. Thereafter the coupons are air-dried and the weight of each coupon is recorded.

Table 3.1: Chemical composition of carbon steel API 5L X70M HFW (wt%)

Fe	C	Si	Mn	P	S	V	Nb	Ti
97.39	0.17	0.45	1.75	0.02	0.01	0.10	0.05	0.06

A 3.0 wt% NaCl solution is prepared to mimic the salinity of the brine. The surfaces of the dried, polished, and cleaned carbon steel coupons are prepared with 0.1 mL of 3.0 wt% sodium alginate (Fig. 3.2). The sodium alginate solution is homogenously spread over the entire surface using a thin strand of nylon. To immobilize the sodium alginate and convert it to Ca-alginate (the simulated biofilm), 0.1 mL of 0.004 M aqueous $CaCl_2$ is applied. The mixture of sodium alginate and $CaCl_2$ on the carbon steel coupons is left to rest for 15 min to crosslink. Thereafter, the coupons are washed with 10 mL of distilled water to remove unreacted sodium alginate, which is soluble in water, and then the coupons are air-dried as the final treatment for preparing the coupons. During washing of test coupons, the formed substance on the surface was insoluble in water evidencing that the formed substance is calcium alginate. SRB and its metabolite H_2S are simulated by adding 0.4 M sodium sulfide ($Na_2S.\ xH_2O$: Assay ~ 60%) to either distilled water or the brine solution before the experiments.

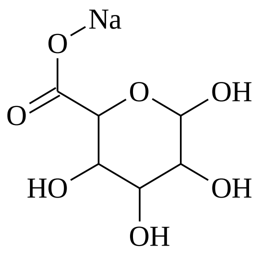

Fig. 3.2:Structure of sodium alginate used for simulation of a biofilm

3.3.2 Experiment set-up and pH measurements

The carbon steel coupons are tested in a three-electrode electrochemical cell coupled with a Potentiostat/Galvanostat: PGSTAT204/AUT50663 from Metrohm (Autolab B.V., Amsterdam, The Netherlands). The software used is NOVA version 1.11.2 (ibid). Furthermore, the cell is coupled with a thermostat-water bath, pH meter, and CO_2 gas cylinder (Fig. 3.3). The pH meter allows monitoring of the pH of the solution in the electrochemical cell during the test.

The carbon steel coupons (with or without biofilm) are used as working electrodes, platinum as an auxiliary electrode, and saturated silver-silver chloride (Ag/AgCl) in 3.0 M KCl solution as a reference electrode. The solution (distilled water or brine solution) in the electrochemical cell is purged with CO_2 (flow rate ~150 mL/min) for 30 min before the experiment and during the experiment to create an O_2 deprived medium and to serve as a product from SRB dissimilatory sulfate reduction. The volume of the solution (distilled water or brine solution) in the electrochemical cell is 500 mL, including a volume of 3 mL of 0.4 M $Na_2S.xH_2O$ added as a source of H_2S.

The corrosion tests are done for two different exposure times of 60 and 120 min and with or without simulated biofilm (Table 3.2). This gives four tests per temperature. All tests are done in duplicate. Further, the pH of the solution is measured at the start of the test (initial pH) and also after 60 and 120 min (final pH). After the test, the carbon steel coupon is removed from the cell and placed in a desiccator.

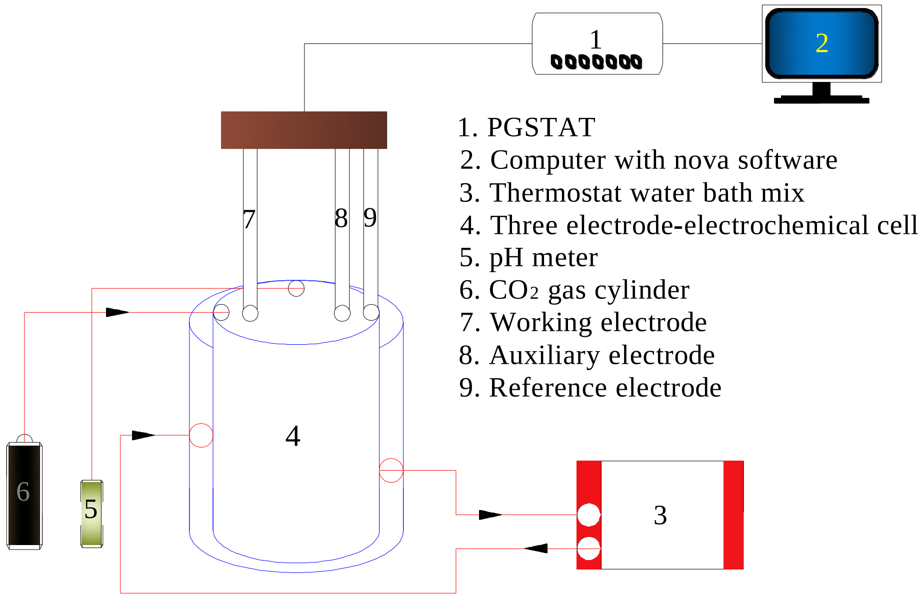

Fig. 3.3:Schematic diagram of the set-up for carbon steel corrosion tests under a simulated microbial environment

Table 3.2: Test matrix for the investigation of the role of biofilm on the corrosion of carbon steel

	Experiment	Temperature (°C)	Simulated biofilm	Time (min)
Distilled water	1, 2, 3	30, 45, 60	no	60
	4, 5, 6	30, 45, 60	yes	60
	7, 8, 9	30, 45, 60	no	120
	10, 11,12	30, 45, 60	yes	120
Brine solution	13, 14, 15	30, 45, 60	no	60
	16, 17, 18	30, 45, 60	yes	60
	19, 20, 21	30, 45, 60	no	120
	22, 23, 24	30, 45, 60	yes	120

3.3.3 Electrochemical corrosion measurements

Electrochemical corrosion measurements, i.e., PotentioDynamic Polarization (PDP) and Electrochemical Impedance Spectroscopy (EIS), are measured in the electrochemical cell after 60 and 120 min. The PotentioDynamic Polarization (PDP) is done at a range of −200 to +200 mV from the corrosion potential (E_{corr}) with a scan rate of 10 $\mathrm{mVmin^{-1}}$. s. The Tafel slopes (b_a and b_c) are determined after a stable open circuit potential is achieved by extrapolating the linear Tafel regions to the corrosion potential (E_{corr}). For a better corrosion rate estimation, the Tafel slopes in combination with the polarization resistance (R_p) from EIS are used to determine the corrosion current density (I_{corr}) (eqs 3.5 – 3.7):

$$\beta = \left(\frac{b_\mathrm{a} b_c}{2.303\ (b_\mathrm{a} + b_c)} \right)$$

(3.5)

$$R_p = \frac{\Delta E}{\Delta I} \quad = \left(\frac{\beta}{i_\mathrm{corr}} \right) \tag{3.6}$$

$$i_\mathrm{corr} = \frac{1}{R_P} \left(\frac{b_\mathrm{a} b_c}{2.303\ (b_\mathrm{a} + b_c)} \right)$$

(3.7)

The corrosion rate (CR) is calculated from the corrosion current density (I_{corr}) together with Faraday’s law (eq. 3.8):

$$\text{Corrosion Rate }(\mathrm{CR}) = \frac{315 \times}{\rho n F} \frac{Z I_\mathrm{corr}}{} \tag{3.8}$$

in which b_a and b_c are Tafel slopes for anodic and cathodic curves respectively (in $\mathrm{mVdec^{-1}}$), β is the Stern–Geary Coefficient ($\mathrm{mVdec^{-1}}$), I_{corr} is the corrosion current density ($\mu A/cm^2$), ρ is the density of iron (7.8 g /cm^3), F is Faraday’s constant (96500 C/mol), Z is the atomic weight (g/mol), n is the number of exchanged electrons, ΔE is the change in potential (mV), and ΔI is the change in current (mA).

Electrochemical Impedance Spectroscopy (EIS) is studied as a function of the frequency of an applied alternating current. It is measured under a sinusoidal excitation potential of 10 mV in the frequency range from 0.5 mHz to 10 kHz. Furthermore, the electrochemical circle fitting -analysis on EIS data is done using the NOVA software to generate the polarization resistance (R_p), solution resistance (R_s), and constant phase elements (pseudo-capacitance/admittance - Y_o), and phase shift/index (n). The EIS which is non-destructive is performed first followed by PDP which is destructive for surfaces.

3.3.3.1 Kinetic parameters of the activation corrosion process

Corrosion kinetic parameters "*apparent activation corrosion energy*" (E_{act}), "*enthalpy of activation*" (ΔH_{act}), and "*entropy of activation*" (ΔS_{act}) are calculated using the Arrhenius equation (3.9) and the transition state equation (3.10). The kinetic parameters of the activation corrosion process have a direct influence on the passivity developed on the material surface (Go et al., 2020; Khadom et al., 2009).

$$\log I_{corr} = \log A - \frac{E_{act}}{2.303\,RT} \tag{3.9}$$

$$I_{corr} = \frac{RT}{Nh} e^{\frac{\Delta S_{act}}{R}} e^{-\frac{\Delta H_{act}}{RT}} \tag{3.10}$$

I_{corr} is the corrosion current density (μA/cm^2), E_{act} is the activation corrosion energy (J/mol), R is the universal gas constant of 8.314J/ (mol·K), T is the testing temperature (K), A is the pre-exponential factor, h is Plank's constant, *N* is Avogadro's number, ΔS_{act} is the entropy of activation (J/K), and ΔH_{act} is the enthalpy of activation (J).

3.3.3.2 Statistical T-test

The T-test is part of inferential statistics used to compare the means of two different sets of observed data and to find to what extent such difference is 'by chance'. A T-test is selected because it likely determines whether biofilm affects the corrosion current density. Paired and independent t-tests are performed using the IBM SPSS statistics 27 software.

3.3.4 Characterization of corrosion products

The analytical techniques used to characterize the corrosion products on the surface of the carbon steel coupons are SEM-EDS and XRD. A Scanning Electron Microscope (SEM, Model JSM-6010LV/LA) equipped with Energy Dispersive Spectrometer (EDS) is used for determining the elemental composition. The corroded test coupons are adhered to on the carbon tabs before the analysis to enhance the surface conductivity and prevent possible charging problems. An acceleration voltage of 20.0 kV and a working distance of 10.0 mm are used during the analysis.

X-Ray Diffraction (XRD) (Bruker D2 phaser) is used for qualitative characterization of the corrosion products on carbon steel. The equipment operates in Bragg-Brentano geometry with CuKα radiation and a LYNXEYE detector as well as Bruker's corundum standard reference material. The patterns are collected with a Cu X- ray tube (1.54184 Å, 10 mA, 30kV) from 6^{o} to 80^{o} in 2θ range with the step size of 0.012^{o} and integration time of 0.1s. In addition, a detector slit of 8 mm is inserted while a standard divergence slit of 0.6 mm is used to control the illuminated area. Identification of the obtained diffractograms is performed with DIFFRA.EVA software. XRD has a detection limit that depends on the density, valence electrons, and crystal structure of the compounds in the sample. However, the rule of thumb is that XRD has a detection limit of ~1% by volume (Schwantes et al., 2017; Treiman et al., 2010). In this study, the duration of the measurement of each sample is 24 hours. A non-treated carbon steel coupon is used as a reference.

3.3.5 Characterization of the dissolved metal ions in solution

The collected solutions after the electrochemical measurements are investigated with Inductive Coupled Plasma- Optical Emission Spectrometry (ICP-OES) (Perkin Elmer 8300DV) to quantify Fe, Si, and Mn ions dissolved in the solution as an indication of carbon steel corrosion in set conditions. Before the analysis, calibration lines are constructed by the dilution of standard solutions (Merck, multi IV 1000 mg/L). The results are corrected with blanks of blank experiments (experiments without carbon steel in the cell). The quantity of metal ions released (in µg/ (g.cm^2)) corresponds to the concentration of dissolved metal ions in the solution (mg/L) normalized to the weight of the working electrode (g), its exposed geometrical surface area (cm^2), and the total solution volume (L).

3.4 Results

The results on electrochemical parameters are presented first, followed by corrosion rates, kinetic parameters of activation corrosion, statistical T-tests, pH, dissolved metal ions in solution, SEM-EDX, and XRD. The discussion of the results is done in section 3.5.

3.4.1 Electrochemical results

The PDP results to investigate the role of biofilm in distilled water (reference experiments) are shown in Table 3.3 and with a brine solution in Table 3.4. Further, the electrochemical results with EIS on the role of biofilm on corrosion are shown in Tables 3.5 and 3.6.

Table 3.3: PDP results for test coupons in distilled water as a function of temperature (30, 45, and 60 °C) and time (60 and 120 min) without and with simulated biofilm

Time (min)	Biofilm	Temperature (°C)	E_{corr} (mV, Ag/AgCl)	I_{corr} (mAcm^{-2})	b_a (mVdec^{-1})	b_c (mVdec^{-1})	R_p (Ω) x 10^3
60	no	30	-682 ± 2	0.09 ± 0.01	1073 ± 71	741 ± 36	3.410
		45	-688 ±5	0.17± 0.01	1106 ± 26	1012 ± 43	2.105
		60	-697 ± 1	0.23± 0.05	1121 ± 39	1030 ± 26	1.633
	yes	30	-680± 5	0.05 ± 0.01	1034 ± 15	466 ±8	4.618
		45	-686 ± 5	0.11 ± 0.01	1053 ±71	712± 1	2.738
		60	-690± 5	0.11 ± 0.02	1100 ± 12	765 ± 71	2.408
120	no	30	-683± 4	0.05 ± 0.01	1033 ± 33	512 ± 41	4.645
		45	-687 ± 4	0.08 ± 0.01	1037 ± 38	597 ± 93	3.173
		60	-710 ± 1	0.20 ± 0. 03	2103 ± 650	1064 ± 156	2.339
	Yes	30	-692 ± 1	0.07 ± 0.04	1318 ± 149	598 ± 90	3.936
		45	-697 ± 1	0.12 ± 0.09	1372 ± 46	640 ± 8	2.679
		60	-716 ± 2	0.22 ± 0.01	2345 ± 847	1111 ± 169	2.269

Table 3.4: PDP results for test coupons in brine solution as a function of temperature (30, 45, and 60 °C) and time (60 and 120 min) without and with simulated biofilm

Time (min)	Biofilm	Temperature (°C)	E_{corr} (mV, Ag/AgCl)	I_{corr} (mAcm^{-2})	b_a (mVdec^{-1})	b_c (mVdec^{-1})	R_p (Ω)
60	no	30	-684 ± 1	0.56 ± 0.02	103 ± 0	31 ± 7	490
		45	-714 ± 1	1.42 ±0.00	159 ± 6	57 ± 2	294
		60	-697 ± 1	0.94 ± 0.01	125 ± 3	44 ± 4	431
	yes	30	-710 ± 3	0.63 ±0.02	109 ± 64	34 ± 14	432
		45	-716 ± 5	1.46 ± 0.01	149 ± 29	57 ± 3	273
		60	-711 ± 1	1.16 ± 0.01	145 ± 34	54 ± 3	309
120	no	30	-697 ±1	1.18 ± 0.00	134 ± 8	56 ±14	553
		45	-718 ± 1	1.32 ±0.04	137 ± 1	58 ± 7	379
		60	-714± 1	1.29±0.00	142 ± 17	56 ±5	482
	yes	30	-686 ± 2	0.58 ± 0.00	95 ± 8	32 ± 10	643
		45	-721 ± 1	1.42 ± 0.00	122 ± 0	67 ± 0	287
		60	-710 ± 1	0.93 ±0.00	106 ± 18	47± 18	563

Table 3.5: EIS results for test coupons in distilled water as a function of temperature (30, 45, and 60 °C) and time (60 and 120 min) without and with simulated biofilm

Time	Biofilm	T	Rp	Rs	CPEs	
					*Y*o	*n*
(min)		(°C)	(kΩ)	(kΩ)	(μF x 10^{-4})	
60	no	30	2.061	0.078	3.597	0.999
		45	1.327	0.048	6.938	1.000
		60	1.029	0.036	8.665	1.000
	yes	30	2.811	0.089	3.252	0.999
		45	1.748	0.068	5.067	0.999
		60	1.736	0.065	5.279	1.000
120	no	30	2.930	0.093	3.320	0.999
		45	2.044	0.071	4.234	1.000
		60	1.556	0.056	5.753	1.000
	Yes	30	2.782	0.073	4.485	0.999
		45	1.612	0.065	5.498	1.000
		60	1.513	0.053	6.165	1.000

Table 3.6: EIS results for test coupons in brine solution as a function of temperature (30, 45, and 60 °C) and time (60 and 120 min) without and with simulated biofilm

Time	Biofilm	T	Rp	Rs	CPEs	
					*Y*o	*n*
(min)		(°C)	(Ω)	(Ω)	(μF x 10^{-2})	
60	no	30	18.507	1.407	2.106	1.000
		45	12.825	0.215	2.519	1.000
		60	15.160	0.289	2.238	1.000
	yes	30	17.775	1.205	2.176	1.000
		45	12.275	0.205	2.593	1.000
		60	14.721	0.269	2.274	1.000
120	no	30	14.559	0.249	2.365	1.000
		45	13.471	0.216	2.488	1.000
		60	13.563	0.229	2.402	1.000
	yes	30	17.950	1.229	2.154	1.000
		45	13.214	0.210	2.501	1.000
		60	15.192	0.290	2.206	1.000

3.4.1.1 Corrosion rates

The conversion of electrochemical results to more comprehensive corrosion rates (mm/year) is performed using equation 3.8 and the corrosion rates are shown in Fig.3.4.

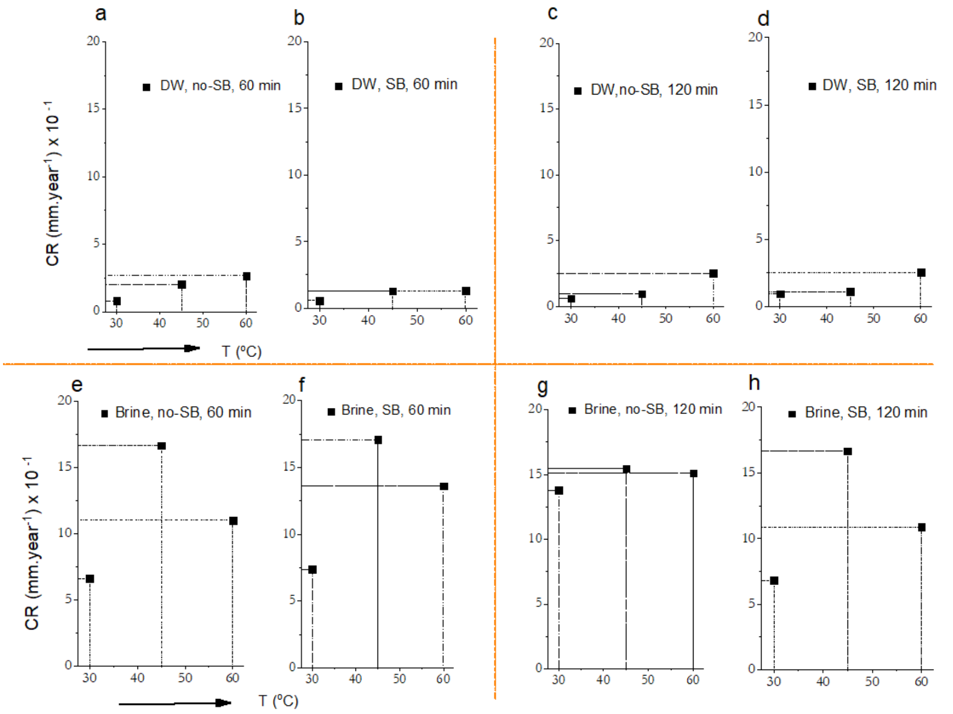

Fig. 3.4:Corrosion rates (CR) of carbon steel coupons in distilled water (DW) and brine solution as a function of temperature (30, 45, and 60 °C) and time (60 and 120 min) without and with simulated biofilm (no-SB respectively SB)

3.4.1.2 Kinetic parameters of activation corrosion

Taking into account equations 3.9 and 3.10, linear regression of log (I_{corr}) versus (1/T), and *In* (I_{corr}/T) versus (1/T) are used to estimate the *apparent activation corrosion energy* (E_{act}), *enthalpy of activation* (ΔS_{act}), and *entropy of activation* (ΔH_{act}). The results are tabulated in Table 3.7.

Table 3.7: Kinetic parameters of activation corrosion for test coupons without and with simulated biofilm in distilled water and brine under exposure times of 60 and 120 min

Medium	Time (min)	Biofilm	E_{act} (kJ/mol)	ΔH_{act} (kJ)	ΔS_{act} (kJ/K)
DW	60	no	26.37	23.72	-0.22
		yes	22.38	19.74	-0.23
	120	no	38.55	35.90	-0.18
		yes	31.97	29.33	-0.20
Brine	60	no	15.06	12.42	-0.24
		yes	17.53	14.89	-0.23
	120	no	12.55	9.90	-0.27
		yes	13.77	11.13	-0.25

Note: DW = Distilled water

3.4.1.3 Statistical T-test

The p-values from paired t-test comparing the two mean values of I_{corr} for test coupons (from Table 3.3 and 3.4) with or without biofilm in distilled water or brine are shown in Table 3.8. Further, the p-values from the independent t-test to compare the influence of the presence or absence of biofilm on the same continuous dependent variable (I_{corr}) are shown in Table 3.9.

Table 3.8: p-values of paired t-test on two means I_{corr} of test coupons with or without biofilm in distilled water or brine

I_{corr}	p-value
Test coupons with vs without biofilm in distilled water	0.393
Test coupons with vs without biofilm in brine	0.527
Test coupons without biofilm in distilled water vs without biofilm in brine	0.001
Test coupons with biofilm in distilled water vs with biofilm in brine	0.002

Table 3.9: p-values of independent t-test on the influence of the presence or absence of biofilm on the same continuous dependent variable (I_{corr}) in distilled water or brine

	Equal variance	Levene's test of equality of variances p	t-test for equality of means p (2-tailed)
$I_{\text{corr (60 min, DW)}}$	Assumed	0.374	0.180
	not assumed		0.206
$I_{\text{corr (120 min, DW)}}$	Assumed	0.875	0.697
	not assumed		0.697
$I_{\text{corr (60 min, brine)}}$	Assumed	0.981	0.767
	not assumed		0.767
$I_{\text{corr (120 min, brine)}}$	assumed	0.130	0.311
	not assumed		0.360

3.4.2 pH results

One of the most influential parameters for the degradation of metallic material like carbon steel in acidic media is the pH (Zuo, 2007). The initial and final pH in a $Na_2S.xH_2O$ (H_2S)/CO_2 environment is shown in Table 3.10.

Table 3.10: Initial and final pH of carbon steel corrosion in distilled water and brine solution experiments

Time (min)	Biofilm	Temperature (°C)	pH Distilled water Initial	 Final	 Brine solution Initial	 Final
60	no	30	3.69	5.30	3.67	5.06
		45	3.47	4.97	3.50	4.80
		60	3.37	4.90	3.41	4.82
	yes	30	3.67	5.35	3.69	5.06
		45	3.08	5.23	3.52	4.71
		60	3.01	5.02	3.51	4.87
120	no	30	3.67	5.48	3.67	5.01
		45	3.48	5.40	3.50	4.85
		60	3.38	5.03	3.43	4.89
	yes	30	3.68	5.40	3.68	5.03
		45	3.05	5.38	3.53	4.83
		60	3.03	4.92	3.50	4.87

3.4.3 ICP-OES results

The amount of metal ions released into distilled water or brine solution as a result of electrochemical corrosion is investigated using ICP-OES to further determine the influence of biofilm on corrosion of carbon steel. Fig. 3.5 shows the concentration units of dissolved metal ions (sum of Fe, Si, and Mn) in both distilled water and brine solution.

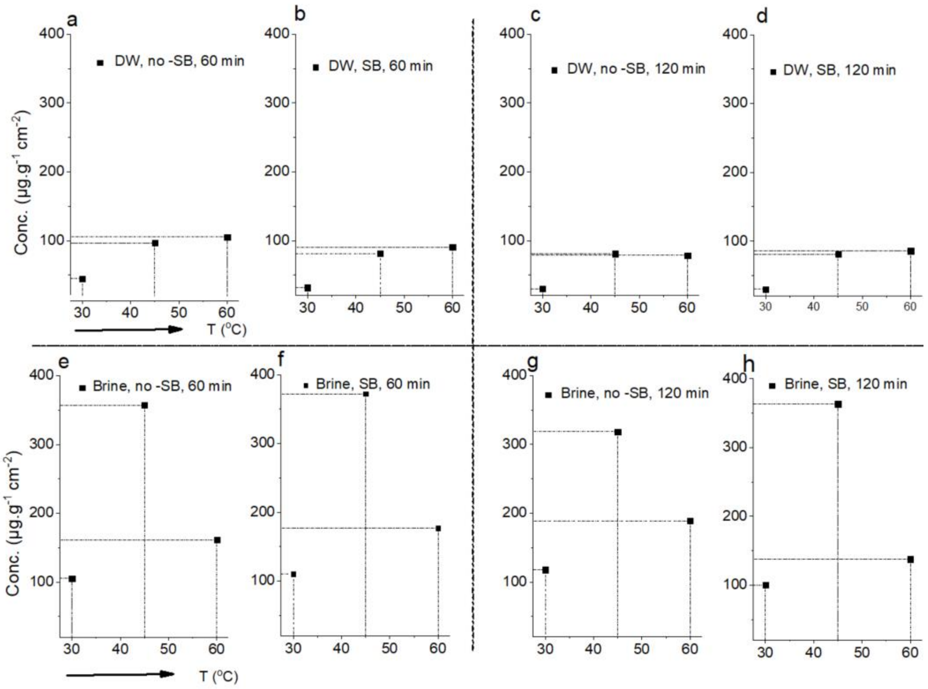

Fig. 3.5:The concentration of dissolved Fe, Si and Mn (µg/g cm^2) versus temperature (30, 45 and 60 °C); (a-d) in distilled water (DW) and (e-h) in brine solution as a function of time (60 and 120 min) and without and with simulated biofilm (no-SB respectively SB).

3.4.4 SEM-EDS results

The elemental composition of the corrosion products scanned by SEM-EDS is shown in Table 3.11 for test coupons in distilled water and brine. Fifteen representative examples are shown.

Table 3.11: Representative examples of SEM-EDS results of corrosion products on test carbon coupons in distilled water and brine

	Element in Mass %								
	C	O	Na	Al	S	Cl	Si	Mn	Fe
Sample 8: (DW, 120 min, SB, 45 °C)	6.80	42.32	-	-	-	2.16	-	0.81	47.90
Sample 12: (DW, 120 min, SB, 60 °C)	6.47	42.70	-	-	-	0.50	-	0.87	49.50
Sample 15: (Brine, 60 min, SB, 30 °C)	14.63	41.33	-	-	-	-	0.11	0.60	43.32
Sample 18: (Brine, 120 min, no -SB, 45 °C)	7.50	42.07	-	-	-	1.19	-	0.69	48.55
Sample 19: (Brine, 60 min, SB, 45 °C)	8.85	30.55	-	0.03	-	-	-	0.95	59.62
Sample 21: (Brine, 60 min, no- SB, 60 °C)	6.11	42.69	-	-	0.33	2.19	-	0.73	0.72
Sample 23: (Brine, 60 min, SB, 60 °C)	7.40	38.31	0.75	-	-	0.71	-	47.96	52.10

Note: SB = simulated biofilm, no -SB = No simulated biofilm, DW = Distilled water

3.4.5 XRD results

X-Ray Diffraction (XRD) analyses are performed on coupons exposed in distilled water and brine solution to investigate the presence of corrosion products on carbon steel occurring in a crystalline phase. Carbon steel not used in tests is considered as a reference (blank coupon). All coupons have been measured, however not all diffractograms are shown. Only diffractograms depicting major changes are shown in Fig.3.6.

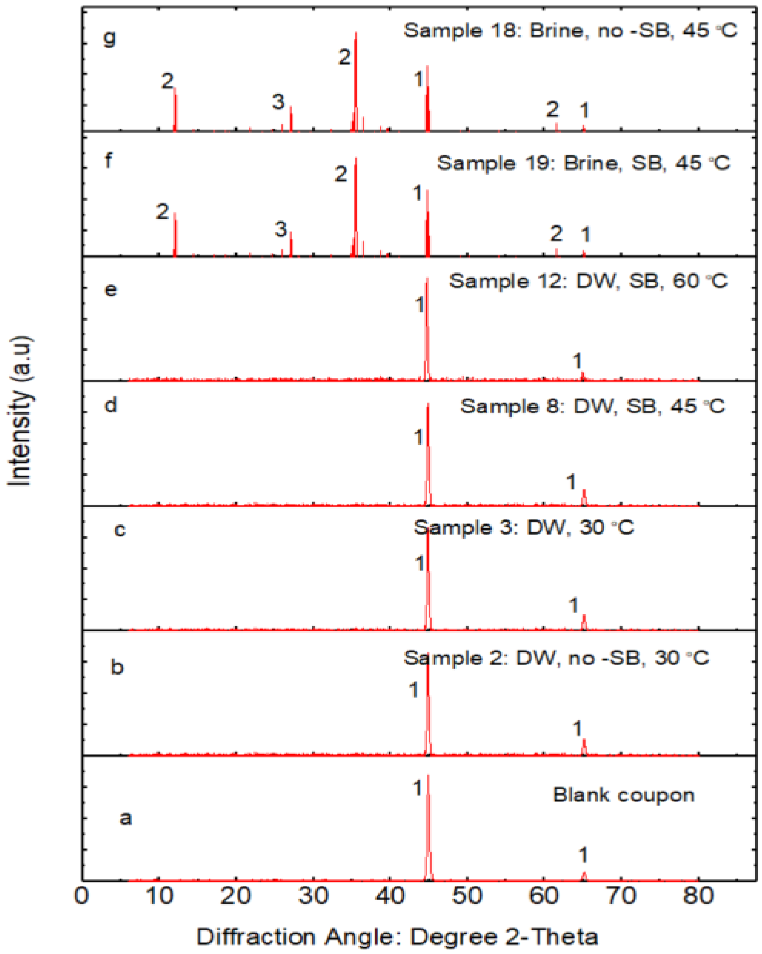

Fig. 3.6:XRD diffractograms for carbon steel as a function of time (60-120 min) with and without simulated biofilm (SB and no-SB) in distilled water and brine.

3.5 Discussion

The electrochemical test results on the role of biofilm on carbon steel corrosion are discussed first, followed by kinetic parameters of activation corrosion, statistical T-tests, pH, and ICP-OES. Further, the results of the SEM-EDS and XRD analyses of the corroded coupon surfaces are discussed.

3.5.1 Electrochemical results

The difference between the standard potential (*E*) of iron of -680 mV (Standard Calomel Electrode (SCE)) and the corrosion potentials (E_{corr}) show a positive overpotential (η_a) for all test coupons in Table 3.3 and 3.4. A positive overpotential indicates that the anodic reaction dominates over the cathodic reaction. The anodic reaction is controlled by reaction presented by chemical equation 3.11 while the cathodic reactions are likely controlled by reactions presented by chemical equations 3.3 and 3.12(a, b and c).

$$Fe(s) \longrightarrow Fe^{2+}(aq) + 2e^- \qquad (11)$$

$$HCO_3^-(aq) \longrightarrow CO_3^{2-}(aq) + H^+(aq) \qquad (12a)$$

$$H^+(aq) + e^- \longrightarrow H_{ads} \qquad (12b)$$

$$2H_{ads} \longrightarrow H_2\,(g) \qquad (12c)$$

Notes: aq = aqueous, g = gas, s = solid, ads = adsorbed

The higher polarization resistances (R_p) and Tafel slopes (b_a and b_c) in distilled water than in brine solution imply lower corrosion current densities (i_{corr}) in distilled water than in brine solution (Pan et al., 2017). The addition of biofilm on the coupon surfaces decreases the corrosion current densities for test coupons without simulated biofilm in distilled water experiments with 60 min exposure time by 0.04, 0.06, and 0.12 mAcm^{-2} at temperatures of 30, 45, and 60 ^{o}C, respectively. In addition, doubling the exposure time does not show a significant difference in the corrosion current densities between the test coupons with and without simulated biofilm. Changing the electrolyte from distilled water to brine solution, the corrosion current densities are four to five times higher in brine than in distilled water for 60 min tests. The corrosion current densities at 60 min do not significantly increase for test coupons with simulated biofilm compared to coupons without simulated biofilm in brine solution at 30, 45, and 60 °C. Doubling the exposure time results in a slight decrease of the corrosion current densities at 45 °C for test coupons with and without simulated biofilm compared to test coupons at 60 min. The opposite trend is observed at 30 and 60 °C. The above results imply that the presence of simulated biofilm in brine and distilled water experiments does not significantly increase the corrosion current densities (I_{corr}).

The EIS results (Table 3.5 and 3.6) show that the presence of biofilm on the test coupons leads to an increase in R_p and R_s values for the test coupons without simulated biofilm in distilled water experiments with 60 min exposure time and temperatures of 30, 45 and 60 °C. This result is similar to the PDP results. There is no significant change of R_p and R_s values between test coupons with and without biofilm if the exposure time is doubled. Further, there are no significant differences in the pseudo-capacitances/admittance (Y_o) for both test coupons with and without simulated biofilm. Changing of electrolyte to brine solution, similar trends as for the PDP results are observed. In addition, there are no significant differences in the Y_o for both test coupons with and without simulated biofilm. These results further support that the presence of simulated biofilm does not influence corrosion.

3.5.1.1 Corrosion rates

In distilled water with CO_2 and $Na_2S.xH_2O$ (H_2S), the corrosion rates increase with temperature independently whether biofilm is present or not (Fig. 3.4a-d). Moreover, for 60 min exposure time, a reduction in corrosion rates is obtained for 30, 45, and 60 °C with biofilm, whereas for 120 min exposure no significant change in corrosion rates are obtained at all (about 0.125 mm/year less for 60 min and 0.02 mm/year less for 120 min). This likely indicates that the impact of biofilm and temperature on the corrosion reactions are pronounced at 60 min exposure time while at 120 min exposure time, only the impact of temperature is observed. This is in agreement with the PDP and EIS results. In brine solution with CO_2 and $Na_2S.xH_2O$ (H_2S), the influence of the biofilm is negligible as there are no significant differences in corrosion rates between test coupons with and without biofilm (about 0.14 mm/year less for 60 min and 0.5 mm/year less for 120 min) (Fig. 3.4e-h). The higher corrosion rates observed in brine than in distilled water are likely due to NaCl which is responsible for inducing the higher corrosion rates because the Cl^- ions can attack the protective layer established by corrosion products. The corrosion rate maximum of carbon steel in brine solution at 45 °C indicates evidence of the formation of a strong protective layer at 60 °C (see further section 3.5.3).

Likely, the use of both $Na_2S.xH_2O$ and CO_2 in presence of simulated biofilm in the tests cause the anaerobic corrosion rates to fall within a range of 0.25 to 1.6 mm/year. This range is comparable to the anaerobic corrosion rates for biotic- SRB experiments which are reported to be within a range of 0.2 to 1.18 mm/year (Beech and Gaylarde, 1999; Fatah et al., 2013; Jack et al., 1996; Miranda et al., 2006).

3.5.1.2 Kinetic parameters of the activation corrosion process

The *apparent activation corrosion energy* and the positive *enthalpy of activation* in the presence of simulated biofilm in distilled water experiments shown in Table 3.7 are slightly lower than without biofilm. According to Go et al (2020), this implies that the biofilm likely underwent a chemisorption mechanism and therefore the biofilm offers a marginal inhibiting effect on corrosion by reducing the contact of the test coupons with the corrosive environment. This is in agreement with the PDP and EIS results in distilled water experiments. On the other hand, the positive enthalpy of activation reflects the endothermic nature of metal dissolution processes on both test coupons with and without biofilm. The negative values of activation entropy reflect the increase in disordering that is achieved by the formation of an activated complex. These results are in agreement with the literature (Go et al., 2020; Khadom et al., 2009; Zarrouk et al., 2011). Moreover, the *apparent activation corrosion energy*, *enthalpy of activation,* and *entropy of activation* for test coupons with and without biofilm in brine shown in Table 3.7 are only slightly different implying that the biofilm does not influence these activation parameters. Further, the E_{act} and ΔH_{act} values vary in the same way in the presence and absence of simulated biofilm. The difference between the two parameters is close to 2.65 which implies that the effect of the presence or absence of simulated biofilm is equal on E_{act} and ΔH_{act}.

3.5.1.3 Statistical T-test

The p-values obtained from the paired t-test (Table 3.8) show no significant difference between the I_{corr} for test coupons with and without biofilm in either distilled water or brine experiments. This further supports the PDP and EIS results. On the other hand, the p-value for I_{corr} between test coupons without biofilm in distilled and brine shows a significant difference. The same is observed between test coupons with biofilm in distilled water and brine. This is also in agreement with PDP and EIS results as the Cl^- is known to be responsible for inducing higher corrosion on test coupons in brine. The independent t-test results (Table 3.9) show that the p-values between the two groups (biofilm and no biofilm at 60 min and 120 min in distilled water and brine) on the continuous variable, I_{corr} are not significantly different. This further supports that biofilm does not influence corrosion.

3.5.2 pH results

The pH ranges from 3.0 - 5.5 in a $Na_2S.xH_2O$ (H_2S)/CO_2 environment in as well distilled water as brine (Table 3.10). This pH range is within the optimum environmental pH for the growth of Acidophilic SRB (Kushkevych et al., 2021; Tran et al., 2021). From the literature, the produced H_2S is more soluble than CO_2 at this pH range implying that reaction 3.3 is dominant over reaction 12a (Ma et al., 2000). The main source of HS^- in reaction 3.3 is the dissociation of the sodium sulfide species described by chemical equation 3.4.

The trend of corrosion rates of carbon steel in distilled water and brine solution with and without biofilm is confirmed by similar trends in the pH values. The final pH decreases in distilled water when the temperature increases; higher temperature promotes the media to ionize more H^+ that leads to lowering of the solution pH (Zhang et al., 2015). Fig. 3.4a-d illustrates how a higher temperature, i.e., more hydrogen in solution, accelerates the corrosion rates from about 0.1 mm/year at 30 ^{o}C to about 0.25 mm/year at 60 ^{o}C in distilled water.

Corrosion of test coupons in brine solution causes a larger decrease in pH at 45 ^{o}C compared to 60 ^{o}C. The decrease in pH at 45 ^{o}C is likely due to the dissolved chloride ions in the solution enhancing the effect of hydrogen ions. The pH in brine solution is lower than in distilled water, resulting in higher corrosion rates of carbon steel coupons. Increasing pH shifts the corrosion potential to a more negative value and hence the corrosion rate increases. The presence of the simulated biofilm does not show any significant influence on the surface chemistry of the carbon steels as is reflected by the absence of any significant impact on the pH of the solution.

3.5.3 Dissolution of metal ions

The metal ion concentration trends shown in Fig. 3.5 are similar to the trends shown by corrosion rates obtained from the electrochemical data (Fig. 3.4) and pH results (Table 3.10). Increasing temperature of the distilled water drives more metal ions in the solution: 25μg/(g.cm^2) at 30 °C to 90 μg/(g.cm^2) at 60 °C, independent of the presence of a biofilm. The driving of metal ions into the solution implies the dissolution of corrosion products. In distilled water experiments, there are no significant differences in the increase of metal ions into a solution for test coupons with and without biofilm.

In brine solution, the ICP-OES results show that the sum of dissolved ions reaches a maximum concentration at 45 ^{o}C (Fig. 3.5e-h): ~350 μg/(g.cm^2), independent from the presence of a biofilm. Further, the ICP-OES results at 60 □C show the sum of dissolved ions to be < 200 μg/(g.cm^2). This indicates evidence of the formation of a protective layer at 60 °C that consequently impedes the diffusion of ferrous ions into the solution. The literature discusses the formation of a $FeCO_3$ on the carbon steel surface that forms a protective layer reducing corrosion (Kvarekval et al., 2002). However, $FeCO_3$ layers only form at pH > 5.5, which is higher than the pH of the solutions under investigation (Table 3.10) (Hernandez et al., 2012). Possibly formation of FeS or iron oxide layers on the carbon steel surfaces is responsible for the decrease in the dissolution of Fe if the temperature of the brine solution increases.

The ICP-OES results, therefore, show that biofilm on carbon steel corrosion does not influence the concentration of metal cations released into the solution. This is contrary to the literature that points out that the biofilm could stimulate the dissolution of the underlying steel by chelation of Fe ions because of its acidic nature (Beech et al., 1998; Dong et al., 2011).

3.5.4 SEM-EDS

The major elements in corrosion products for test coupons in distilled water and brine solution are Fe, C, and O while the minor element is Cl (Table 3.11). The trace element on corrosion products for test coupons in distilled water is Mn while for test coupons in brine the trace elements are Na, S, Si, Al, and Mn. In all SEM-EDS results, Fe species occupy the highest mass percentage of all. Since Fe is part of the composition of the test coupons its detection in the highest percentage indicates the severe corrosivity of the test coupons. The highest mass percentage of all Fe species is observed on test coupon sample 19 exposed in brine solution at 45 ^{o}C. This observation marks the maximum corrosivity of the test coupon and it is supported by maximum corrosion rate (~1.6 mm/year) and minimum pH (4.71). Further, the ICP-OES at this condition also shows the maximum concentration of ions in the solution (~350 µg/g cm^2). These results suggest that at this condition there is a high rate of formation of deposits on the surface and at the same time a high rate of dissolution of the formed deposits. Furthermore, SEM-EDS results show that there are no significant differences in the mass percentage of ions detected (~ 4.1%) on test coupons with and without simulated biofilm as evidenced, for example, by samples number 21 and 23. The highest mass percentage of major elements detected, in particular Fe and O, strongly confirm the presence of these species in corrosion products as detected by XRD in section 3.5.5.

3.5.5 XRD

The XRD diffractogram for a blank coupon in Fig.3.6a shows only the presence of iron peaks (peak 1) at 45 and 65^o. The same peaks are present in all diffractograms (Fig.3.6b-g) for carbon steel in distilled water and brine experiments. Diffractograms in distilled water experiments (Fig.3.6b-e) do not show any different peaks for test coupons with and without biofilm possibly due to low corrosion rates of carbon steel in distilled water (< 0.3 mm/year) and hence little or no corrosion products can be detected. Corrosion rates of carbon steel in brine solutions are much higher (0.6-1.6 mm/year) due to chloride ions; hence, corrosion products have been formed on the coupon surface. Carbon steel corrosion products with and without simulated biofilm in NaCl solution have similar peaks with the same intensity: α-FeOOH (peak 2) and sulfur (peak 3) (Fig. 3.6f-g). This is in agreement with the results discussed before (sections 6.1 through 6.3) that simulated biofilm does not influence corrosion. Corrosion rates (Fig. 3.4) and ICP-OES results (Fig. 3.5) suggest the formation of a protective layer on carbon steel surfaces at 60 ^oC in NaCl solutions. Ferric oxyhydroxide (α-FeOOH) detected by XRD is likely the layer offering the protection. FeS which is the most expected corrosion product is not detected with XRD most likely due to either a low concentration of the FeS species, in essence, below the detection limit of the XRD. Considering the low concentration of sulfur in 3mL of 0.4 M $Na_2S.xH_2O$ = 0.0012 mol $Na_2S.xH_2O$ added to the electrochemical cell before the experiment, the concentration of a protective layer in the form of FeS is believed to be below the detection limit of the XRD. Another reason is also likely the low amount of H_2S formed in the reactor and which could not be stoichiometrically sufficient to form FeS or transform the ferric oxyhydroxide (α-FeOOH) to FeS (chemical equation 13).

$$3H_2S + 2FeOOH \longrightarrow 2FeS + S + 4H_2O \qquad (13)$$

The detection of iron oxyhydroxide with XRD confirms that it is iron oxyhydroxide that undergoes dissolution to release iron species as detected with ICP-OES. This dissolution is controlled by the chemical reaction between the goethite and H^+ (chemical equation 14).

$$2FeOOH + H_2S + 4H^+ \longrightarrow 2Fe^{2+} + S^o + 4H_2O \qquad (14)$$

3.6 Conclusion

In this paper, the role of biofilm in the Microbiologically Influenced Corrosion (MIC) of carbon steel (API 5L X70M HFW) by Sulfate Reducing Bacteria (SRB) is investigated. Simulated biofilm made of calcium alginate, abiotic sulfide (to mimic SRB metabolic end product H_2S), CO_2 (to mimic CO_2 from SRB dissimilatory sulfate reduction), and simulated brine (3.0 wt% NaCl) are used to simulate the SRB environment.

The electrochemical results (PDP and EIS) show that the presence of simulated biofilm in reference experiments (distilled water) at only 60 min exposure demonstrates a small inhibiting effect while at 120 min exposure time and in brine solution experiments neither inhibition nor acceleration of corrosion is observed. These results in distilled water (120 min exposure time) and brine solution experiments in the presence of simulated SRB products (H_2S and CO_2)

disagree with the literature that reports that a biofilm is associated with either inhibition or acceleration of aggressive and localized forms of corrosion (Bao et al., 2012; Li et al., 2013; Procópio, 2019; Starkey, 1985). The PDP and EIS results show that the impact of temperature on the corrosion is more important than the effect of biofilm in distilled water (120-exposure time) and brine experiments. The impact of Cl$^-$ on corrosion is clear in brine experiments. The kinetic corrosion activation parameters show that the effect on the presence or absence of simulated biofilm does not influence E_{act} and ΔH_{act}. The paired T-tests on I_{corr} between test coupons with and without biofilm show that p-values are greater than 0.05 supporting that there is no significant difference between test coupons with and without biofilm. On the other hand, the p-value for I_{corr} between test coupons without biofilm in distilled and brine shows a significant difference. A similar case is observed between test coupons with biofilm in distilled water and brine. These results strongly support the effect of Cl- on corrosion. Independent t-test on the group with and without biofilm over the continuous variable, I_{corr} shows that the p-value is greater than the expected statistical value of 0.05, implying no significant difference between the two groups over I_{corr}. The ICP-OES results show that there are no differences in metal ions driven into solution in the presence or absence of simulated biofilm in both distilled water and brine solution. Moreover, the ICP –OES results show a maximum concentration of metal ions at $45^{\square}$C in a brine solution likely due to a strong enhancement of H$^+$ by Cl$^-$ which in turn results in driving more metal ions into the solution. The opposite is true at 60 °C when the kinetics allow the formation of α-FeOOH as a protective layer on carbon steel in brine. The pH results also show that there is no significant change in the final pH between the solution with and without simulated biofilm, supporting that biofilm on carbon steel does not influence corrosion in the presence of $NaS_2.xH_2O$ (H_2S) and CO_2 in the acidophilic SRB environment shown in this study.

Surface analyses results with SEM-EDS show that there are no significant differences in mass percentages of ions detected (~ 4.1%) on test coupons with and without simulated biofilm. In addition, the highest mass percentage of major elements detected are Fe and O which strongly confirm the presence of α-FeOOH detected by XRD. On the other hand, the XRD that is sensitive to crystalline phases shows that there are no differences in the phases formed in the presence or absence of simulated biofilm. This observation further supports the results mentioned before showing that the biofilm has likely no influence on corrosion. The corrosion products detected with XRD are only α-FeOOH and sulfur. Concentrations below the detection limit or a low amount of H_2S are likely the reason for not detecting the FeS by the XRD.

4 The role of organic acid metabolites in geo-energy pipeline corrosion in a sulfate reducing bacteria environment[7]

4.1 Introduction

Water in geological reservoirs and installations for oil, gas, and non-volcanic geothermal energy normally contains NaCl and minor other elements such as Ca^{2+}, Mg^{2+}, SO_4^{2-}, I^-, Br^-, CO_3^{2}, and HCO_3^- (Dresel and Rose, 2010; Magot et al., 2000; Magot et al., 1997; Muramatsu et al., 2000; Nogara and Zarrouk, 2018a). This mix is commonly denoted "brine". According to Magot et al (1997), the presence of SO_4^{2-} and CO_3^{2-} in water is evidence for the existence of microbes with metabolic processes, e.g. sulfate reduction and acetogenesis. Water is a suitable medium to support the growth of microbes and dissolve metabolic byproducts. The dissolved metabolic byproducts in water result in the formation of a corrosive solution that in conjoint interactions with chloride ions limit the application of metallic materials in the oil, gas, and geothermal industry (Ibrahim et al., 2018; Kiani Khouzani et al., 2019; Provoost et al., 2018).

Corrosion of metallic materials is a serious multibillion-dollar problem in the geo-energy industry (oil, gas, and geothermal) as corrosion reduces mechanical properties leading to loss of materials, and ultimately failure (Abadeh and Javidi, 2019; Ahmad, 2006; Cramer and Covino, 2003; Li and Ning, 2019; Popoola et al., 2013; Reinecker et al., 2019; Wang et al., 2019).

---

[7] This chapter is based on: Madirisha, M., Hack, R., & Van der Meer, F. (2022). The role of organic acid metabolites in geo-energy pipeline corrosion in a sulfate reducing bacteria environment. Heliyon, 8, e09420 .

Metallic materials used in the geo-energy industry are susceptible to different forms of corrosion, such as general and localized corrosion, and pitting (Dariva and Galio, 2014; Streicher, 2011). Localized corrosion mainly caused by biotic factors, also known as Microbial Influenced Corrosion (MIC) is a major cause for pipeline leakage (Alabbas and Mishra, 2013; Clarke and Aguilera, 2001; Li et al., 2018). MIC is a problematic type of corrosion because MIC is difficult to identify compared to abiotic corrosion. After all, it does not have a specific form (Little et al., 2020; Riskin and Khentov, 2019). Further, the type and capability of microbial metabolites that are causing corrosion are uncertain too (Little et al., 2006). The most dominant and troublesome species of MIC are Sulfate Reducing Bacteria (SRB) that exist in complex microbial communities (Audiffrin et al., 2003; Hussain et al., 2016; Wolf et al., 2016).

4.2 Microbial Influenced corrosion due to sulfate reducing bacteria

Sulfate reducing bacteria (SRB) are ubiquitous anaerobes which are the most studied corrosive microbes in the geo-energy industry because sulfate ions are frequently present (Jia et al., 2017). SRB require an electron donor and acceptor to provide energy for their metabolism. Low-molecular-weight organic compounds are used as electron donors where they provide energy and carbon for growth. SRB usually use sulfate as the terminal electron acceptor, reducing it to HS^{-}. According to Gu et al (2019), SRB consume also elemental iron as an electron donor when there is a lack of low-molecular-weight organic compounds (carbon source). In SRB corrosion, bacterial biofilms shuttle electrons from extracellular iron oxidation across the cell wall to reach the cytoplasm where sulfate reduction takes place under biocatalysis (Gu et al., 2019b; Li et al., 2018). Cross-cell wall electron transfer is known as extracellular electron transfer (EET) (Jia et al., 2018; Li et al., 2015a). Thus, this first type of microbial influenced corrosion (MIC) is referred to as EET-MIC. The transfer of electrons during EET-MIC can either be direct or mediated with electron shuttles. In the latter case, some SRB are reported to posses outer-membrane cytochromes (OMCs) that exchange electrons directly with the electron shuttles (Li et al., 2019; Wang et al., 2020). The second type of MIC is attributed to secreted corrosive metabolites such as H_2S, CO_2, and organic acids. This type of MIC is called metabolite MIC (M-MIC) and which makes the central focus of this paper.

4.3 Influence of organic acid metabolites on corrosion

The distribution of microbes in a microbial community is not homogeneous (Almela et al., 2021b; Davis and Isberg, 2016). Different interacting species of microbes are known to be present producing different metabolites which in turn result in metabolic heterogeneity within bacterial communities (Kim et al., 2015; Wong et al., 2021). Different microbial species can share a living space, for example, SRB with methanogens, SRB with acetogenic, and SRB with fermentative bacteria (acid-producing bacteria). SRB and methanogens compete for acetate and H_2 while SRB and acetogenic compete for propionate, butyrate, and ethanol. SRB depend on fermentative bacteria (Fig.4.1) which cleave and ferment the complex organic matter to low-molecular-weight organic compounds. SRB do not metabolize complex organic compounds, such as those included as substrates in the test medium, instead metabolizes short-chain organic acids (low-molecular-weight organic acids). In this context, an oxidant such as sulfate serves as the terminal electron acceptor to adsorb the electrons released from organic carbon oxidation. Fermentative bacteria produce a variety of low molecular weight organic compounds, and these include organic acids (acetic, L-ascorbic, gluconic, glucuronic, formic, peroxides and oxalic, oxalacetic, butyric, succinic, propionic, fumaric, citric, malic, and glyoxylic acid, kojic, phenylacetic, indolylacetic, dihydroxydibenzenecarboxylic, glutaconic and 4-hydroxymandelic acids), ketones, and alcohols (ethanol, propanol, and butanol) (Bao et al., 2012; Kushkevych et al., 2021; Lugauskas et al., 2009; Naranjo et al., 2015; Sand and Gehrke, 2003; Tran et al., 2021).

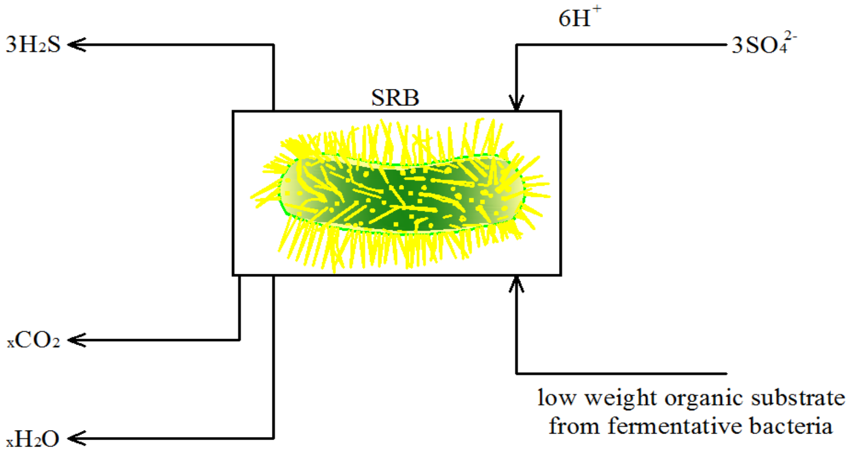

Fig. 4.1:Dependency of SRB on fermentative bacteria for nutrition

In the absence or low concentration of an external electron acceptor, fermentative microbes such as acid producing bacteria and SRB strains oxidize an organic carbon (e.g aromatic and aliphatic hydrocarbons in oil and gas) and produce energy through substrate-level phosphorylation (Xu et al., 2016). Organic acids are the main products also in this type of anaerobic fermentation. The combinations of different metabolites in a microbial community are likely to have a particular kinetic effect on corrosion that is specific to the combination of metabolites (Videla and Herrera, 2009). For example, organic acids are reported to react with materials of natural and/or synthetic origin causing swelling, total or partial dissolution, and, finally, deterioration (Caneva et al., 2008). Organic acids undergo reactions with materials by either the action of protons or chelation with metal ions and therefore promote corrosion by destroying the oxide layer formed on the material surface (Caneva et al., 2008). Despite the direct role of organic acids on materials being commonly known, their role in combination with SRB environment is still unclear. The presence of organic acid metabolites in a SRB environment e.g organic acid from fermentative bacteria might result in an aqueous medium with unique corrosion kinetics (Bao et al., 2012; Bonis and Crolet, 1989; Crolet and Bonis, 1983). A study on organic acid metabolites in combination with a SRB environment is important to establish the possible interactions of SRB with other chemical species and with the metals in installations for oil, gas and non-volcanic geothermal energy.

The present study aims to investigate the role of organic acid metabolites, namely acetic and L-ascorbic acid (0.2 and 1.0 mM) on corrosion of geo-energy pipelines made from carbon steel, in a simulated SRB environment. The carbon steel corrosion study is simulated in an electrochemical cell with different temperatures (30, 45, and 60 ^{o}C) and exposure times (60 and 120 min). Electrochemical techniques are used to monitor the corrosion parameters and the results obtained are supported further by kinetic corrosion of activation, multiple linear regression of corrosion current densities, Inductively Coupled Plasma - Optical Emission Spectrometry (ICP-OES), pH, and X-Ray Diffraction (XRD).

4.4 Materials and methods

4.4.1 Preparation of test coupons

The carbon steel working electrodes in the electrochemical cell (further referred to as "test coupons") are prepared from carbon steel used for gas pipelines (API 5L X70M HFW), which is made available

by the Tanzania Petroleum Development Corporation. The chemical composition is shown in Table 4.1. The test coupons are the circular disk of 1.5 mm thick and 7 mm radius. Each one is wet polished with a sequence of silicon carbide papers of decreasing particle size, i.e., 100, 200, 400, 600, 800, and 1000 grit. Thereafter, the test coupons are rinsed with distilled water and degreased in ethanol by sonication for about 15 minutes and afterward rinsed with acetone and dried. Thereafter, the coupons are air-dried and the weight of each coupon is recorded.

Table 4.1: Chemical composition of carbon steel API 5L X70M HFW (wt %)

Fe	C	Si	Mn	P	S	V	Nb	Ti
97.39	0.17	0.45	1.75	0.02	0.01	0.10	0.05	0.06

4.4.2 Preparation of biofilm and organic acid metabolites

A simulated biofilm is prepared since it is often present in microbes bound on surfaces that grow into structured communities (Alabbas and Mishra, 2013; Blackwood, 2018; Parthipan et al., 2017; Zuo, 2007). Calcium alginate is used to simulate biofilm because it is comparable to the structure and properties of biofilm in real situations as shown by various authors (Chang et al., 2010; Nassif et al., 2020). In addition, calcium alginate in a combination with SRB metabolites is reported to result in corrosion rates (0.25 to 1.6 mm/year) which are comparable to published corrosion rates obtained in SRB experiments (0.20

to 1.2 mm/year). This implies that the simulated H_2S, CO_2, and biofilm are representative of the SRB media for corrosion studies (Madirisha et al., 2022c).

In preparation of calcium alginate, the surfaces of the dried, polished, and cleaned test coupons are prepared with 0.1 mL of 3.0 wt% sodium alginate (Fig. 4.2). The sodium alginate solution is homogenously spread over the entire surface using a thin strand of nylon. To immobilize the sodium alginate and convert it to Ca-alginate (the simulated biofilm), 0.1 mL of 0.004 M aqueous $CaCl_2$ is applied. The sodium alginate/$CaCl_2$ on the test coupons are left to rest for 15 min. Thereafter, the coupons are washed with 10 mL of distilled water to remove unreacted Na-alginate, which is soluble in water, and then the coupons are air-dried as the final treatment for preparing the coupons. Furthermore, organic acids: acetic acid and L-ascorbic (Fig.4.2) are prepared at the concentration of 0.2 and 1.0 mM. The pH of 2.6 at the concentration of 0.2 and 1.0 mM acetic or L-ascorbic acid is prepared. The type and concentration of acids are chosen to represent organic acids produced by non-SRB.

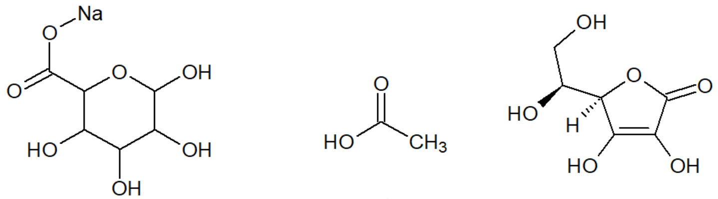

Sodium alginate

Acetic

L-ascorbic

Fig. 4.2:Structure of sodium alginate and organic acids (acetic and L-ascorbic) used to simulate the biofilm and organic acid metabolites, respectively

4.4.3 Electrochemical cell

The electrochemical experiments are performed in a three-electrode electrochemical cell coupled with a Potentiostat/Galvanostat: PGSTAT204/AUT50663 from Metrohm (Autolab B.V., Amsterdam, The Netherlands). The software used is NOVA version 1.11.2 (ibid.). Furthermore, the cell is coupled with a thermostat-water bath, pH meter, and CO_2 gas cylinder (Fig.4.3). The pH meter allows continuous monitoring of the solution in the electrochemical cell during the test. The test coupons with biofilm are used as working electrodes, platinum as the auxiliary electrode, and saturated silver-silver chloride (Ag/AgCl) in 3.0 M KCl solution as reference electrodes. The brine in oil, gas, and non-volcanic geothermal energy installation is simulated with a 3.0 wt% NaCl solution. The solution of simulated brine and organic acid metabolite in the electrochemical cell is purged with CO_2 (flow rate ~150 mL/min) for 30 min before and during the experiment to create an O_2 deprived medium and at the same time serve as a product from SRB dissimilatory sulfate reduction. The test matrix (Table 4.2) is made such that the volume of the solution in the electrochemical cell is 500 mL total, including 3.0 wt% NaCl solution (to simulate the brine), organic acid metabolites, and 0.4 M $Na_2S.xH_2O$ (to mimic H_2S) in a volume ratio of 487: 10: 3, respectively. The corrosion tests are done at different temperatures of 30, 45, and 60 ^{o}C, with two different exposure times of 60 and 120 min. All tests are done in duplicate. Further, the pH of the solution is measured at the start of the test (initial pH) and also after 60 and 120 min (final pH). After the test, the test coupon is removed from the cell and placed in a desiccator.

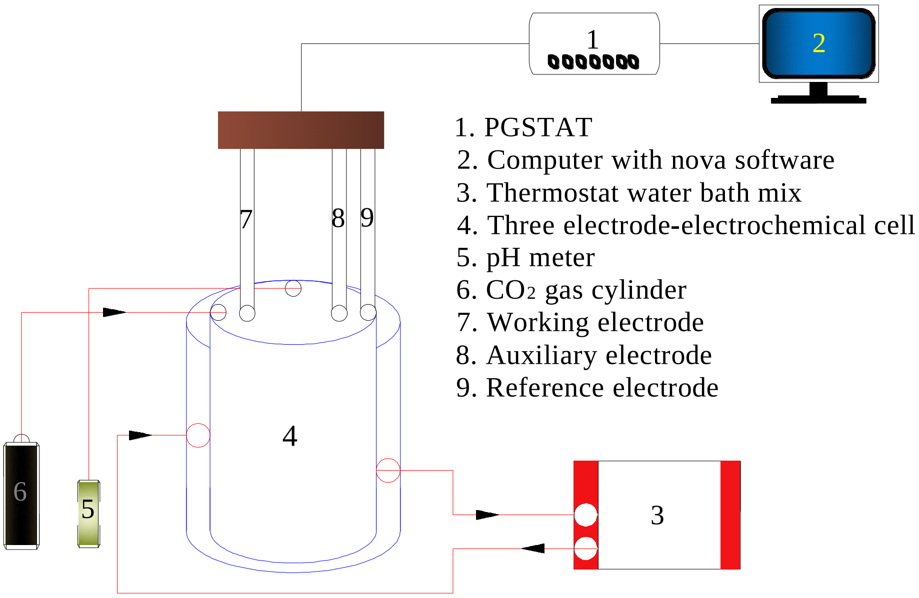

Fig.4.3: Schematic diagram of the set-up for carbon steel corrosion tests

Table 4.2: Experiments for the investigation of the role of organic acid metabolites on the corrosion of carbon steel

Acid	Experiment	Temperature (°C)	Concentration of acid (mM)	Time (min)
Acetic acid	1, 2, 3	30, 45, 60	0.2	60
	4, 5, 6	30, 45, 60	1.0	60
	7, 8, 9	30, 45, 60	0.2	120
	10, 11,12	30, 45, 60	1.0	120
L-Ascorbic acid	13, 14, 15	30, 45, 60	0.2	60
	16, 17, 18	30, 45, 60	1.0	60
	19, 20, 21	30, 45, 60	0.2	120
	22, 23, 24	30, 45, 60	1.0	120

4.4.4 Methods

4.4.4.1 Electrochemical corrosion measurements

The electrochemical corrosion measurements by Electrochemical Impedance Spectroscopy (EIS) and by PotentioDynamic Polarization (PDP) are done in the electrochemical cell after 60 and 120 min. The Electrochemical Impedance Spectroscopy (EIS) is carried out in a frequency range of 0.5 mHz to 10 kHz with a perturbation amplitude of 10 mV. The measurements are all performed at the open circuit potential and are taken after 60 min and 120 min exposure time. Furthermore, the electrochemical circle fitting -analysis on EIS data is done using the NOVA software to generate the polarization resistance (R_p), solution resistance (R_s), and constant phase elements (CPE): pseudo-capacitance/admittance (Y_o), and phase shift/index (n).

The PotentioDynamic Polarization (PDP) is measured by sweeping the potential at a rate of 10 mVmin^{-1} in the range of -200 to 200 mV vs Ag/AgCl reference electrode, i.e cathodically and anodically from open circuit potential. The Tafel slopes (b_a and b_c) are determined after a stable open circuit potential is achieved by extrapolating the linear Tafel regions to the corrosion potential (E_{corr}). All polarization measurements are performed after the electrochemical impedance measurements.

4.4.4.2 Gravimetric analysis

Gravimetric analysis is done by conversion of the obtained corrosion current density to the more comprehensive electrochemical weight loss. This follows Faraday's law (equation (4.1)) (Apostolopoulos et al., 2013; Munoz et al., 2007; Sanchez et al., 2017):

$$\Delta W(g) = \frac{P\int Idt}{F} \tag{4.1}$$

Where P is the equivalent weight of iron with a valence of 2; I is corrosion current density; t = time; the integral $\int Idt$ corresponds to the area under the curve obtained in the electrochemical measurements (I_{corr} - time curve); and F is the Faraday constant of about 9.65 x 10^4 C mol^{-1}.

Kinetic parameters of activation corrosion

Corrosion kinetic parameters; *apparent activation corrosion energy* (E_{act}), *enthalpy of activation* (ΔH_{act}), and *entropy of activation* (ΔS_{act}) are calculated using Arrhenius equation (4.2) and transition state equation (4.3). The kinetic parameters of activation corrosion have a direct influence on the passivity developed on the material surface (Go et al., 2020; Khadom et al., 2009).

$$\log I_{\mathrm{corr}} = \log A - \frac{E_{\mathrm{act}}}{2.303RT} \tag{4.2}$$

$$I_{\mathrm{corr}} = \frac{RT}{Nh} \mathrm{e}^{\frac{\Delta S_{act}}{R}} \mathrm{e}^{-\frac{\Delta H_{act}}{RT}} \tag{4.3}$$

A is the pre-exponential factor, R is the universal gas constant of 8.314 J/(mol·K), T is the testing temperature (K), N is Avogadro's number, h is Plank's constant.

4.4.4.3 Characterization of the dissolved metal ions in solution

After electrochemical measurements, the collected solutions are investigated with Inductive Coupled Plasma- Optical Emission Spectrometry (ICP-OES) (Perkin Elmer 8300DV) to quantify Fe, Si, and Mn ions dissolved in the solution as an indication of carbon steel corrosion. Prior to the ICP-OES analysis, working standard solutions are prepared by stepwise dilution of a multi-element (1000 mg/L) ICP standard solution (Merck). The prepared working standard solutions are filled into ICP-OES tubes and inserted into the autosampler of the ICP-OES equipment. Calibration of blanks (DW and brine) is done followed by calibration of standards ranging from low to high concentration. Thereafter, the blank samples in ICP-OES tubes are inserted into the autosampler followed by the samples collected after electrochemical measurements ready for ICP-OES analysis. Correction of the ICP-OES results for samples is done by subtracting ICP-OES results of blanks of distilled water and brine. The quantity of metal ions released in solution (in μg/ (g.cm^2)) corresponds to the concentration of dissolved metal ions in the solution (mg/L) normalized to the weight of the working electrode (g), its exposed geometrical surface area (cm^2), and the total solution volume (L).

4.4.4.4 Inferential statistics

Inferential statistics is the branch of statistics allowing to make predictions ("inferences") from the data collected. Regression analysis is chosen to ascertain the extent of the relationship between the outcome variable (dependent variable) and predictor variables (independent variables). The regression analysis is performed by using the IBM SPSS statistics 27 software. Multiple linear regression is performed on corrosion current density (I_{corr}) as a function of temperature, exposure time, the concentration of acids, and pH of the solution.

4.4.4.5 Characterization of corrosion products

X-Ray Diffraction (XRD) (Bruker D2 phaser) is used for qualitative characterization of corrosion products on the test coupons. The equipment operates in Bragg-Brentano geometry with CuKα radiation and a LYNXEYE detector as well as Bruker's corundum standard reference material. The patterns are collected with a Cu X-ray tube (1.54184 Å, 10 mA, 30kV) from 6° to 80° in the 2θ range with the step size of 0.012° and integration time of 0.1s. In addition, a detector slit of 8 mm is inserted while a standard divergence slit of 0.6 mm is used to control the illuminated area. Identification of the obtained diffractograms is performed with the DIFFRA.EVA software. XRD has a detection limit that depends on the density, valence electrons, and crystal structure of the compounds in the sample. However, the rule of thumb is that XRD has a detection limit of ~1% by volume (Schwantes et al., 2017; Treiman et al., 2010). In this study, the duration of the measurement of each sample is 24 hours. A non-treated carbon steel coupon is used as a reference.

4.5 Results

4.5.1 Electrochemical results

The electrochemical results of the PDP and EIS measurements determining the influence of acetic acid (0.2 and 1.0 M) and L-ascorbic acid (0.2 and 1.0 M) are shown in Tables 4.3, 4.4, 4.5, and 4.6.

Table 4.3: Electrochemical parameters (PDP) for test coupons in brine solution as a function of time (60-120 min), acetic acid (0.2 and 1.0 mM), and temperature (30-45-60 °C)

t (min)	[Acetic] (mM)	T (°C)	E_{corr} (mV, Ag/AgCl)	I_{corr} (mAcm^{-2})	b_a (mVdec^{-1})	b_c (mVdec^{-1})	R_p (Ω)
60	0.2	30	-668 ± 2	0.07 ± 0.00	241 ± 14	61 ± 3	286 ± 3
		45	-670 ± 1	0.08 ± 0.00	220 ± 11	60 ± 1	275 ± 1
		60	-672 ± 4	0.09 ± 0.00	192 ± 2	55 ± 1	273 ± 1
	1.0	30	-682 ± 1	0.12 ± 0.01	253 ± 17	66 ± 5	198 ± 4
		45	-684 ± 2	0.13 ± 0.01	235 ± 15	62 ± 2	192 ± 1
		60	-686 ± 1	0.14 ± 0.01	204 ± 2	56 ± 3	125 ± 1
120	0.2	30	-643 ± 1	0.06 ± 0.02	179 ± 8	62 ± 2	280 ± 3
		45	-666 ± 3	0.07 ± 0.01	166 ± 4	60 ± 1	275 ± 1
		60	-670 ± 3	0.08 ± 0.02	146 ± 10	63 ± 4	247 ± 5
	1.0	30	-680 ± 2	0.11 ± 0.00	248 ± 11	75 ± 10	213 ± 1
		45	-686 ± 1	0.13 ± 0.00	216 ± 1	72 ± 0	161 ± 1
		60	-692 ± 2	0.14 ± 0.00	196 ± 5	64 ± 2	113 ± 1

Table 4.4: Electrochemical parameters (PDP) for test coupons in brine solution as a function of time (60-120 min), L-ascorbic acid (0.2 and 1.0 mM), and temperature (30-45-60 °C)

t (min)	[L-ascorbic] (mM)	T (°C)	E_{corr} (mV, Ag/AgCl)	I_{corr} (mAcm^{-2})	b_a (mVdec^{-1})	b_c (mVdec^{-1})	R_p (Ω)
60	0.2	30	-681 ± 2	0.89 ± 0.00	136 ± 11	59 ± 3	528 ± 21
		45	-705 ± 1	1.17 ± 0.01	179 ± 4	59 ± 5	402 ± 27
		60	-708 ± 1	1.68 ± 0.00	341 ± 14	58 ± 8	380 ± 1
	1.0	30	-711 ± 1	1.88 ± 0.01	390 ± 42	87 ± 7	194 ± 1
		45	-713 ± 3	2.12 ± 0.00	431 ± 27	89 ± 4	182 ± 7
		60	-717 ± 2	2.77 ± 0.01	538 ± 82	96 ± 6	79 ± 1
120	0.2	30	-685 ± 1	0.97 ± 0.00	179 ± 4	54 ± 1	417 ± 4
		45	-707 ± 2	1.49 ± 0.00	229 ± 3	66 ± 6	364 ± 1
		60	-710 ± 1	1.84 ± 0.00	239 ± 4	67 ± 1	312 ± 1
	1.0	30	-715 ± 2	2.22 ± 0.00	399 ± 70	85 ± 15	163 ± 2
		45	-721 ± 1	2.94 ± 0.00	413 ± 81	88 ± 15	118 ± 1
		60	-748 ± 2	3.32 ± 0.00	576 ± 94	130 ± 17	72 ± 1

Table 4.5: Polarization resistance, solution resistance and CPEs (Y_o and n) (EIS) for test coupons in brine solution experiments as a function of time (60-120 min), acetic acid (0.2 and 1.0 mM) and temperature (30-45-60 °C)

t (min)	[Acetic] (mM)	T (°C)	R_p (Ω)	R_s (Ω)	CPEs	
					Y_o (x 10^{-2} µF)	n
60	0.2	30	22.60 ± 0.11	2.24 ± 0.05	1.799	1.000
		45	15.55 ± 0.01	0.98 ± 0.00	2.201	1.000
		60	14.24 ± 0.12	0.77 ± 0.06	2.493	1.000
	1.0	30	17.03 ± 0.21	0.82 ± 0.14	2.362	1.000
		45	15.40 ± 0.06	0.58 ± 0.08	2.395	1.000
		60	12.62 ± 0.42	0.21 ± 0.06	2.522	1.000
120	0.2	30	15.74 ± 0.63	0.46 ± 0.15	2.557	1.000
		45	13.63 ± 0.51	0.32 ± 0.08	2.519	1.000
		60	13.18 ± 0.01	0.31 ± 0.06	2.616	1.000
	1.0	30	13.62 ± 0.54	0.40 ± 0.02	2.225	1.000
		45	12.22 ± 0.01	0.32 ± 0.00	2.243	1.000
		60	09.03 ± 0.13	0.29 ± 0.08	2.444	1.000

Table 4.6: Polarization resistances, solution resistances and CPEs (Y_o and n) (EIS) for test coupons in brine solution experiments as a function of time (60-120 min), L-ascorbic acid (0.2 and 1.0 mM) and temperature (30-45-60 °C)

t (min)	[L-ascorbic] (mM)	T (°C)	E_{corr} (mV, Ag/AgCl)	I_{corr} (mAcm^{-2})	b_a (mVdec^{-1})	b_c (mVdec^{-1})	R_p (Ω)
60	0.2	30	-681 ± 2	0.89 ± 0.00	136 ± 11	59 ± 3	528 ± 21
		45	-705 ± 1	1.17 ± 0.01	179 ± 4	59 ± 5	402 ± 27
		60	-708 ± 1	1.68 ± 0.00	341 ± 14	58 ± 8	380 ± 1
	1.0	30	-711 ± 1	1.88 ± 0.01	390 ± 42	87 ± 7	194 ± 1
		45	-713 ± 3	2.12 ± 0.00	431 ± 27	89 ± 4	182 ± 7
		60	-717 ± 2	2.77 ± 0.01	538 ± 82	96 ± 6	79 ± 1
120	0.2	30	-685 ± 1	0.97 ± 0.00	179 ± 4	54 ± 1	417 ± 4
		45	-707 ± 2	1.49 ± 0.00	229 ± 3	66 ± 6	364 ± 1
		60	-710 ± 1	1.84 ± 0.00	239 ± 4	67 ± 1	312 ± 1
	1.0	30	-715 ± 2	2.22 ± 0.00	399 ± 70	85 ± 15	163 ± 2
		45	-721 ± 1	2.94 ± 0.00	413 ± 81	88 ± 15	118 ± 1
		60	-748 ± 2	3.32 ± 0.00	576 ± 94	130 ± 17	72 ± 1

4.5.1.1 Gravimetric results

The gravimetric results based on electrochemical weight loss of test coupons in acetic and L-ascorbic acids are presented in Fig. 4.4 and 4.5 respectively.

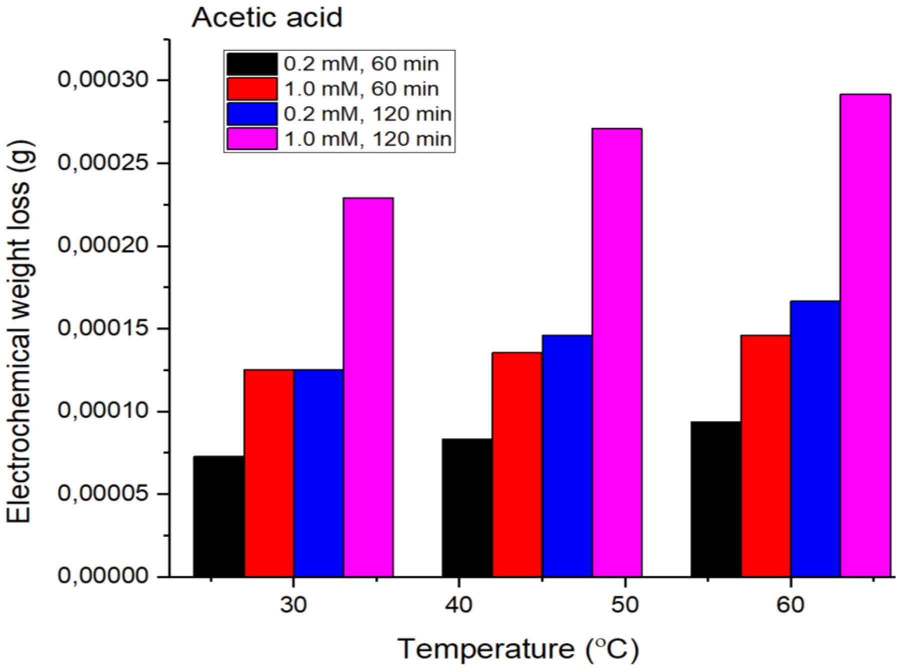

Fig. 4.4:Electrochemical weight loss of test coupons in 0.2 and 1.0 mM acetic acid, exposure time of 60 and 120 min, and temperature of 30, 45, and 60 °C

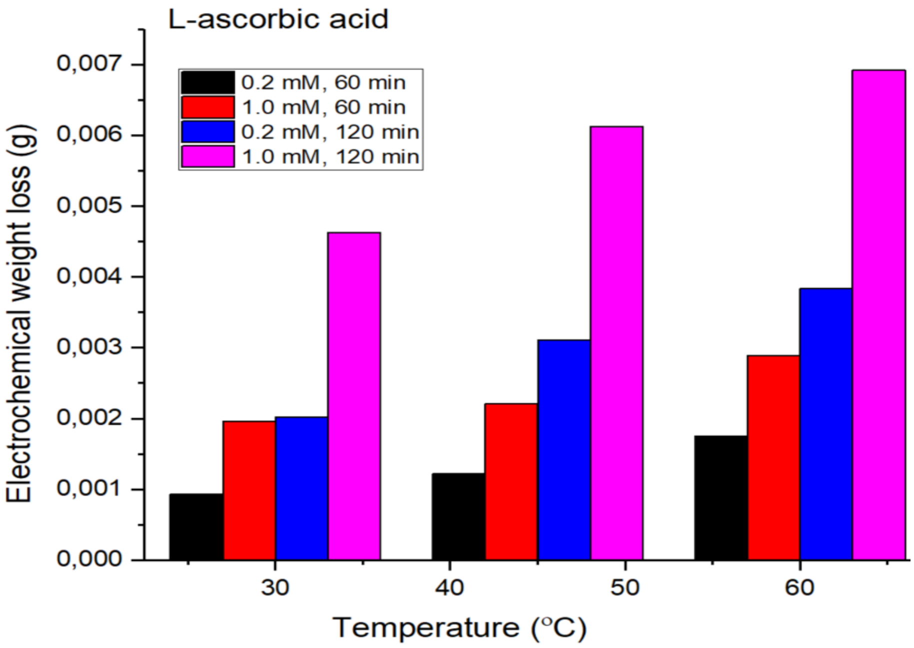

Fig. 4.5:Electrochemical weight loss of test coupons in 0.2 and 1.0 mM L-ascorbic acid, exposure time of 60 and 120 min, and temperature of 30, 45, and 60 °C

4.5.1.2 Kinetic parameters of activation corrosion

The apparent activation corrosion energy (E_{act}) is estimated from the linear regression plot shown in Fig.4.6 of Arrhenius equation (equation 4.2). Further, the enthalpy of activation (ΔH_{act}) and entropy of activation (ΔS_{act}) are also estimated from the linear regression plot shown in Fig. 4.7 of transition state equation (equation 4.3). The numerical results are shown in Table 4.7.

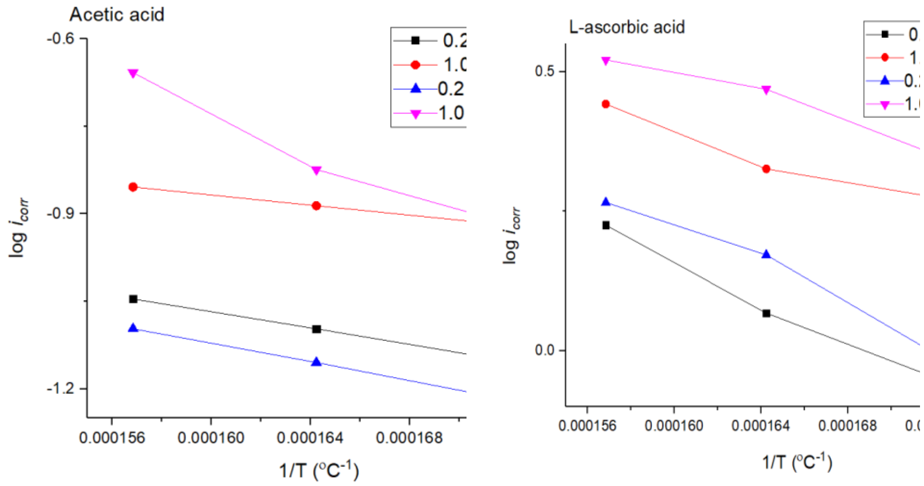

Fig. 4.6: Plot of 1/T vs log i_{corr} as a function of concentration (0.2 and 1.0 mM) of acetic and L-Ascorbic acids and exposure time (60 and 120 min), (a) Acetic (b) L-ascorbic

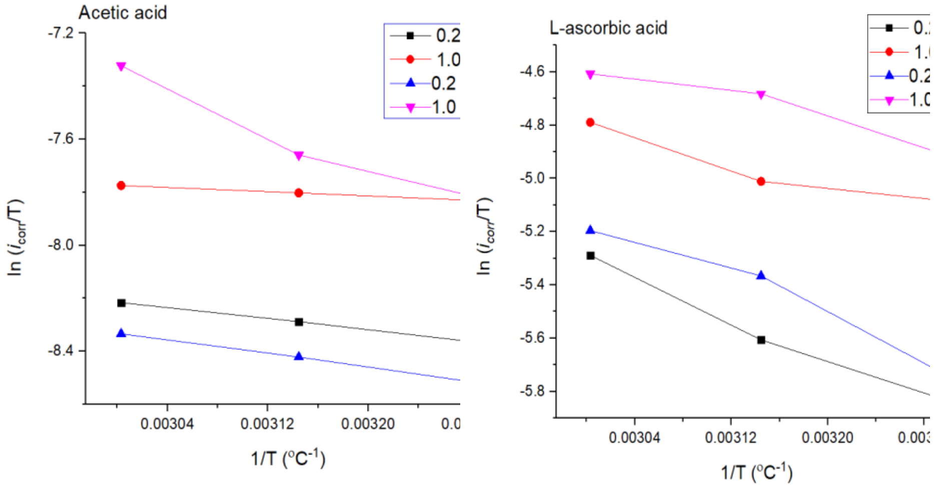

Fig. 4.7: Plot of 1/T vs In (i_{corr}/T) as a function of concentration (0.2 and 1.0 mM) of acetic and L-Ascorbic acids and exposure time (60 and 120 min), (a) Acetic (b) L-ascorbic

Table 4.7: The apparent activation corrosion energy (E_{act}), enthalpy of activation (ΔH_{act}) and entropy of activation (ΔS_{act}) as the function of temperature (30, 45, 60 °C) and corrosion current density (I_{corr})

Acid	Conc. (mM)	Time (min)	E_{act} (kJ/mol)	ΔH_{act} (kJ)	ΔS_{act} (kJ/K)
Acetic	0.2	60	7.03	4.39	-0.26
	1.0		4.31	1.67	-0.27
	0.2	120	8.05	5.41	-0.26
	1.0		6.78	4.14	-0.27
L-Ascorbic	0.2	60	17.89	15.25	-0.21
	1.0		10.84	8.28	-0.22
	0.2	120	18.03	15.39	-0.21
	1.0		11.33	8.69	-0.22

4.5.2 pH results

The final pH after the experiments is plotted against temperature (Fig. 4.8). Discussion of the results is in section 5.

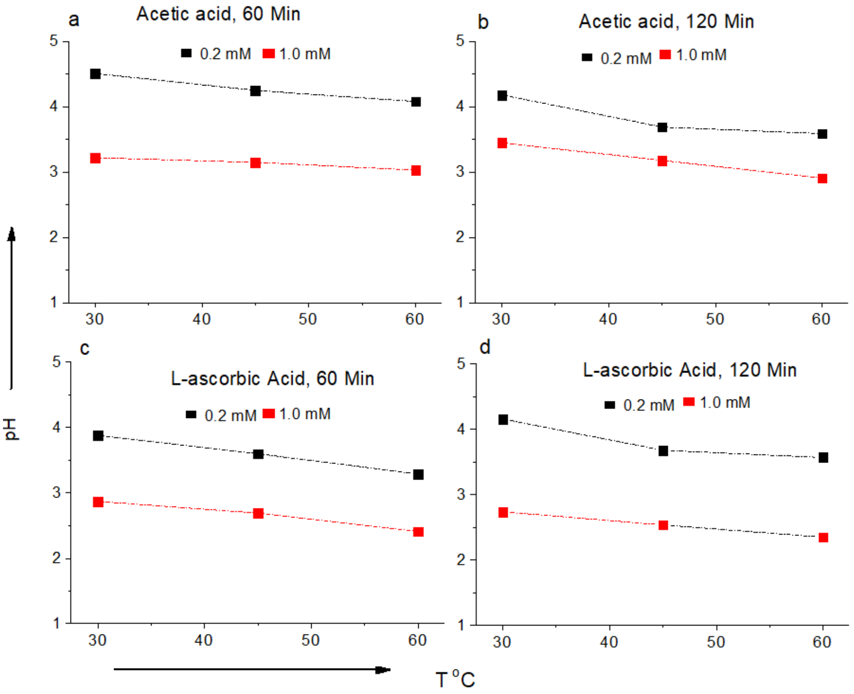

Fig.4.8: Final pH of the brine solution with acetic, and L-ascorbic (0.2 and 1.0 mM) acids as a function of time, biofilm, and temperature (30-45-60 °C) (the

lines between the markers have no meaning but are for identification of trends only)

4.5.3 ICP-OES results

The ICP-OES results on dissolved metal ions in solution are shown in Fig. 4.9 and further discussed in section 5.

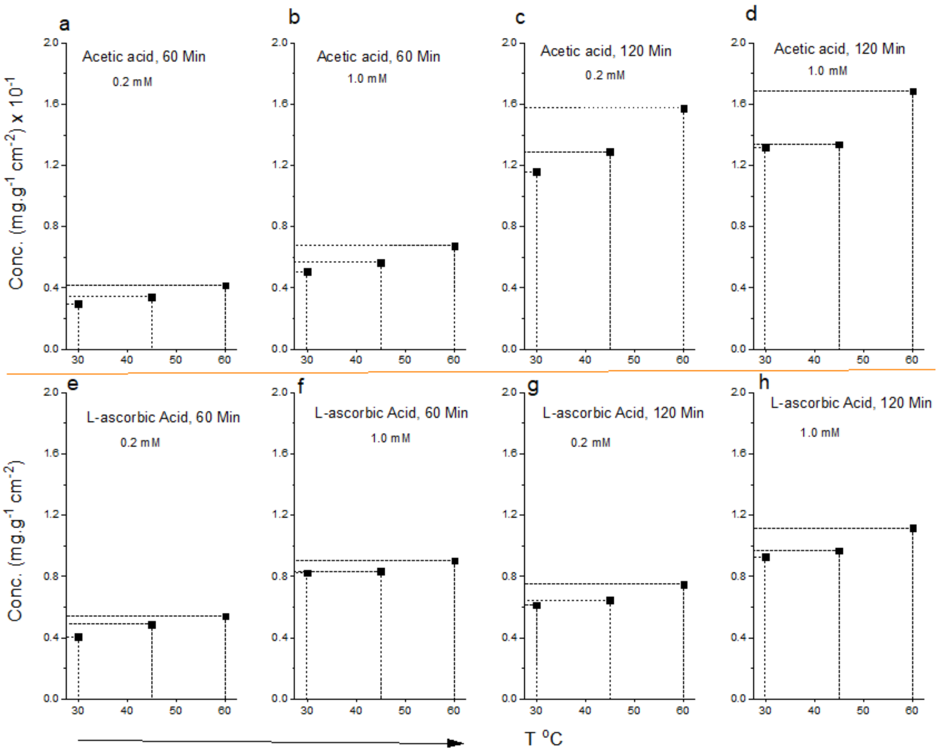

Fig. 4.9: Dissolved cations (Fe, Si, and Mn) in a brine solution with acetic and L-ascorbic (0.2 and 1.0 mM) acids experiments as a function of time (60 and 120 minutes) and temperature (30-45-60 °C) (the lines between the markers have no meaning but are for identification of trends only)

4.5.4 Multiple Linear Regression

The data shown in Table 4.8 is analyzed by multiple linear regression to predict the corrosion current density (I_{corr}) as a function of temperature, exposure time, the concentration of acids, and pH of the solution. The data in Table 4.8

do not show any quadratic, polynomial, exponential, or logarithmic relation due to near-collinearity among model terms. The R^2, p, and coefficient values are shown in Table 4.9.

Table 4.8: Corrosion current density, temperature, exposure time, the concentration of acids, and pH of the solution.

Acid	I_{corr}	T (°C)	Time (min)	Conc. (mM)	pH
Acetic	0.07	30	60	0.2	3.35
	0.08	45	60	0.2	3.01
	0.09	60	60	0.2	2.96
	0.12	30	60	1	2.68
	0.13	45	60	1	2.63
	0.14	60	60	1	2.48
	0.06	30	120	0.2	3.33
	0.07	45	120	0.2	2.99
	0.08	60	120	0.2	2.94
	0.11	30	120	1	2.71
	0.13	45	120	1	2.61
	0.14	60	120	1	2.54
L-ascorbic	0.89	30	60	0.2	2.84
	1.17	45	60	0.2	2.66
	1.68	60	60	0.2	2.41
	1.88	30	60	1	2.47
	2.12	45	60	1	2.27
	2.77	60	60	1	2.22
	0.97	30	120	0.2	2.93
	1.49	45	120	0.2	2.65
	1.84	60	120	0.2	2.46
	2.22	30	120	1	2.54
	2.94	45	120	1	2.31
	3.32	60	120	1	2,.24

Table 4.9: R^2, p and coefficient values of prediction of corrosion current density (I_{corr}) as a function of temperature, exposure time, the concentration of acids, and pH of the solution

Acid	R^2	p	Model equation
Acetic	0.992	0.000	I_{corr} (acetic) = 0.001T + 0.000t + 0.075C + 0.014pH - 0.014
L-ascorbic	0.970	0.000	I_{corr} (L-ascorbic) = 0.033T + 0.006t + 1.602C + 0.254pH - 1.711

Notes: R^2: coefficient of determination; p-value: the probability of obtaining; T: temperature; C: concentration; t: exposure time

4.5.5 XRD results

XRD diffractograms of test coupons corroded in presence of acetic and L-ascorbic acid are shown Fig.4.10 and 4.11, respectively. All coupons have been measured, however only diffractograms depicting major changes are shown.

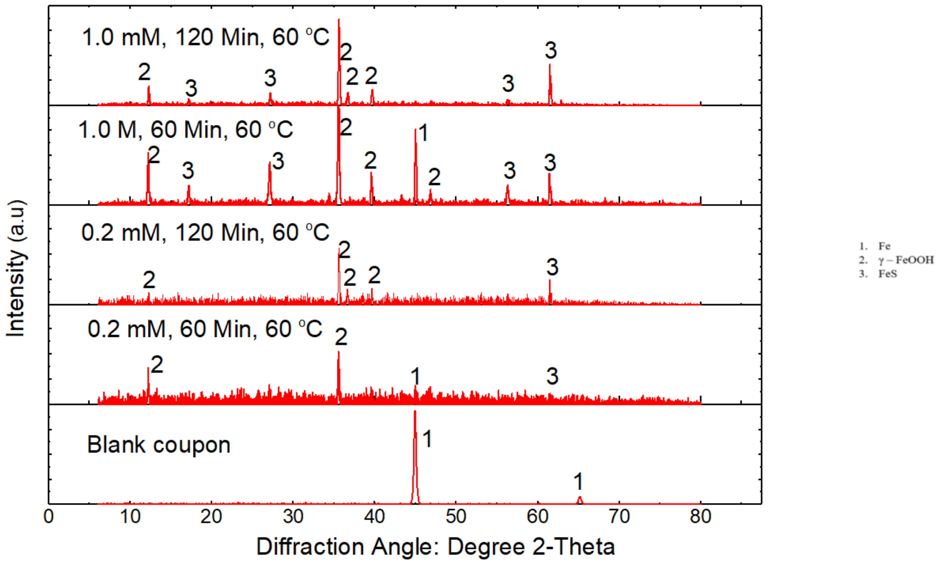

Fig. 4.10: XRD patterns for test coupons in brine solution with acetic acid (0.2 and 1.0 mM) as a function of time (60 and120 min) at 60 °C

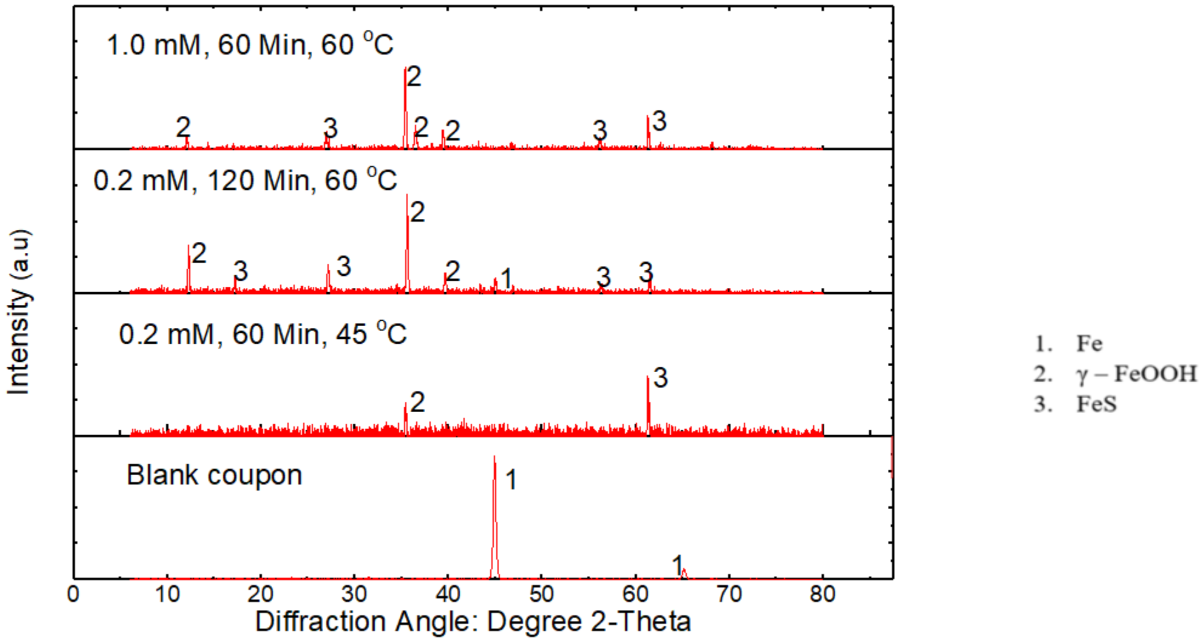

Fig. 4.11: XRD patterns for test coupons in brine solution with L-ascorbic acid (0.2 and 1.0 mM) as a function of time (60 and120 min) and temperature (45 and 60 ^{O}C)

4.6 Discussion

4.6.1 PotentioDynamic Polarization (PDP)

The PDP results presented in Table 4.3 for test coupons under influence of acetic acid (0.2 and 1.0 M) in a simulated SRB environment show that the corrosion potentials (E_{corr}) at exposure times of 60 and 120 min are less negative than the standard potential (E) of iron which is -680 mV (Standard Calomel Electrode (SCE)). A negative over potential implies that the reduction reaction (cathodic reaction) dominates the corrosion process. The possible cathodic chemical equations are equations 4.4, 4.5, and 4.6:

$$2H_2S + 2e^- \longrightarrow 2HS^- + H_2 \qquad 4.4$$

$$2HAc + 2e- \longrightarrow H_2 + 2Ac^- \qquad 4.5$$

$$2H_2CO_3 + 2e^- \longrightarrow H_2 + 2HCO_3^- \qquad 4.6$$

Furthermore, an increase in corrosion current densities and Tafel slopes is observed when temperature increases. The increase in corrosion current in the presence of acetic acid when temperature increases are likely due to a rapid increase in the amount of hydrogen species as a consequence of an increase in the extent of chemisorption of acetic acid on the metal surface as described by the chemical equations (4.7 and 4.8) (Amri et al., 2011; Singh and Gupta, 2000) or dissociation of H_2S according to equation (4.4).

$$HAc_{(ad)} \rightleftharpoons H^+ + Ac^- \rightleftharpoons H_{(ad)} + Ac^- \qquad 4.7$$

$$H_{(ad)} + H^+ \rightleftharpoons H_2 \qquad 4.8$$

On the other hand, an increase in corrosion current densities when the concentration of acetic acid increases can be explained by Le-Chatelier's Principle. To elaborate, an increase in the concentration of acetic acid in equation 4.7 favors the right-hand side reaction and hence rapidly favors the cathodic reaction. An increase in corrosion current upon an increase in acetic concentration and temperature is likely also linked to the absence of dimer and polymer formation associated with acetic acid. The absence of dimer and polymer formation is likely to increase the mobility of the ions (hydrogen ions and anionic conjugate base) (Singh and Mukherjee, 2010).

The corrosion current densities in the presence of acetic acid in this study are two times lower than without acetic acid under similar experimental conditions reported in Madirisha et al (2022c). In addition, a significant change in the Tafel slope is observed. Lower corrosion current densities evidenced in the presence of acetic acid in the SRB environment imply an inhibitory effect occurring on the working electrode while the significant change in Tafel slopes indicates the change in species involved in the reaction. The inhibitory effect demonstrated by acetic acid in a simulated SRB environment highlights the novelty of this work.

Replacing acetic acid with L-ascorbic acid results in corrosion potentials greater than the standard potential (*E*) of iron (Table 4.4) which is -680 mV (Standard Calomel Electrode (SCE)) which implies that the anodic reaction is dominant compared to the cathodic reaction. The possible anodic reaction involved is the dissolution of iron to ferrous ions given by equation 4.9 while the cathodic reactions are given by equations 4.4, 4.6, and 4.10.

$$\mathrm{Fe} \longrightarrow \mathrm{Fe}^{2+} + 2e^{-} \qquad 4.9$$

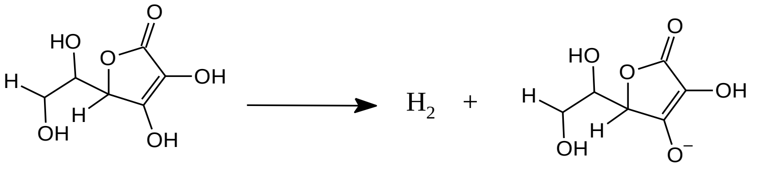

4.10

In the presence of L-ascorbic acid, the I_{corr}, E_{corr}, and Tafel slopes increase while R_p decreases when temperature increases. Comparing the corrosion current densities with those reported in the SRB environment without L-ascorbic acid under similar experimental conditions in Madirisha et al (2022c), the corrosion current densities are approximately two times higher implying higher corrosion rates. The increase in corrosion current densities caused by L-ascorbic acid under the SRB environment is likely associated with the formation of a chelating complex of high solubility that easily forms with Fe^{2+} (Fig. 4.12). The increase in corrosion current densities in the presence of either 0.2 or 1.0 mM L-ascorbic acid under a simulated SRB environment is not found in the literature. Corrosion experiments with L-ascorbic acid alone have shown the acid to serve as the corrosion inhibitor for corrosive ions (Chidiebere et al., 2015; Fuchs-Godec et al., 2013; Hong et al., 2016).

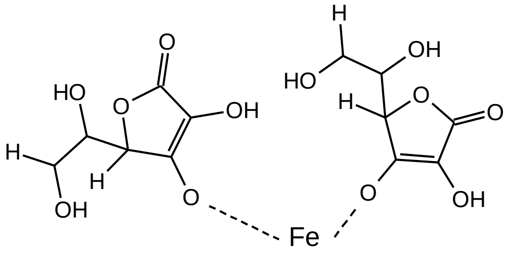

Fig.4.12: Formation of a chelating complex between Fe^{2+} and L- Ascorbic acid

4.6.2 Electrochemical Impedance Spectroscopy (EIS)

The increase in temperature and concentration of acetic acid shown in the EIS results in a decrease of R_p and R_s, and an increase of Y_0 (Table 4.5). The decrease in resistance (R_p and R_s) implies an increase in corrosion current densities. Moreover, the conversion of Y_0 data into equivalent capacitance (C) which is governed by equation 4.11 shows that when $n = 1$ in Table 4.5, the pseudocapacitance (Y_o) is equal to equivalent capacitance (C_{dl}) and thus the CPEs are equivalent to pure capacitors. If $Y_o = C_{dl}$, the trend demonstrated by

Y_o is also similar to C_{dl}. and their increase reflects an increase in corrosion rate. These results further support the PDP results.

$$C_{dl} = Y_0^{\frac{1}{n}} R_p^{\frac{1-n}{n}} \tag{4.11}$$

The EIS results for L-ascorbic acid show a drop in R_p and R_s when the concentration of L-ascorbic acid and temperature is increased (Table 4.6). The drop in R_p and R_s further supports the PDP results that L-ascorbic acid increases corrosion instead of acting as the corrosion inhibitor as reported in the literature (Ferreira et al., 2004; Fuadi, 2019). This increase in corrosion rate is in agreement with the increase in Y_0 since n = 1 based on equation 4.11.

4.6.3 Electrochemical weight loss

The electrochemical weight loss for test coupons in either acetic or ascorbic acid shown in Fig.4.4 and 4.5 increases with an increase in temperature and concentration of the acid. This implies an increase in corrosion current densities. The electrochemical weight loss is maximum at 60 °C for 1.0 mM of acid and 120-exposure time and minimum at 30 °C for 0.2 mM of acid and 60-exposure time. In addition, the electrochemical weight loss in the presence of L-ascorbic acid is higher than in the presence of acetic acid which in turn implies higher corrosion. These observations are in agreement with the PDP and EIS results.

4.6.4 Kinetic parameters of activation corrosion

The kinetic parameters of activation corrosion, i.e. *apparent activation corrosion energy* (E_{act}) and *enthalpy of activation* (ΔH_{act}), in the presence of either acetic or ascorbic acid decrease with an increase in acid concentration. This implies an increase in corrosion current and thus the dissolution of metal.

The reaction at the metal surface requires a small activation energy and activation enthalpy to proceed if the acid solution concentration is increased. The positive sign for both E_{act} and ΔH_{act} reflects the endothermic nature of the corrosion process while the increase of ΔS_{act} implies an increase in disordering takes place on going from reactants to the activated complex (Go et al., 2020; Okewale and Adesina, 2020). These observations on kinetic parameters of activation corrosion support the PDP and EIS results.

4.6.5 Multiple Linear Regression

The R^2 values in Table 4.9 with the multiple linear regression results show a strong correlation between the variables (0.992 and 0.970). The concentration of acids, temperature, exposure time, and pH have a high influence on the corrosion current densities in either acetic or L-ascorbic acid. The p-value in acetic or L-ascorbic shows a significant correlation because it is less than the statistical accepted value which is 0.05. On the other hand, the coefficient values of independent variables in Table 4.9 show that the concentration of acid has more influence on corrosion current densities than on pH, temperature, and exposure time. The influence of the concentration of acid on corrosion current densities is more pronounced in L-ascorbic than acetic experiments which in turn implies higher corrosion current densities in the presence of L-ascorbic. These regression results strongly support the PDP, EIS, and pH measurement results

4.6.6 pH

The final pH decreases towards a pH of 3 (highly acidic) when acetic acid is introduced into the simulated SRB environment (60 °C and 120 minutes) and the temperature increases to 60 °C (Fig.4.8). Moreover, under the same simulated conditions, with L-ascorbic acid instead of acetic acid, the pH decreases even more to 2.5 at 60 °C. This decrease in pH values if the temperature increases imply the increase in corrosion current densities as confirmed in Table 4.3 and 4.4. Further, the change in concentration from 0.2 to 1.0 mM of either acetic or L-ascorbic acid decreases the pH values and consequently increases the corrosion current densities too. The decrease in L-ascorbic acid is more than in acetic which implies higher corrosion current densities. The observed decrease in pH in both acetic and L-ascorbic acid leading to an increase in corrosion current densities further supports the PDP and EIS results.

4.6.7 Dissolved metal ions in solution

The general trend observed in Fig. 4.9 is that the concentration of metal ions (Fe, Si, and Mn) in solution increases as temperature and concentration of the organic acid metabolite increase. This trend is consistent with the trend of corrosion current densities. The increase in metal ions into solution when temperature or concentration increases relates to the increase in H^+ and decrease in pH.

According to Madirisha et al (2022c), the ICP-OES results of carbon steel corrosion under SRB conditions, with biofilm and in brine solution show an average concentration of Fe, Si, and Mn of 220 μg/gcm^2 (at 60 and 120 minutes). Carbon steel corrosion under the same conditions, with the addition of acetic acid (60 and 120 minutes), in both concentrations (0.2 and 1.0 mM), results in a decrease of the dissolved ion concentration to 60 μg/gcm^2 for 0.2 mM and 170 μg/gcm^2 for 1.0 mM. The addition of L-ascorbic (1.0 mM) instead of acetic acid increases the dissolution of the carbon steel coupon even more to dissolved ion (Fe, Si, and Mn) concentrations of 800 µg/gcm^2 and 1100 µg/gcm^2, at 60 minutes and 120 minutes exposure time, respectively. These results further support the PDP and EIS on inhibition and acceleration of corrosion demonstrated by acetic and L-ascorbic acids in a simulated SRB environment, respectively.

4.6.8 X-Ray Diffraction (XRD)

Corrosion products on the carbon steel due to acetic acid/L-ascorbic acid under a simulated SRB environment are characterized with XRD (examples in Fig. 4.10 and 4.11). Carbon steel not exposed to experiments is considered as a reference. The examples show the diffractograms depicting the most explicit changes. The XRD reveals the occurrence of corrosion products namely FeS and γ-FeOOH in the presence of acetic or L-ascorbic acid in a simulated SRB environment. The presence of these corrosion products under a simulated SRB environment is in agreement with the literature that when SRB are present in the environment, the first corrosion products are ferric (oxyhydroxide) such as lepidocrocite, transformed to the iron sulfide by hydrogen sulfide, chemical equation 4.12 (El Hajj et al., 2013). The presence of corrosion products on test coupons in the presence of acetic or L-ascorbic acid in a simulated SRB environment further supports the occurrence of deterioration on the test coupons.

$$3H_2S + 2FeOOH \longrightarrow 2FeS + S + 4H_2O \qquad 4.12$$

4.7 Conclusion

The role of simulated organic acid metabolites, namely acetic and L-ascorbic acids on corrosion of geo-energy pipeline made of carbon steel in the presence of simulated Sulfate Reducing Bacteria (SRB) is investigated at different temperatures (30, 45, and 60 °C) and exposure times (60 and 120 minutes). The simulated SRB environment consists of simulated biofilm made of calcium alginate, abiotic sulfide (to mimic SRB metabolic end product H_2S), CO_2 (to mimic CO_2 from SRB dissimilatory sulfate reduction), and simulated brine (3.0 wt% NaCl). The electrochemical results show that acetic and L-ascorbic acids in a simulated SRB environment accelerate corrosion. Further, the electrochemical weight loss increases with the increase in temperature and concentration of the acetic/L-ascorbic acid which in turn implies an increase in corrosion current densities. These observations are further supported by the kinetic corrosion activation parameters which show an endothermic nature of the corrosion process characterized by a small activation energy and activation enthalpy to proceed if the acid solution concentration is increased. The R^2 from multiple linear regression of corrosion current densities shows that concentration of acids, temperature, exposure time, and pH have a high influence on the corrosion current densities. The p-values in acetic or L-ascorbic show a significant correlation of the variables on corrosion because p-values are less than the statistical accepted value which is 0.05. On the other hand, the coefficient values in the presence of L-ascorbic acid are higher than in acetic acid implying higher corrosion current densities. Furthermore, the ICP-OES shows that the dissolution of metal ions in solution is more in the presence of L-ascorbic than in the presence of acetic acid. The increase of dissolution of carbon steel is accompanied by the decrease of the pH solution when acetic acid and L-ascorbic acid are added. The XRD results also confirm the occurrence of corrosion in the presence of acetic/L-ascorbic acid. This is evidenced by the formation of FeS and γ-FeOOH.

Comparison of electrochemical results in this study with the results in a simulated SRB environment without acetic or L-ascorbic acid shows that the corrosion current densities in the presence of acetic acids in an SRB environment are two times lower than those in a simulated SRB environment without acetic acid under similar experimental conditions (Madirisha et al., 2022c). This observation shows that acetic acid in the presence of a simulated SRB environment demonstrates an inhibitory effect. On the other hand, the corrosion current densities in the presence of L-ascorbic acid in a simulated SRB environment are approximately two times higher than without L-ascorbic acid implying that L-ascorbic acid accelerates corrosion. The effect on corrosion current densities demonstrated by acetic and L-ascorbic acids in a simulated SRB environment is not found in the literature. Furthermore, the ICP-OES results support the corrosion inhibitory and acceleration effects due to the presence of acetic and L-ascorbic acid, respectively. Taking into account the ICP-OES results (average concentration of Fe, Si, and Mn is 220 ug/gcm^2) of test coupons under SRB conditions without acetic or L-ascorbic acid reported in Madirisha et al (2022c), adding acetic acid with concentrations 0.2 and 1 mM (60 and 120 minutes), decreases the dissolved metal ion concentration to 60 µg/gcm^2 for 0.2 mM and 170 µg/gcm^2 for 1.0 mM. The addition of L-ascorbic (1.0 mM) instead of acetic acid increases the dissolution of the carbon steel test coupons even more to dissolved ion (Fe, Si, and Mn) concentrations of 800 µg/gcm^2 and 1100 µg/gcm^2, at 60 minutes and 120 minutes exposure time, respectively. The results complement the existing literature on the role of acetic and L-ascorbic acids on corrosion of carbon steel in an SRB environment and highlight the novelty of this research. The results have a direct impact on the role of other microbial metabolites in the corrosion of carbon steel.

5 The influence of chelating agents on clays in geothermal reservoir formations: implications to reservoir acid stimulation[8]

5.1 Introduction

Geothermal energy is a renewable resource that may provide long-term energy with low carbon footprint and maintenance costs (Archer, 2020; Bahadori et al., 2013; Junrong et al., 2015; Li et al., 2015b; Owusu and Asumadu-Sarkodie, 2016; Wang et al., 2016a). The majority of the world's geothermal reserves are contained in subsurface sandstone and carbonate formations that often contain sizeable quantities of fine-grained materials such as clay minerals; kaolinite, chlorite, smectite, mixed layer illite-smectite, and illite (Ahmad et al., 2018; Fulignati, 2020; Jiang, 2012; Moeck, 2014; Toth and Bobok, 2016). The clay minerals may be concentrated in layers or distributed in the coarse-grained materials in the reservoir. Clay layers also often form the impervious boundary on top of the permeable reservoir rocks, the so-called, "caprock" (Gunderson et al., 2000; Kuila and Prasad, 2013; Toth and Bobok, 2016). The amount and distribution of clay minerals have a significant impact on the fundamental principles of quality of the reservoir especially the permeability (Ahmad et al., 2018). Clay minerals are sensitive to chemicals and therefore injecting chemicals in a reservoir, such as done for chemical stimulation, may cause unwanted results. Sometimes chemical stimulation to improve the permeability of a reservoir causes the reverse and the result is a reduction in

---

[8] *This chapter is based on: Madirisha, M., Hack, R., & Van der Meer, F. (2022). The influence of chelating agents on clays in geothermal reservoir formations: Implications to reservoir acid stimulation. Geothermics, 99, 102305.*

permeability. This effect is often denoted "formation damage" (Liang et al., 2017; Shafiq et al., 2018; Wilson et al., 2014). Formation damage may result in flow barriers or baffles that hinder the flow of fluids (Xiao et al., 2016b; Xiong and Holditch, 1995). Smectite and kaolinite, as well as other phyllosilicates often are envisioned as the barriers for fluid flow in formation damage (Ahmad et al., 2018; Gray et al., 2013; Metz et al., 1995; Priisholm et al., 1987). In this study, the interactions are investigated between two clay minerals often responsible for the decrease in reservoir permeability in formation damage and three biodegradable chelating agents (Fig.5.1) which are nitrilotriacetic, iminodiacetic and ethylenediamine-N,N'-disuccinic acids (further abbreviated in this article as BCA3, BCA2, and BCA1, respectively). These three chemical agents have been chosen for the research as these have different functional groups (FGs) that are likely to interact with the clays differently as the number of functional groups determines the reactivity of the chemical agent. BCA3, BCA2, and BCA1 have 4, 3, and 6 functional groups, respectively. The biodegradable chelating agents are typical examples for dozing chemicals used in reservoir chemical stimulation which are characterized by lower dissolution rate and large balanced path through the undamaged or damaged formation (Li et al., 2015c; Nitters et al., 2016; Portier et al., 2007; Rose et al., 2010). The experiments in this study are conducted under simulated conditions common in many geothermal reservoirs; i.e., temperature 230 °C and pressure 85 bars, and in brine and CO_2 environment. Before the experiments in brine, experiments in distilled water under the same conditions are conducted as a control study. The novelty of this study is to achieve a better understanding of the compatibility in terms of geochemical reaction (dissolution – precipitation) between clay minerals and biodegradable chelating agents. The outcome is of importance for forecasting the effects of reservoir stimulation to enhance permeability.

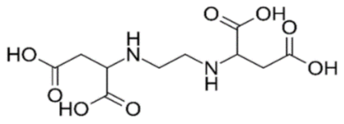

1

Ethylenediamine-N, N′-disuccinic acid (BCA1)

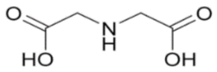

2

Iminodiacetic acid (BCA2)

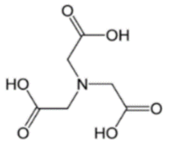

3

Nitrilotriacetic acid (BCA3)

Fig. 5.1: Biodegradable chelating agents (BCA) - aminopolycarboxylic acids

5.2 Chemical injection and permeability of reservoir rocks

Poor permeability in both convective (hydrothermal) and non-convective (enhanced) geothermal systems is a recurring problem (Aqui and Zarrouk, 2011b; de Pater and Shaoul, 2019; Vilarrasa et al., 2020). Poor permeability often requires re-drilling existing and drilling of new wells. Alternatively, a cheaper solution may be reservoir stimulation by injection to improve permeability. An acid injection is the most dominant permeability stimulation technique in use (Aqui and Zarrouk, 2011b). The most often used acids for reservoir stimulation are HF, HCl, CH_3COOH, HCOOH, H_2NSO_3H, and $ClCH_2COOH$ (Peksa et al., 2016; Portier et al., 2007; Rose et al., 2010). However, it is often reported that the acids interact with clay minerals in the reservoir and pose problems such as dissolution - precipitation and matrix un-consolidation (Portier et al., 2007; Simon and Anderson, 1990; Tariq et al., 2017a; Thomas et al., 2002). The dissolution may cause matrix un-consolidation due to part of the grain skeleton vanishing or precipitation may clog the pores and channels between pores in the grain skeleton. The surface area of clay minerals is a key parameter for predicting dissolution-precipitation in clay minerals because a larger surface area of a clay mineral gives a higher reactivity (Hao et al., 2019; Metz et al., 1995; Metz et al., 2005).

Clay-rich sandstone and heterogeneous dolomite reservoirs are suitable for acidizing using chelating agents (Portier et al., 2009; Tariq et al., 2017b). Chelating agents such as aminopolycarboxylic acids (APCAs) are reported to have limited reactions with the clay minerals, reducing the rates of secondary and tertiary reactions such as precipitation as temperature increases t (Gdanski, 1997; Lucas et al., 2020; Rose et al., 2010). This is an advantage for use in many geothermal reservoirs because temperatures in geothermal reservoirs are often higher and hence less precipitation is likely to occur when using APCAs for stimulation than using mineral acids (HF and HCl). APCAs contain several carboxylate groups bound to one or more nitrogen atoms and therefore are capable of forming water-soluble complexes by coordinating electrophilic species (mainly metal ions) through oxygen and nitrogen donor atoms and by forming one or more heteroatomic rings (Bucheli-Witschel and Egli, 2001; Salvatore and Salvatore, 2015; Tariq et al., 2017a). These structural features enable APCAs to retard precipitation in reservoirs containing clay minerals and characterized by high temperatures. Further, APCAs are less corrosive, thermally stable, and more effective even under high-temperature conditions (Aldakkan et al., 2018; Hassan and Al-Hashim, 2016). For the above reasons, the application of synthetic APCAs in reservoir stimulation would be an advantage. However, the use is limited because of environmental concerns (Pinto et al., 2014). Natural APCAs that are not hampered by environmental concerns are an alternative to conventional acids and synthetic APCAs and are often preferable. This study, therefore, uses BCA1, BCA2, and BCA3 as natural APCAs.

5.3 Materials and Methods

5.3.1 Materials

The materials used in this research are clay minerals kaolinite-natural (KN) and montmorillonite-K10 (MM) in powdered form, CO_2 gas, brine, distilled water, and biodegradable chelating agents (BCAs); namely: BCA1, BCA2, and BCA3). The clay minerals are supplied by Sigma Aldrich Company (https://www.sigmaaldrich.com/european-export.html) while the CO_2 gas is supplied by TOL Gases Limited (formerly Tanzania Oxygen Limited) (http://www.tolgases.com/). KN and MM are selected because these are reported to be the most critical clay minerals causing permeability reduction during acid stimulation (Ahmad et al., 2018). KN and MM are sensitive to reactions in an aqueous solution and acidic environments (Riyono et al., 2018). BCA1, BCA2, and BCA3 are selected because these APCAs are environmental-friendly, not very corrosive, and stable at high temperatures (Pinto et al., 2014). The brine was collected in December 2020 from Iyola, one of the Songwe Hot Springs in South Western Tanzania (Fig. 5.2). The hydrothermal fluids originate in the basement and sedimentary rift deposits of the Songwe Basin (Alexander et al., 2016). The stratigraphy consists of a metamorphic basement, Karoo sandstone, red sandstone, and lake beds (clays etcetera).

The hydrothermal fluids likely circulate through faults in the basement and accumulate in the overlying sandstones. Arriving at the surface, the drop in pressure causes CO_2 to escape and precipitation of carbonates which resulted in thick travertine deposits. The hydrothermal fluids by now brine, rise to the surface through water channels in the travertine rocks (Mayo and Mnzava, 2010; Roberts et al., 2004). The brine is neutral to slightly alkaline with pH 6.9 - 8.8 and mixed with Na-HCO_3-Cl-SO_4 fluids containing non -condensable gas (CO_2) (Hinz et al., 2018). The brine of the springs in Songwe was thought to be of possible volcanic origin or influenced by volcanic activity, but in recent publications, the volcanic origin or influence is regarded as highly unlikely (Hinz et al., 2018; Alexander et al., 2016). Therefore, the brine of the Iyola Spring in the Songwe district is expected to be characteristic of sedimentary reservoirs. This is confirmed by ICP-OES and pH measurements were done for this study. The brine contains mainly Na^+ and $Mg^{2+,}$ and the pH is between neutral to alkaline, which are properties characteristic for brine in sedimentary reservoirs (Nogara and Zarrouk, 2018b). Extensive chemical analyses of the brine are reported in Mnzava and Mayo (2010). Distilled water is supplied by the Arusha Technical College, Tanzania. The distilled water is prepared according to ISO 3696:1987 (https://www.iso.org/standard/9169.html). A CO_2 gas environment is used because many geothermal reservoirs have a low concentration of oxygen and a high CO_2 level (Gunnlaugsson et al., 2014a). The analytical methods used are porosimetry, infrared reflectance spectroscopy, X-ray diffraction (XRD), Inductively Coupled Plasma - Optical Emission Spectrometry (ICP-OES), Fourier-transform infrared spectroscopy (FT-IR), and pH, conductivity, and salinity measurements.

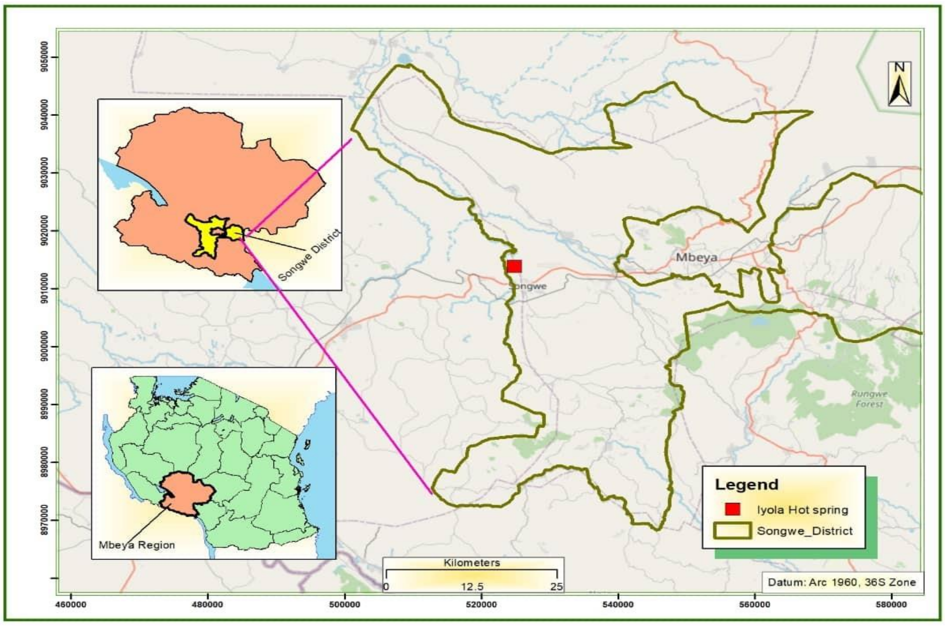

Fig. 5.2: Map of Songwe district showing Iyola hot spring, where brine was sampled (map courtesy: Mabala E. Z. 2021)

5.3.1.1 Experiment Matrix

The clays used are very hygroscopic and therefore sample preparation has to be done with care to avoid too much humidity from the air to be taken up by the clay samples. Therefore, each sample is prepared separately. A sample of a little more than 10 g of a clay mineral is weighed and dried overnight in an oven at 60 °C. Then, the sample is trimmed to exact 10.0 g, weighted again, and placed in a 500 mL beaker. 145 mL of distilled water (DW) or brine and 5 mL of chelating agents (BCAs) are added to the beaker. This procedure is repeated 12 times. 3 formulated solutions of MM clay and 3 formulated solutions of KN clay are prepared with DW and BCAs while the other six are prepared similar but with brine instead of DW. Two experiments are done as reference experiments of which one is with MM clay and the other with KN clay, each with 150 mL of DW. The volume of each beaker of the formulated solution is then 150 mL for as well the beakers with and without a chelating agent and irrespective of whether the beaker contains DW or brine. The experiment matrix of in total of 14 experiments is shown in Table 5.1. The starting temperature (T_1) is the room temperature of approximately 25 °C while the initial pressure (P_1) is chosen to be 21 bar. This combination of T_1 and P_1 allows for reaching a temperature of 230 °C (T_2) and a pressure of 85 bar (P_2) within a time span of approximately 3 hour after the heater in the reactor is switched on. These conditions (T_2 and P_2) are common in geothermal reservoirs. The experiment itself starts when T_2 and P_2 are reached and run for 2 hour. During the 2 hour, the T_2 and P_2 are maintained in the reactor. 2 hour is considered to be long enough to study the interaction of the biodegradable chelating agents and the clay minerals. The large surface area of the clay minerals allows fast reaction kinetics such that in 2 hour the reaction kinetics can be established (Stoch, 1990).

Table 5.1: Experiment matrix for investigating the interaction of biodegradable chelating agents and clays under CO_2 environment

Experiment	Clay g	DW/ brine mL	BCA mL	Total volume mL	T_1 °C	P_1 bar	T_2 °C	P_2 bar	Time hour
MM + DW+ CO_2	10	150	0	150	25	21	230	85	2
KN + DW + CO_2	10	150	0	150	25	21	230	85	2
MM + DW + BCA + CO_2	10	145	5	150	25	21	230	85	2
MM + brine + BCA + CO_2	10	145	5	150	25	21	230	85	2
KN + DW + BCA + CO_2	10	145	5	150	25	21	230	85	2
KN + brine + BCA + CO_2	10	145	5	150	25	21	230	85	2

Notes: MM = montmorillonite-K10, KN = kaolinite-natural, DW = Distilled water, BCA = Biodegradable Chelating Agent (BCA1, BCA2 or BCA3); T_1 = Initial temperature, T_2 = Final temperature, P_1 = Initial pressure, P_2 = Final pressure

5.3.1.2 Experiment set up

The experiments are conducted in a 500 mL desktop high-pressure hydrothermal reactor (Model: TGYF-B, Henan Lanphan Industry Co.Ltd, China). It allows a maximum pressure of 220 bar by a temperature of 300 °C. The formulated solutions are poured into the internal cup of the reactor (Fig. 5.3) and purged with CO_2 at approximately 21 bar (P_1), whereafter the heater is switched on. The experiment starts (countdown) when the temperature reaches 230 ^{o}C (T2) and pressure of 85 bar (P_2). The experiment is stopped after 2 hour and the internal cup is removed and put in a sink containing water for cooling. After cooling down to 100 ^{o}C, the solution is drained from the internal cup into a beaker which is kept in a trough with water to cool down further to room temperature. Thereafter, the supernatant (which is the liquid above the solid residue) is poured in a 50 mL falcon tube for analysis while the beakers with remaining sediments are placed in an oven at a temperature of 60 ^{o}C and left overnight to dry also for further analysis.

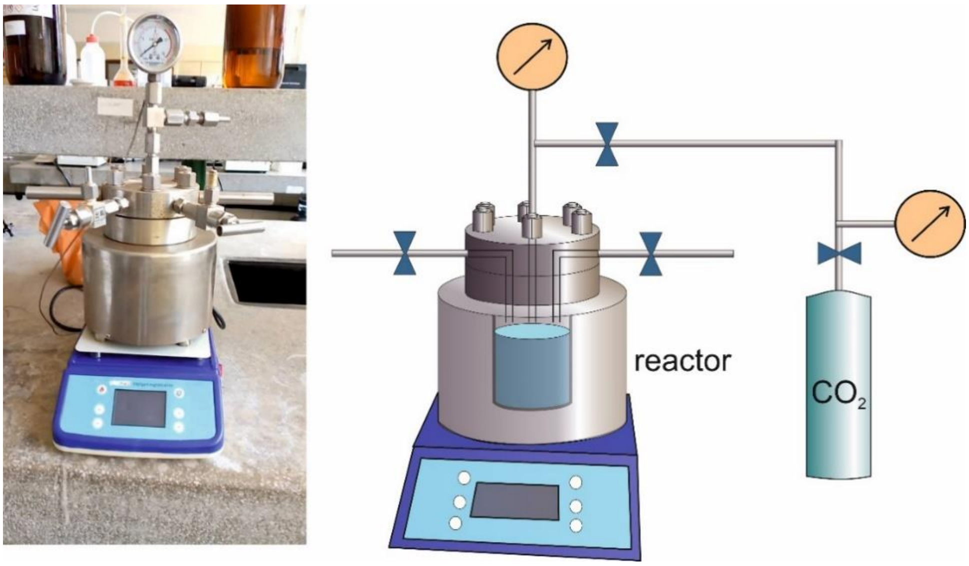

Fig. 5.3: Photo and diagram of the reactor for investigating the interaction of biodegradable chelating agents and clays under CO$_2$ environment

5.3.2 Analytical methods

Powdered clay mineral samples as blanks and powdered sediments collected after the experiments are characterized by porosimetry, Attenuated Total Reflection Fourier Transform Infra-Red (ATR-FTIR), infrared reflectance spectroscopy, and X-ray powder diffraction (XRD). The supernatants collected from post-experiment solutions are analyzed for dissolved metal ions using ICP-OES. The pH, conductivity, and salinity using pH and conductivity meters, are measured of the formulated and post-experiment solutions.

5.3.2.1 Porosimetry

A nitrogen adsorption porosimeter (NOVA 1200e, PRUS Version 11.03, Quantachrome Corporation, Japan) is used to analyze the surface area, pore size distribution, and pore volume of the blank samples and sediments. The device is warmed up for a minimum of 30 min before starting the analysis. Then, the samples are degassed at 140 °C with a reduced pressure for 2 hour. The aim of degassing is to remove adsorbed water. The degassed sample is filled in an instrument-specific glass holder and weighted three times on a microbalance. The actual porosimeter test is done by allowing boiling nitrogen gas (i.e., at 77 K) to be adsorbed by the degassed sample. The difference in volume adsorbed at different fractions of equilibrium and saturation pressures of nitrogen are recorded automatically and the characteristic isotherm is generated by NOVA Win software (PRUS Version 11.03). The isotherm is used to determine the BET (Brunauer-Emmett-Teller) surface area, and BJH (Barrett, Joyner, and Halenda) pore area and volume. The BET surface area is the summation of both the external area and pore area. BET surface and BJH pore area and volume characterize the reactivity of the clay minerals. The inability to measure the reactive surface area of a mineral powder that is exposed to an aqueous phase makes the BET methodology appropriate for dissolution and precipitation experiments with mineral powder although BET surface area may be larger than the reactive surface area (Helgeson et al., 1984; Metz et al., 2005).

5.3.2.2 Attenuated Total Reflection Fourier Transform Infra-Red (ATR-FT-IR)

The surface and structure of the blank samples and sediments are investigated by Attenuated Total Reflection Fourier Transform Infra-Red (ATR-FT-IR). The vibrational spectra are analyzed with an Alpha ATR-FT-IR Spectrometer (Model Bruker optic GmbH 2011 U.S.A model) installed with Bruker OPUS Spectroscopy Software (version 7 ed.2011). Each solid sample is positioned directly on top of a diamond crystal and the incident IR beam penetrates through the crystal and interacts with the sample, which is pressed onto the crystal. The analysis is done in the wavenumber range of 400 - 4500 cm^{-1}.

5.3.2.3 Infrared reflectance spectroscopy

The infrared reflectance spectra of the blank samples and sediments are measured using a TerraSpec Halo Spectroradiometer (ASD-FieldSpec 4). The TerraSpec Halo Spectroradiometer measures single reflectance spectra between Visible-Near (VNIR) and Short-Wave Infrared (SWIR) (350 to 2500 nm) via a non-destructive contact measurement (Kenaston, 2019). The equipment samples at intervals of 1.4 nm for the region 350-1000 nm and 2 nm for the region 1000-2500 nm. The measurements are done with direct contact between the 2 cm diameter probe window of the ASD and the clay sample. Reflectance values are measured in the 350–2500-nm wavelength range. Before the measurement, the machine is switched on and left to warm up for 40 minutes and optimized to ensure the correct working of the sensor. Calibration of the machine is done using white reference material (white reference spectralon) which reflects all light. The calibration is conducted until the reflectance of spectralon is 1.

5.3.2.4 X-ray powder diffraction (XRD)

The chemical composition of the blank samples and sediments are analyzed with X-ray powder diffraction (XRD) using a Bruker D2 Phaser XRD operating in Bragg-Brentano geometry with CuKα (1.54184Å, 30 kV, and 10 mA) radiation and a LYNXEYE detector as well as Bruker’s corundum standard reference material. The equipment is set to operate at 5° to 70° in 2θ range with a step size of 0.014°.

5.3.2.5 Inductively Coupled Plasma - Optical Emission Spectrometry (ICP-OES)

The supernatants are investigated with Inductively Coupled Plasma - Optical Emission Spectrometry (ICP-OES) (Thermo Scientific iCAP 6000 Series) to quantify the amount of Al, Si, Ca, Na, and Mg metal ions that are dissolved in the solution during the interaction of clays with BCAs in brine or distilled water under CO_2 environment. The total concentration of metal ions is the addition of the concentrations of individual metal ions. 95.0 mL of supernatant is placed into a 150 mL Pyrex beaker and 5.0 mL of concentrated HNO_3 solution (analytical grade; from Merck, Darmstadt, Germany) is added. This is heated on a hot plate at 100 °C for ca. 3 hour. During this time, the sample is refluxed so that the mixture is not allowed to dry. The digested solution is filtered through Whatman no. 40, 125 mm filter paper into a 25.0 mL volumetric flask which is further filled to the mark with deionized water. Working standard solutions are prepared by stepwise dilution (0.25, 0.5, and 1.0 ppm) of a multi-element (1000 μg mL^{-1}) ICP standard solution (Merck). The prepared working standard solutions are filled into ICP-OES tubes and inserted into the autosampler of the ICP-OES equipment. Calibration of blanks (DW and brine) is done followed by calibration of standards ranging from low to high concentration. Thereafter, the sample blanks are inserted into the autosampler followed by samples of the supernatants. Correction of the ICP-OES results for samples 1-14 is done by subtracting ICP-OES results of blanks of distilled water and brine.

5.3.2.6 pH, conductivity, and salinity measurements

The pH, conductivity, and salinity of the formulated solution non-dozed and dozed with BCAs without purging with CO_2 before the experiment (initial values) and those of post-experiment solutions (final values) are measured at a temperature of 25 °C. The pH, conductivity, and salinity meters are calibrated before taking the measurements. The pH meter is calibrated with buffer solutions of pH = 7 and 4 while the conductivity and salinity are calibrated with distilled water. The sensors are cleaned with distilled water after every measurement.

5.4 Results

The results from the analyses described in section 5.3 are presented in this section. The results on surface properties and structural changes of the clay minerals (MM and KN) are presented first, followed by the results on dissolved ions in solution, pH, conductivity, and salinity. Multiple regression analyses conclude the section.

5.4.1 BET surface area, and BJH pore area and volume

The BET surface area (BET-SA) and BJH pore area (BJH-PA) and pore volume (BJH-PV) per gram of the blank samples and sediments are shown in Tables 5.2 and 5.3.

Table 5.2: BET surface area (BET-SA), BJH pore area (BJH-PA), and volume (BJH-PV) per gram of the MM blank sample and MM sediments

Test	BCA	Sample	BET-SA (m^2/g)	BJH-PA (m^2/g)	BJH-PV (cc/g)
MM	No BCA	blank	256.4	180.9	0.4
MM + DW + CO_2	No BCA	1	773.6	611.1	0.9
	BCA1	2	530.4	306.9	0.5
	BCA2	3	1074.0	692.8	1.2
	BCA3	4	452.4	302.8	0.6
MM + brine + CO_2	BCA1	5	601.4	397.8	0.6
	BCA2	6	950.7	613.0	1.0
	BCA3	7	982.4	630.6	1.0

Table 5.3: BET surface area (BET-SA), BJH pore area (BJH-PA) and volume (BJH-PV) per gram of the KN blank sample and KN sediments

Test	BCA	Sample	BET-SA (m^2/g)	BJH-PA (m^2/g)	BJH-PV (cc/g)
KN	No BCA	blank	599.4	344.2	0.5
KN + DW + CO_2	No BCA	8	836.7	518.2	0.8
	BCA1	9	1007.0	564.4	0.8
	BCA2	10	1767.0	996.6	1.5
	BCA3	11	704.6	365.6	0.6
KN + brine + CO_2	BCA1	12	1759.0	969.1	1.5
	BCA2	13	1220.0	688.5	1.1
	BCA3	14	878.4	471.9	0.7

5.4.2 Attenuated Total Reflectance Fourier Transform Infrared Spectroscopy (ATR-FTIR)

The changes in surface area, pore area, and volume of the MM and KN clays due to dozing with BCAs in a CO_2 environment are supported by ATR-FTIR analyses which show differences in absorption peaks and intensities (see supplementary Fig. S5.1, S5.2, S5.3, and S5.4 in appendix). These results are further discussed in section 5.5.

5.4.3 Infrared reflectance spectroscopy

The reflectance spectra for different wavelengths of the MM and KN blank samples and MM and KN sediments are shown in Figs 5.4, 5.5, 5.6, and 5.7. These are discussed in section 5.5.

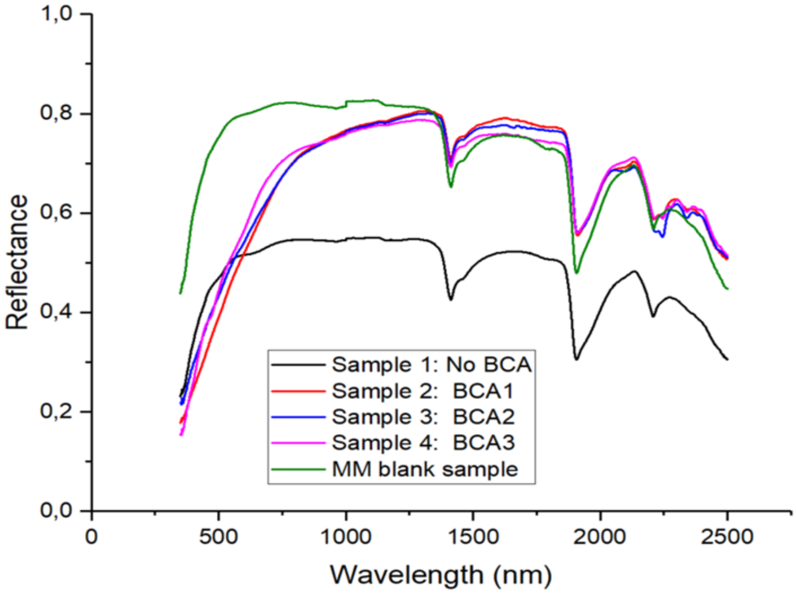

Fig. 5.4: Reflectance vs wavelength for the MM blank sample and MM sediments of experiments non-dozed and dozed with BCAs in distilled water under CO_2 environment

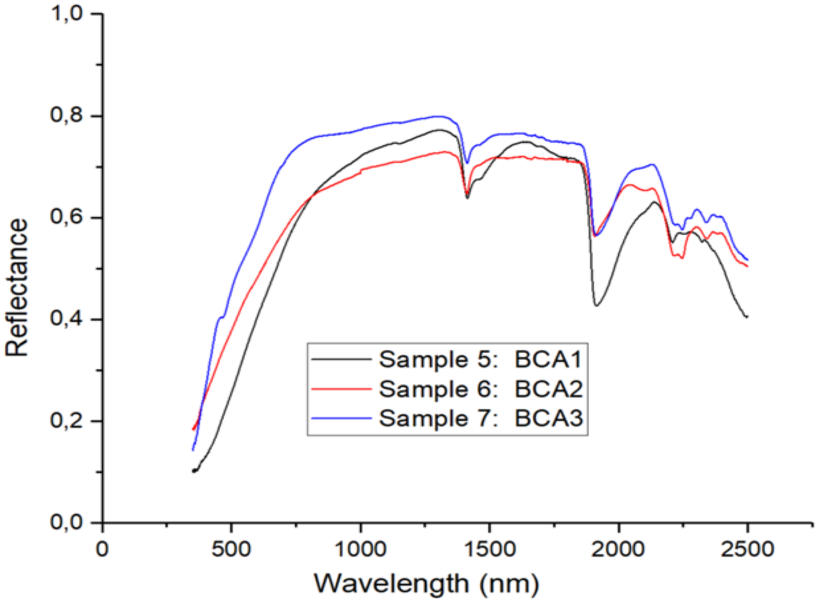

Fig. 5.5: Reflectance vs wavelength for the MM sediments of experiments dozed with BCAs in brine under CO_2 environment

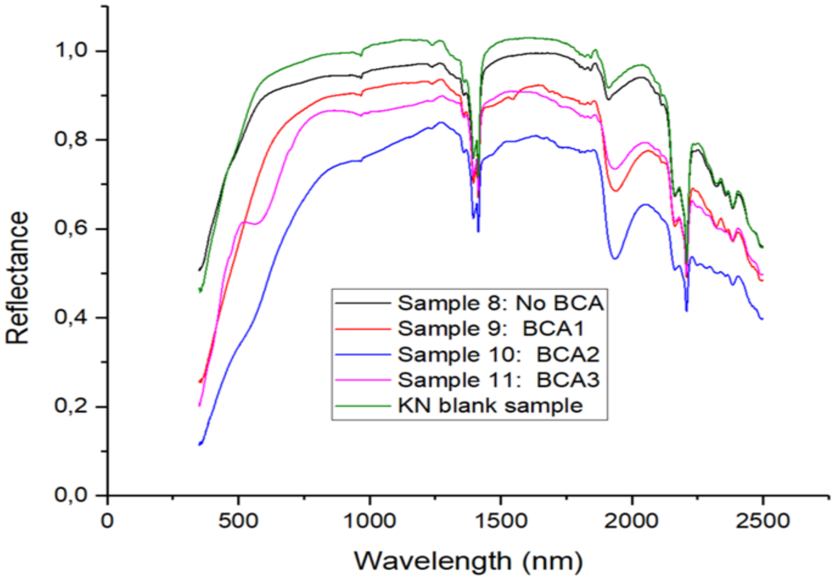

Fig.5.6: Reflectance vs wavelength for the KN blank sample and KN sediments of experiments non-dozed and dozed with BCAs in distilled water under CO_2 environment

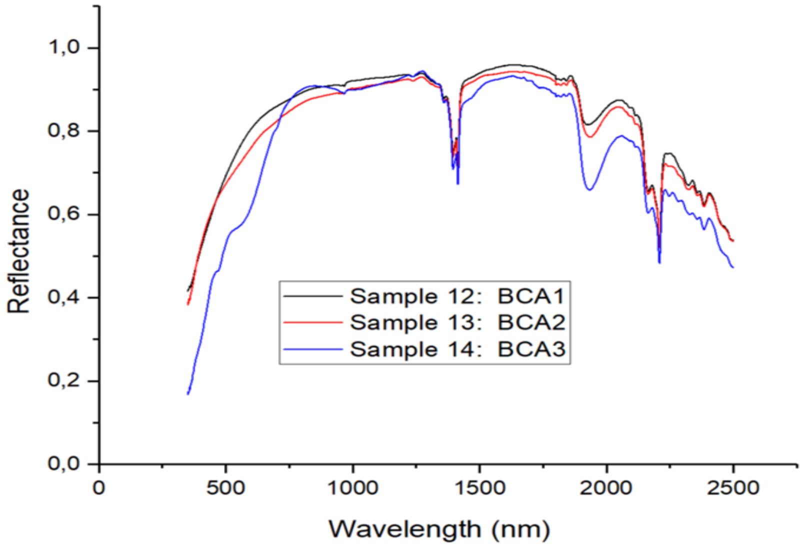

Fig. 5.7: Reflectance vs wavelength for the KN sediments of experiments dozed with BCAs in brine under CO_2 environment

5.4.4 X-ray powder diffraction

The diffractograms of the blank samples and sediments showing changes in overall crystallinity phases are shown in Supplementary Figs. S5.5 and S5.6 (in appendix) are further discussed in section 5.5.

5.4.5 ICP-OES

The ions that dissolve in solution during the experiments are determined with Inductively Coupled Plasma - Optical Emission Spectrometry (ICP-OES) analyses of the supernatants (See Supplementary Tables S5.1 and S5.2 in appendix). Results for blank samples of DW and brine are included. The concentrations of metal ions dissolved from the surface of the minerals [C_{total}] are normalized with the surface area (BET-SA) of the MM and KN to give [$C_{nor\ total}$] as shown in Table 5.4 (Hodson, 2006; Hodson et al., 1997).

Table 5.4: Normalized total concentration of dissolved metal ions in supernatants for MM or KN non-dozed and dozed with BCAs in distilled water and brine under CO_2 environment

Supernatant	BCA	Sample	[$C_{nor\ total}$] (ppm.g/m^2)	
			[C_{total}]/(BET-SA of blank clay)	[C_{total}]/(BET-SA of non-dozed or dozed clay)
MM+ DW + CO_2	No BCA	1	1.0×10^{-3}	3.4×10^{-4}
	BCA1	2	7.6×10^{-2}	3.7×10^{-2}
	BCA2	3	3.8×10^{-3}	9.1×10^{-4}
	BCA3	4	4.9×10^{-2}	2.8×10^{-2}
MM + Brine + CO_2	BCA1	5	1.2×10^{-1}	5.0×10^{-2}
	BCA2	6	7.6×10^{-3}	2.1×10^{-3}
	BCA3	7	9.0×10^{-2}	2.0×10^{-1}
KN + DW + CO_2	No BCA	8	2.0×10^{-3}	1.5×10^{-3}
	BCA1	9	5.2×10^{-2}	3.1×10^{-2}
	BCA2	10	1.1×10^{-2}	3.8×10^{-3}
	BCA3	11	3.4×10^{-2}	2.9×10^{-2}
KN + Brine + CO_2	BCA1	12	3.7×10^{-2}	1.3×10^{-2}
	BCA2	13	3.9×10^{-3}	1.9×10^{-3}
	BCA3	14	1.8×10^{-2}	1.2×10^{-2}

Note: [C_{total}] = total concentration of dissolved metal ions in ppm; [$C_{nor\ total}$] = Normalized total concentration of dissolved metal ions

5.4.6 pH, conductivity, and salinity

The change in surface area of the clay minerals is supported by changes in pH, electrical conductivity, and salinity. Fig. 5.8 and 5.9 show electrical conductivity versus pH while Fig. 5.10 and 5.11 show electrical conductivity versus salinity.

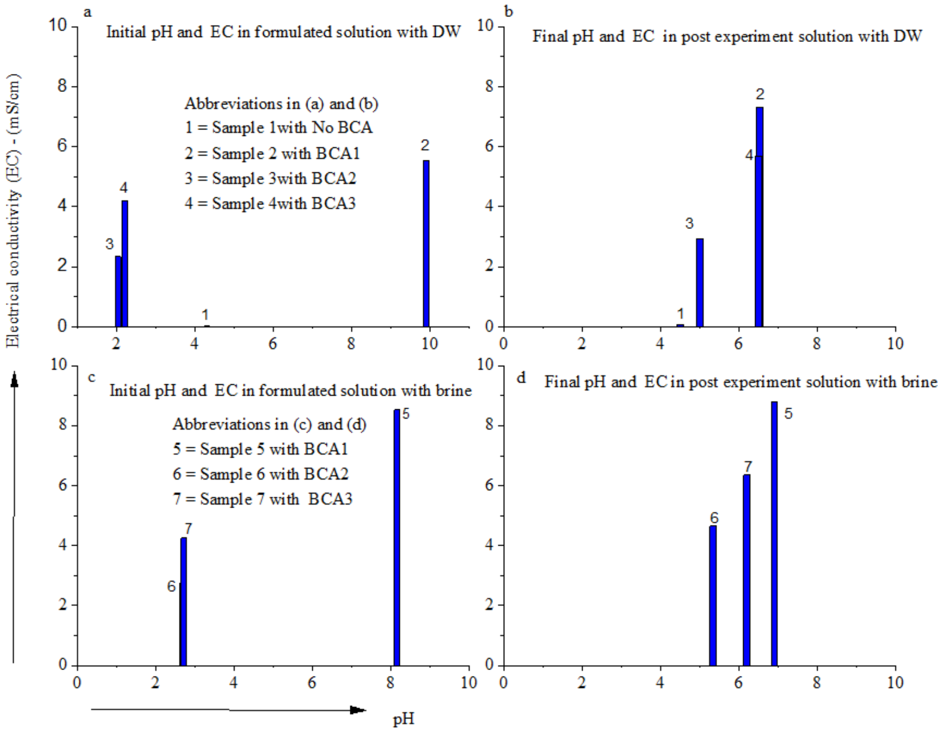

Fig. 5.8: Electrical conductivity versus pH of formulated solutions and post-experiment solutions of MM; a) formulated solution with distilled water; b) post-experiment solution with distilled water; c) formulated solution with brine; d) post-experiment solution with brine

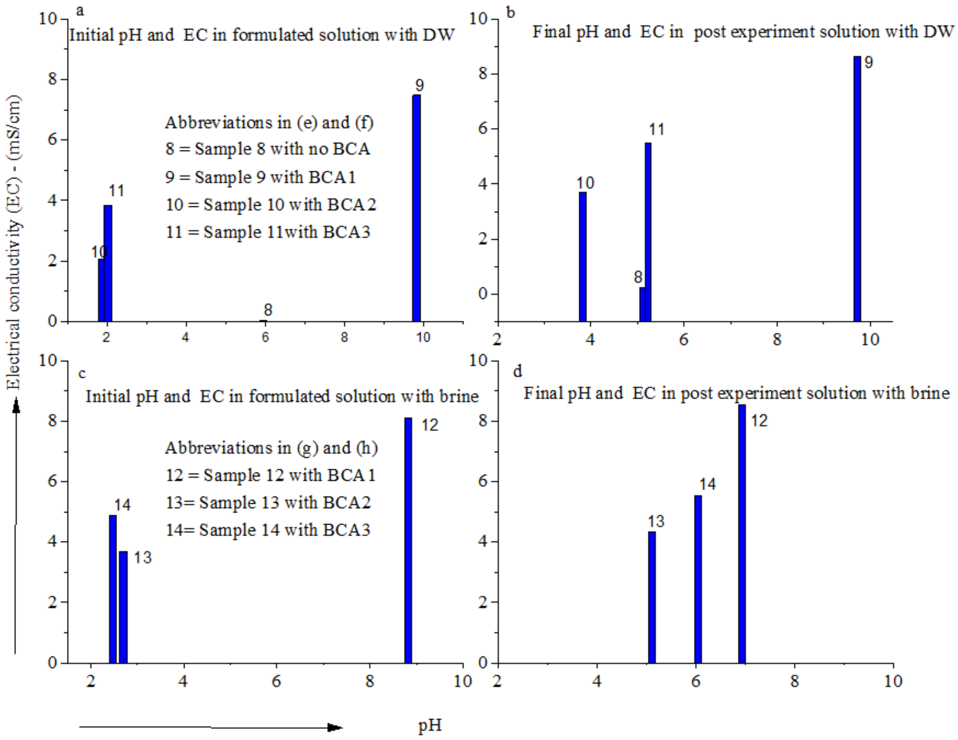

Fig. 5.9: Electrical conductivity versus pH for formulated solutions and post-experiment solutions of KN samples; a) formulated solution with distilled water; b) post-experiment solution with distilled water; c) formulated solution with brine; d) post-experiment solution with brine

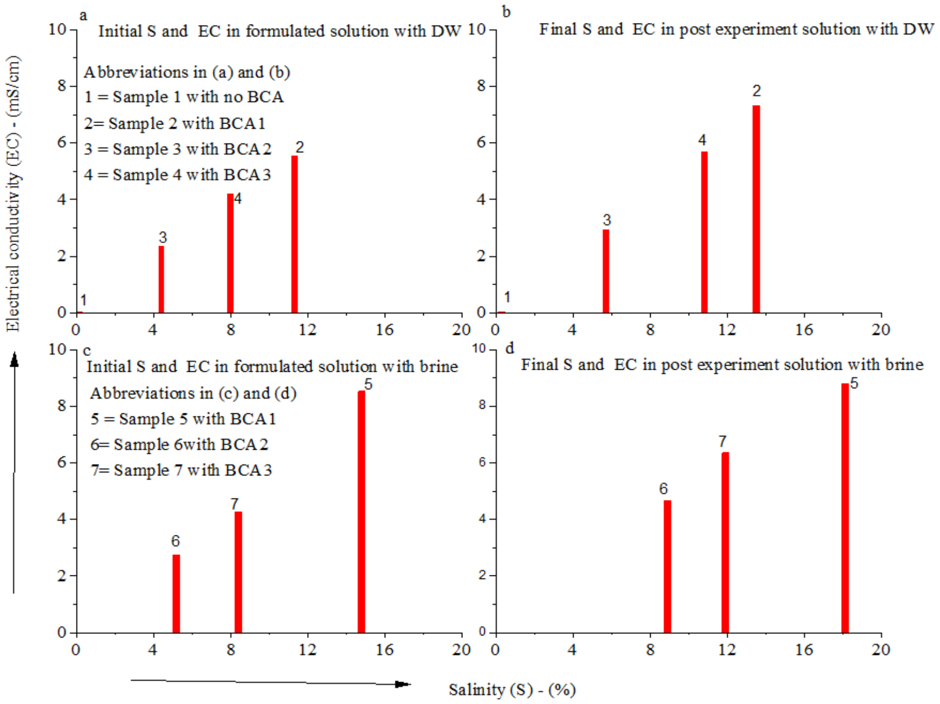

Fig. 5.10: Electrical conductivity versus salinity for formulated solutions and post-experiment solutions of MM samples; a) formulated solution with distilled water; b) post-experiment solution with distilled water; c) formulated solution with brine; d) post-experiment solution with brine

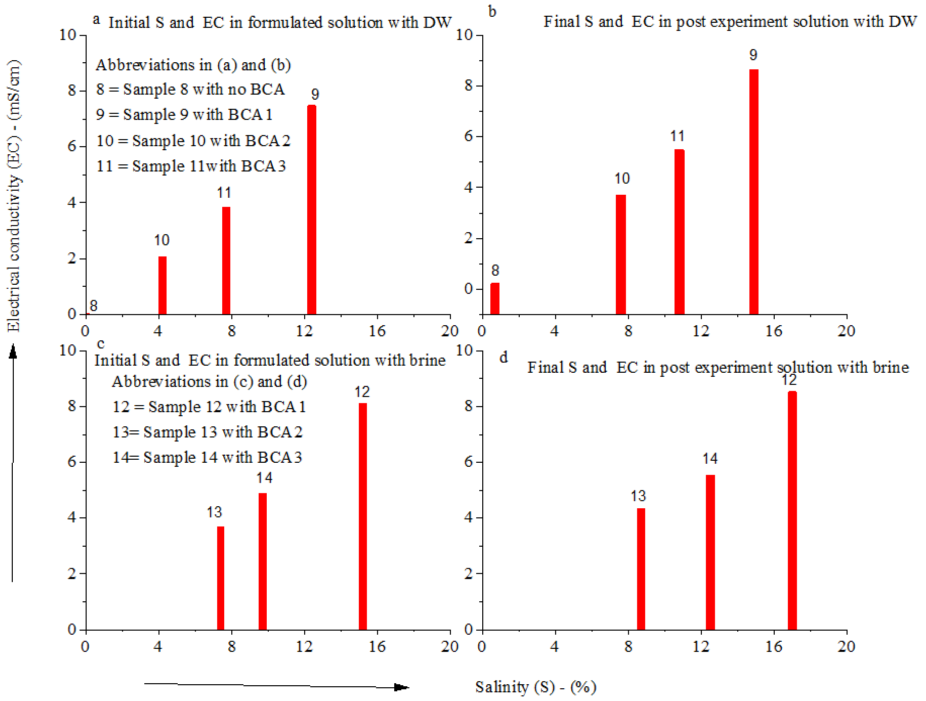

Fig. 5.11: Electrical conductivity versus salinity for formulated solutions and post-experiment solutions of KN samples; a) formulated solution with distilled water; b) post-experiment solution with distilled water; c) formulated solution with brine; d) post-experiment solution with brine

5.4.9 Multiple Linear Regression

The data shown in Table 5 is analyzed by multiple linear regression to predict the total normalized concentration of dissolved metal ions in the supernatant as a function of $pH_{initial}$ and Functional Groups (FG) of BCA in the supernatant of MM or KN with distilled water or brine. The IBM SPSS statistics 27 software is used. The data in Table 5.5 do not show any quadratic, polynomial, exponential, or logarithmic relation. Also, the literature does not suggest anything (Larson et al., 1996) and therefore a multiple linear regression analysis was done on the data. The R, p, and coefficient values are shown in Tables 5.6 and 5.7.

Table 5.5: Normalized total concentration of dissolved metal ions in the supernatant ($C_{nor\ total}$), $pH_{initial}$ of the formulated solution, and FG (number of functional groups of BCA)

	BCA	[$C_{nor\ total}$] (ppm.g/m^2)	$pH_{initial}$	FG
MM+ DW + CO_2	No BCA	1.0×10^{-3}	4.30	0
	BCA1	7.6×10^{-2}	9.91	6
	BCA2	3.8×10^{-3}	2.04	3
	BCA3	4.9×10^{-2}	2.22	4
MM + Brine + CO_2	BCA1	1.2×10^{-1}	8.16	6
	BCA2	7.6×10^{-3}	2.68	3
	BCA3	9.0×10^{-2}	2.72	4
KN + DW + CO_2	No BCA	2.0×10^{-3}	5.10	0
	BCA1	5.2×10^{-2}	9.83	6
	BCA2	1.1×10^{-2}	1.89	3
	BCA3	3.4×10^{-2}	2.03	4
KN + Brine + CO_2	BCA1	3.7×10^{-2}	8.82	6
	BCA2	3.9×10^{-3}	2.70	3
	BCA3	1.8×10^{-2}	2.48	4

[$C_{nor\ total}$] = Normalized total concentration of dissolved metal ions in supernatant

Table 5.6: R and p values on prediction of the normalized total concentration of dissolved metal ions in the supernatant ($C_{nor\ total}$) as a function of $pH_{initial}$ of formulated solution and FG (number of functional groups of BCA)

Supernatant	R^2	p
MM+ DW + CO_2	0.849	0.389
MM + Brine + CO_2	0.802	0.445
KN + DW + CO_2	0.923	0.278
KN + Brine + CO_2	0.935	0.256

Notes: R^2: coefficient of determination. p-value: Probability of obtaining results.

Table 5.7: Coefficient values on prediction of the normalized total concentration of dissolved metal ions in the supernatant ($C_{nor\ total}$) as a function of $pH_{initial}$ of formulated solution and FG (number of functional groups of BCA)

Supernatants	Parameter	Coefficients	Std. Error
MM+ DW + CO_2	Constant	-0.133	0.202
	pH	0.200	0.299
	FGs	0.532	0.335
MM + Brine + CO_2	Constant	-0.217	0.444
	pH	0.300	0.789
	FGs	0.935	0.620
KN + DW + CO_2	Constant	-0.131	0.221
	pH	0.216	0.294
	FGs	0.919	0.331
KN + Brine + CO_2	Constant	-0.217	0.163
	pH	0.363	0.243
	FGs	0.560	0.217

5.5 Discussion

The changes of surface properties and structural changes of the clay minerals (MM and KN) are discussed first, followed by the dissolved metal ions in solution, pH, conductivity, salinity, and the cause-effect statistical relationships.

5.5.1 BET surface area, and BJH pore area and volume

The non-dozed MM and KN clay samples (samples 1 and 8) show an increase in BET surface area (BET-SA), pore areas (BJH-PA), and pore volumes (BJH-PV) in comparison with the blank samples (Table 5.2 and 5.3). The increase in BET-SA, BJH-PA, and BJH-PV without dozing is possibly due to the sorption of CO_2. MM and KN clays are reported to have sorption capacity to carbon dioxide that can be trapped in the interlayer regions (Chen and Lu, 2015; Romanov, 2013). However, considering non-dozed MM or KN clay samples as the reference to dozed samples, a change in BET-SA, BJH-PA, and BJH-PV for dozed samples is observed. These changes in dozed samples are likely influenced by the presence of organic acids such as BCAs that modify the surface of clays because of either complexation, adsorption, intercalation, or cation exchange (Barrios et al., 2001; Hao et al., 2019; Lagaly, 1984; Lagaly et al., 2013). Other literature suggests that the changes in surface area, pore area, and volume are linked to lattice substitution (isomorphic) on the octahedral aluminum layer and tetrahedral silica layer (Altin et al., 1999; Badathala, 2015; Dai and Zhao, 2019; Gu et al., 2019a; Mokaya and Jones, 1995; Rufe and Hochella, 1999). The BET-SA in presence of BCA1 and BCA3 decreases while in the presence of BCA2 increases compared to BET-SA of non-dozed samples. The high number of amine functional groups in BCA1 that might induce alkalinity and the presence of R-groups (-CH_2COOH) in BCA-3 that might induce steric hindrance is likely to lower the reactivity and decrease the BET-SA.

Taking into account the BET-SA of the dozed samples in distilled water as the reference for dozed samples in brine experiments, the BET-SA in the presence of BCA2 decreases while in the presence of BCA3 and BCA1 increase. The reason for these changes is likely that the brine enhances the effect of–COOH thus the overall consequences are stronger for BCA1 with four –COOOH followed by BCA3 and BCA2 that have 2 and 3 -COOH, respectively. Distilled water experiments with KN instead of MM show a similar increase in BET-SA in the presence of BCA2 and the decrease in BET-SA in the presence of BCA3 is observed. In contrast, an increase in BET-SA is observed in the presence of BCA-1 which is likely contributed by the acidic nature of KN. Similar trends and reasons on BET-SA as in brine experiments with MM are observed for brine experiments with KN. The changes therefore in BET-SA, BJH-PA, and BJH-PV due to non-dozing and dozing with BCAs suggest changes of surface properties and structural changes of both MM and KN (Altin et al., 1999; Badathala, 2015; Gu et al., 2019a).

5.5.2 Attenuated Total Reflection Fourier Transform Infrared Spectroscopy (ATR-FTIR)

Comparison of the MM blank sample with sample 1 in Fig. S5.1 shows differences in absorption peaks and intensities. Sample 1 shows a peak at 3435 due to –OH, and other new peaks are present in the range of 1640-1400 cm^{-1}. The intensities of sample 1 are greater than that of the blank sample suggesting changes in the grain size of the clays becoming larger and capable to absorb more light. Further, a comparison of sample 1 which is the reference to samples 2, 3, and 4 shows similar features. However, the peak due to –OH at 3435 cm^{-1}, new peaks in the range of 1640-1400 cm$^{-1,}$ and greatest intensity are most explicit for sample 2. When brine is used instead of distilled water (Fig. S5.2), a similar peak for OH is observed in the range of 3660 – 3420 cm^{-1} and many new peaks are observed in the range of 2400 – 1200 cm^{-1}and the intensities for samples 5, 6, and 7 are considerably weaker than those for samples in distilled water suggesting that the grain sizes in the presence of brine are likely smaller and therefore less light is absorbed.

On the other hand, a comparison of the absorption peaks of samples 8 with the KN blank sample (Fig.S5.3) shows the disappearance of peaks at 1200 – 1700 cm^{-1} and lower intensity. In contrast, samples 9, 10, and 11 show peaks at 1200 – 1700 cm^{-1} when compared to sample 8 which is the reference to dozed samples. Further, samples 9, 10, and 11 show stronger intensity. Similar features are observed to sample 12, 13, and 14 when brine is used instead of distilled water (Fig.S5.4).

The differences in intensity and disappearance of absorption peaks in both non-dozed and dozed MM and KN suggest changes in surface properties and structure. The differences in cation radius, valence charge, and hydration energies of the exchangeable cations are likely to influence the absorption bands and intensity (Madejova and Komadel, 2001). The successive release of the central atoms Al/Si which is accompanied by the gradual transformation of the layered tetrahedral/octahedral sheet is also likely to influence the absorption bands and intensity. Moreover, the absence of strong evidence for chemical bonding of CO_2 and –OH to form carbonates even in the absence of BCAs suggests that CO_2 present in the system was likely physically adsorbed on clays.

5.5.3 Infrared reflectance spectroscopy

The comparison of reflectance spectra of sample 1 with MM blank sample (Fig. 5.4) lays on absorption depth where sample 1 has a lower absorption depth at 1410 and 1910 nm. Dozed samples compared to sample 1 show a similar feature at 1410 and 1910 nm. However, a doublet peak instead of a singlet is observed at 2208 nm on samples 2, 3, and 4. This doublet is likely due to internal re-arrangements that resulted in the formation of (FeMg)OH (Tripathi et al., 2020). Furthermore, weak absorption peaks at the 2300–2500 nm region are observed in sample 2, sample 3, and sample 4 and are related to the presence of Fe-OH and/or Mg-OH in the clay minerals, which are in agreement with the literature (Fang et al., 2018; Zhao et al., 2018). Replacing distilled water with brine, similar characteristics on formation of a doublet at 2208 nm and weak absorption peak at 2350 nm are observed on samples 5, 6, and 7 in Fig. 5.5. In addition, a similar decrease in absorption depth is observed at 1410 and 1910 nm for samples 6 and 7. However, sample 5 shows a decrease and increase in absorption depth at 1410 and 1910 nm, respectively. The decrease or increase in absorption depth is likely due to cation/molecule being exchanged to have either a larger or smaller radius. Cations or molecules with larger radius have a greater internal path and photons may be absorbed. The literature suggests that when a grain size becomes larger, more light is absorbed and the reflectance drops (Van der Meer et al., 2012).

Replacement of KN with MM shows an increase in absorption depth at 1900 nm for sample 8 in comparison with KN blank sample (Fig.5.6). This increase in absorption peak is due to an overtone caused by molecular water. Further comparison of dozed samples and sample 8 which is the reference shows that the right asymmetry of the 1400 nm absorption feature which is overtone caused by water and OH decreased in depth. In addition, the 1900 nm absorption feature for dozed samples increased in-depth compared to sample 8. The characteristic doublets at 2200 nm decreased in-depth in dozed samples as compared to sample 8. This decrease in depth is due to a combination of tones caused by Al-OH and which is in agreement with the literature (Cudahy et al., 2016). Additionally, some weak absorption bands in the 2300 – 2500 nm region which are related to the presence of Fe-OH and/or Mg-OH are observed. Similar characteristics in peaks are also observed on samples 12, 13, and sample 14 in brine tests (Fig. 5.7). The decrease or increase in absorption depth, disappearance, and formation of new peaks, therefore, suggest changes in structural and surface properties of the clay mineral brought by BCAs.

5.5.4 X-ray diffraction (XRD)

The XRD patterns of non-dozed samples in comparison with blank MM and KN did not show any significant change in diffractograms (Fig. S5.5 and S5.6). Similar results are obtained for dozed compared to non-dozed samples. This is likely due to new species formed or chemically removed from the clays as the consequence of the absence or presence of BCAs to be below the detection limit. The rule of thumb is that XRD has a detection limit of ~1% by volume (Schwantes et al., 2017; Treiman et al., 2010).

5.5.5 ICP-OES

The normalized total concentration of metal ions in supernatant shown in Table 5.4 for both MM and KN decreases in the order of BCA1 > BCA3 > BCA2 >No BCA. This suggests the presence of a dissolution-precipitation effect. The higher normalized concentrations of cations in the supernatant in the presence of BCA1 and BCA3 suggest the greater dissolution of MM and KN accompanied by low precipitation of metal ions while the lower normalized concentration of cations in the presence of BCA2 and no-BCA suggest lower dissolution accompanied by high precipitation. The occurrence of high precipitation in the sample with BCA2 or no-BCA is in agreement with the BET-SA results as these samples experienced larger BET-SA and expected to have more ions in solution. The ability of BCA to retain ions in solution is likely linked to the number of functional groups of each BCA. The trend suggests that the higher number of functional groups correlates with a higher concentration of dissolved metal ions in solution i.e low precipitation of metal ions. The reactivity of the chemical compounds such as BCAs is in agreement with the literature that the BCAs have a high propensity of being able to use their functional groups (Adewuyi and Pereira, 2016; Bucheli-Witschel and Egli, 2001; Hassan and Al-Hashim, 2016).

The high concentration of dissolved octahedral/tetrahedral metal ions (Al/Si) in supernatants is because protons of organic acids such as BCAs preferentially attack the isomorphic substituted elements (Belchinskaya et al., 2013; Crundwell, 2014; Dai and Zhao, 2019; Jeon and Nam, 2019; Lagaly et al., 2013; Yariv and Cross, 1979). To elaborate this, the BCAs tend to exist in anionic form (negatively charged form) because of high acidic strength (pKa) and therefore the dissociated protons attack the octahedral and tetrahedral layer elements of the MM and KN (Fig. 5.12). The released metal ions in the clay are then attacked by the anion chelating agents (reaction 5.1) and therefore remain in solution. Other literature suggests that dissolution of the clay minerals to release Al or Si is achieved through a surface complexation mechanism where the chelating agent is adsorbed on the surface of the clay mineral (Carbonaro et al., 2008; Tariq et al., 2017a). Moreover, the presence of other minerals such as Ca, Na, and Mg in solution are likely released from the clay minerals by ion-exchange reactions rather than by destruction of the framework (Hanna and Somasundaran, 1979; Kang and Xing, 2007). The released metal ions into the solution then bind with BCAs.

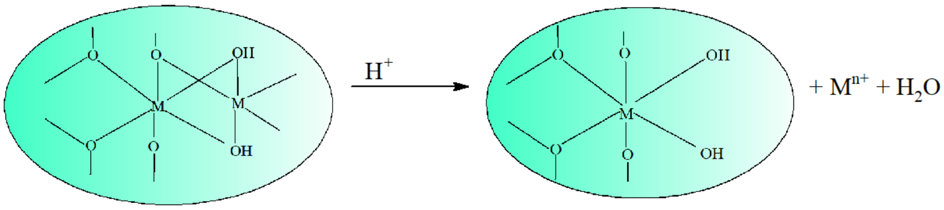

M = Al or Si

Fig. 5.12: Crystal lattice destruction of isomorphic substitution cations in the clay mineral

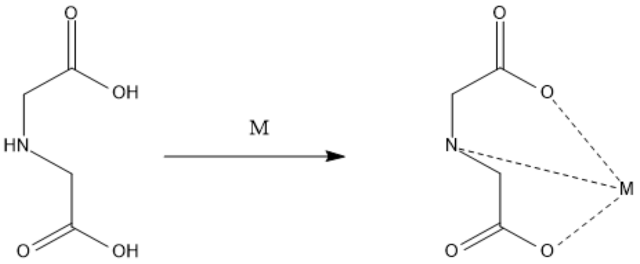

(5.1)

M = Al or Si

5.5.6 pH, conductivity and salinity

The increase in final pH in the presence of BCA2, BCA3, and no BCA, and the decrease in the presence of BCA1 (Fig.5.8b) in comparison with initial pH in Fig 5.8a suggest structural and property changes on MM which consequently lead to variation in accumulation of metal ions in solution. Despite the increase or decrease in final pH, the trend on final pH and electrical conductivity is BCA1 > BCA3 > BCA2 >No BCA which is in agreement with the trend in the total normalized concentration of metal ions. The increase in pH in the presence of BCA2, BCA3, and No BCA suggests that proton (H^+) replaces metal ions in the minerals and therefore the metal ions result in an increased value of pH as it interacts with BCAs. Further, the decrease in final pH in the presence of BCA1 suggests the anion of BCA1 exchanges with the aluminate or silicate anion. The same trend for pH and electrical conductivity is achieved when distilled water is replaced by brine. This trend is in agreement with the normalized concentration of metal ions in the solution. Replacing MM clay mineral with KN, the changes in initial pH and electrical conductivity for the formulated solution and final pH and electrical conductivity for post-experiment solution in either distilled water or brine (Fig. 5.9) follow the same trends as depicted in MM. Furthermore, plots of salinity against conductivity (Fig. 5.10 and 5.11) show that the conductivity increases as salinity increases and the trend is BCA1> BCA3> BCA2> No BCA which is also in agreement with the trend of the total normalized concentration of metal ions.

5.5.7 Multiple Linear Regression

The R- square values in Table 5.6 of the multiple linear regression show a strong correlation between the variables. The pH and functional groups have a high influence on the normalized total concentration of dissolved metal ions in supernatants of MM or KN in distilled water or brine. However, the p-values show that the correlation is not significant because it is greater than the statistical accepted value which is 0.05. On the other hand, the coefficient values in Table 5.7 show that BCAs' functional groups have more influence on the normalized total concentration than the pH. The results of the regression are strongly in agreement with the chemistry that functional groups are the most determinant of reactivity of the compound or molecule. The higher the number of functional groups, the higher the concentration of dissolved metal ions in the solution.

5.6 Conclusion

In this study, biodegradable chelating agents (BCAs) that are often used in acid stimulation interact with clay minerals Kaolinite-natural (KN) and montmorillonite K10 (MM) under simulated geothermal reservoir conditions with temperature 230 °C and pressure 85 bar, in distilled water and a brine solution under a CO_2 environment. Analytical and statistical techniques are used to understand the interaction of BCAs and clay minerals. Porosimetry, Reflection Fourier Transform Infra-Red (ATR-FT-IR), infrared reflectance spectroscopy, and XRD are used to study the surface properties and structural changes of the clay minerals. Moreover, ICP-OES, pH, conductivity, and salinity are used to quantify the interaction of the clay minerals with BCAs under a CO_2 environment. The increase in BET surface area (BET-SA), pore areas (BJH-PA), and pore volumes (BJH-PV) of the non-dozed and dozed MM and KN evidenced by porosimeter results suggest changes in structural and surface properties. ATR-FTIR shows changes in light intensities, disappearance, and formation of new peaks while infrared reflectance spectroscopy shows an increase and decrease in absorption depth, changes in light intensities, and replacement of Al-OH peak with (FeMg)OH. These changes in absorption features are evidence of surface properties and structural changes in both KN and MM which in turn suggest an interaction between the clay minerals and BCAs. XRD shows insignificant variations in peak position and intensity. The ICP-OES, pH, salinity, and conductivity results strongly support the interaction in terms of dissolution.

These results show that BCA1 and BCA3 cause greater dissolution (more dissolved metal ions) which implies lower precipitation of ions from solution than BCA2 and no-BCA. The R values of the multiple linear regression show that the independent variables (pH and chelating functional groups) strongly influence the normalized concentration of dissolved metal ions. Further, the coefficient values show that BCAs' functional groups have more influence than pH. The study, therefore, suggests that BCA1 and BCA3 would be useful in improving permeability in reservoirs containing sizeable quantities of fine-grained materials such as clay minerals.

6 Synthesis

This chapter examines different literature sources on microbial influenced corrosion, and precipitation of clay minerals during reservoir acid stimulation and identifies their relationship to the thesis.

6.1 Introduction

This research aims to improve understanding of Microbial Influenced Corrosion (MIC), and understanding of precipitation of clay during acid stimulation in the reservoir as these both hamper flow assurance problems in the geo-energy industry. For MIC, the research aims at understanding the role of biofilm in corrosion due to Sulfate Reducing Bacteria (SRB) and the role of organic acid metabolites in SRB corrosion in oil and gas exploitation, and non-volcanic geothermal installations. Further, the research aims at understanding the influence of biodegradable chelating agents on the precipitation of clay minerals in the geothermal reservoir formation. The research has two goals: 1) to cover the gap on Microbiologically Influenced Corrosion (MIC) induced by SRB species that are the most important species for MIC, and ii) to cover the gap on clay mineral precipitation during reservoir acid stimulation.

6.2 Microbiologically influenced corrosion (MIC) by Sulfate Reducing Bacteria (SRB)

Microbiologically influenced corrosion (MIC) is more prevalent nowadays because of the pronounced increase of aging equipment (Chatterjee et al., 2021; Jia et al., 2018). MIC is documented as a multi-dollar billion problem in many settings including the geo-energy industry(Jia et al., 2018). The most commonly studied corrosive microbes in MIC are Sulfate reducing bacteria

(SRB) because SRB constitute half of all the instances of MIC failures (Bao et al., 2011). SRB utilizes sulfate as a terminal electron acceptor for anaerobic respiration and uses low molecular weight organic compounds as the carbon source for energy. SRB depends on fermentative bacteria which cleave and ferment the complex organic matter to low-molecular-weight organic compounds. SRB metabolic activities are related to environmental conditions such as environmental pH. Based on environmental pH, SRB can be divided into three groups namely, acidophilic (2.9 to 6.5), alkaliphilic (6.9 to 9.9), and neutrophilic (6–8) (Sen and Johnson, 1999; Sorokin et al., 2015; Widdel, 1988). The metabolic flexibility of SRB helps to increase their chance of survival when environmental conditions change. If sulfate resources (electron acceptors) become limited, SRB may continue to be active due to this association with other microbes such as methanogens, acetogenic, and fermentative bacteria (acid-producing bacteria) (Cord-Ruwisch et al., 1987; Tran et al., 2021). This coexistence helps SRB to obtain enough energy for their survival and growth.

The distribution of microbes in a microbial community is not homogeneous (Almela et al., 2021a; Davis and Isberg, 2016). Given the heterogeneous nature of the SRB environment due to chemical composition, physical parameters, and the complexity of microbiological processes, the identification of the microbial metabolites responsible for corrosion becomes more complicated (Bao et al., 2012). Recent studies have shown that results from abiotic sulfide experiments to simulate SRB corrosion are similar with SRB experiments (Fatah et al., 2013). However, the overwhelming majority of simulations of SRB corrosion with abiotic sulfide are focused on H_2S as the only

SRB metabolic product. The presence of EPS (biofilm), CO_2, and metabolites from other microbes such as low-molecular-weight organic compounds were neglected (Fatah et al., 2013). These metabolites modify the chemistry between the material-solution interface that in turn affects the thermodynamics and kinetics of the material surface (Wong et al., 2021).

In Chapters 3 and 4, the roles of biofilm and organic acid metabolites in SRB corrosion are investigated in the presence of abiotic sulfide (to mimic SRB metabolic end product H_2S) and CO_2 (to mimic CO_2 from SRB dissimilatory sulfate reduction). Understanding the role of biofilm low-molecular-weight organic compounds (organic acid metabolites) has strong implications for the mitigation of corrosion. This enables the quantification of the severity of MIC threat and the relative vulnerability of different materials to MIC which in turn enables the design of materials for casings, pipes, and other installations that can resist corrosive environments. Moreover, this enables the elucidation of other roles of other microbial metabolites.

6.3 Precipitation of clay minerals during reservoir acid stimulation

The exploitation of geothermal wells is dependent on natural or induced mineral precipitation and associated decrease in permeability of the system. This may hinder the fluid flow in well casings or rock fractures and thus decrease the heat extraction from the system. Reacting fluids such as acids are used to react and remove materials that restrict fluid flow, and due to their low cost, reacting fluids are becoming more and more common (Portier et al., 2007). The goal of using reacting fluids is to improve well productivity or injectivity by enhancing rock permeability without damaging the mother rock. The type of rock (local mineralogy), the type of formation damage (in the damaged reservoir), thickness, and the number of the permeable zone are crucial factors when designing the acid treatment (Veldkamp, 2015). For example, disturbance of the chemistry of the reservoir containing clay minerals may lead to precipitation of minerals, blocking pore throats.

Different acid combinations of stimulating agents have been developed to acquire the best results related to permeability, porosity, and precipitation, but still, there are some limitations associated with such combinations (Shafiq and Mahmud, 2017). These include fast spending of acid, precipitation reactions, less penetration of acids, and corrosion of pipelines. New acid combinations are required to be developed for heterogeneous carbonates and clay-rich sandstone acidizing because of the limitations of acid combinations at high-temperature and precipitation of clay minerals. Chelating agents are usually more suitable for heterogeneous carbonates and clay-rich sandstones. However, the use of chelating agents as stand-alone stimulation fluids to improve reservoir permeability is still a premature research field that requires more exploration. In Chapter 5, the influence of biodegradable chelating agents (BCAs) on clay mineral precipitation is evaluated. The results have two strong implications in the geo-energy industry. The BCAs were stable at high temperature $T > 200$ °C. Further, the high number of chemical functional groups and molecular weight enhanced the efficiency of lowering clay mineral precipitation.

7 Conclusion[9]

This chapter provides the conclusion and recommendations for further research.

7.1 Conclusion

The work in this thesis has given an understanding of the flow assurance problems in the geo-energy industry, specifically on Microbial Influence Corrosion (MIC) and precipitation of clay minerals due to reservoir acid stimulation. The role of biofilm in MIC on carbon steel (API 5L X70M HFW) due to Sulfate Reducing Bacteria (SRB) and the role of organic acid metabolites in SRB corrosion are investigated. Simulated biofilm made of calcium alginate, abiotic sulfide (to mimic SRB metabolic end product H_2S), CO_2 (to mimic CO_2 from SRB dissimilatory sulfate reduction), and simulated brine (3.0 wt% NaCl) are used to simulate the SRB environment. In addition, simulated organic acid metabolites, namely acetic and L-ascorbic acids are used. Different temperatures (30, 45, and 60 °C) and exposure times (60 and 120 minutes) are used to establish the corrosion kinetics. For precipitation of clay minerals, the interaction is investigated of biodegradable chelating agents (BCA1, BCA2, and BCA3) and clay minerals kaolinite-natural (KN) and montmorillonite-K10 (MM) in a hydrothermal reactor in which the conditions of a geothermal reservoir are simulated under a CO_2 environment with a temperature of 230 °C and pressure of 85 bars.

---

[9] *This chapter is based on the three published articles (chapter 3,4 and 5).*

The electrochemical results on the role of simulated biofilm show that the simulated biofilm in the reference at 120 min exposure time and brine experiments neither inhibits nor accelerates corrosion. These results are strongly supported by corrosion kinetic adsorption parameters, statistical T-test, ICP-OES, pH, SEM-EDS, and XRD. The results contradict the existing literature on the role of biofilm and this is likely due to the presence of both H_2S and CO_2 as simulated SRB metabolites (Bao et al., 2012; Li et al., 2013; Procópio, 2019; Starkey, 1985). Despite this discrepancy, the obtained corrosion rates (0.25 to 1.6 mm/year) in the simulated SRB environment are comparable to published corrosion rates obtained in SRB experiments (0.20 to 1.2 mm/year). The results highlight the novelty of this research and have a direct impact on the role of other microbial metabolites on the corrosion of carbon steel. In addition, simulated H_2S, CO_2, and biofilm are representative of the SRB media for corrosion studies.

The electrochemical results on the role of organic acid metabolites show that both simulated organic acid metabolites accelerate corrosion in a simulated SRB environment. The results are further supported by electrochemical weight losses, kinetic corrosion activation parameters, multiple linear regression, ICP-OES, pH, and XRD. However, a comparison of electrochemical results with those published in the literature for a simulated SRB environment without acetic or L-ascorbic acid under similar experimental conditions shows that the presence of acetic in this study results in lower corrosion current densities while in presence of L-ascorbic acid results into higher corrosion current densities. This implies that acetic and L-ascorbic acids inhibit and accelerate corrosion, respectively. In addition, the results highlight that H_2S is the key role of corrosion in the presence of organic acid. The results of this study are important new and novel information on the role of acetic and L-ascorbic acids in corrosion of geo-energy pipelines in the SRB environment.

Results on precipitation of clay minerals following the interaction of biodegradable chelating agents (BCA1, BCA2, and BCA3) and clay minerals kaolinite-natural (KN) and montmorillonite-K10 (MM) show that BCA1 and BCA3 cause greater dissolution with lower precipitation as compared to BCA2 and no-BCA (ICP-OES, pH, conductivity and salinity results). The porosimetry, ATR-FTIR, and infrared reflectance spectroscopy show changes in surface properties and structure of MM and KN which in turn suggest chemical interaction to take place. However, XRD results show insignificant changes in the structure of MM and KN. Further, the R -values from multiple linear regression show that pH and BCAs' function groups have a strong influence on the normalized concentration of dissolved ions though the p-values are insignificant. The coefficient values show that the BCAs' functional groups have more influence than pH. BCA1 and BCA 3 would therefore be useful acids for reservoir stimulation in improving permeability, especially in geothermal reservoir formations which contain clay minerals.

7.2 What next?

The following recommendations are suggested for future research on the research topic of flow assurance problems (MIC and precipitation of clay minerals during reservoir acid stimulation) in the geo-energy industry.

1. Investigations on corrosion of SRB in association with other microbes such as methanogens, acetogenic, and fermentative bacteria (acid-producing bacteria).

2. Detection of corrosion products on the surface of carbon steel using techniques that require minimal sample preparation and have fast acquisition time such as hyperspectral sensors.
3. Influence of biodegradable chelating agents on other formation damage mechanisms such as rock−fluid and brine−fluid interactions.
4. Application of biodegradable chelating agents on other upstream activities in the geo-energy industry that are recognized as a cause of formation damage such as enhancing hydrocarbons (oil and gas) recovery, and drilling.

Bibliography

Abadeh, H. K., and Javidi, M. (2019). Assessment and influence of temperature, NaCl and H2S on CO2 corrosion behavior of different microstructures of API 5L X52 carbon steel in aqueous environments. *Journal of Natural Gas Science and Engineering* **67**, 93-107.

Adewuyi, A., and Pereira, F. V. (2016). Nitrilotriacetic acid functionalized Adansonia digitata biosorbent: Preparation, characterization and sorption of Pb (II) and Cu (II) pollutants from aqueous solution. *Journal of advanced research* **7**, 947-959.

Ahmad, K., Kristály, F., and Turzo, Z. (2018). Effects of clay mineral and physico-chemical variables on sandstone rock permeability. *Journal of Oil, Gas and Petrochemical Sciences* **1**, 18-26.

Ahmad, Z., & Institution of Chemical Engineers (Great Britain) (2006). "Principles of Corrosion Engineering and Corrosion Control," Boston, MA: Elsevier/BH.

Aksu, I., Bazilevskaya, E., and Karpyn, Z. (2015). Swelling of clay minerals in unconsolidated porous media and its impact on permeability. *GeoResJ* **7**, 1-13.

Al-Arji, H., Al-Azman, A., Le-Hussain, F., and Regenauer-Lieb, K. (2021). Acid stimulation in carbonates: A laboratory test of a wormhole model based on Damköhler and Péclet numbers. *Journal of Petroleum Science and Engineering* **203**, 108593.

Alabbas, F. M., and Mishra, B. (2013). Microbiologically influenced corrosion of pipelines in the oil & gas industry. *In* "Proceedings of the 8th Pacific Rim International Congress on Advanced Materials and Processing", pp. 3441-3448. Springer.

Aldakkan, B., Gomaa, A. M., Cairns, A. J., Sayed, M., and Alnoaimi, K. (2018). Low viscosity retarded acid system: A novel alternative to emulsified acids. *In* "SPE Kingdom of Saudi Arabia Annual Technical Symposium and Exhibition". OnePetro.

Alexander, B. K., Cumming, W., and Marini, L. (2016). Technical Review of Geothermal Potential of Ngozi and Songwe Geothermal Prospects, Tanzania. *Proceedings, 6th African Rift Geothermal Conference, Addis Ababa, Ethiopia, 2nd – 4th November 2016, UNEP ARGeo Project*.

Ali, S. A., Clark, W. J., Moore, W. R., and Dribus, J. R. (2010). Diagenesis and reservoir quality. *Oilfield Review* **22**, 14-27.

Almela, P., Justel, A., and Quesada, A. (2021a). Heterogeneity of microbial communities in soils from the Antarctic Peninsula region. *Frontiers in microbiology* **12**, 280.

Almela, P., Justel, A., and Quesada, A. (2021b). Heterogeneity of Microbial Communities in Soils From the Antarctic Peninsula Region. *Frontiers in microbiology* **12**, 628792.

Altin, O., Özbelge, H. Ö., and Dogu, T. (1999). Effect of pH in an aqueous medium on the surface area, pore size distribution, density, and porosity of montmorillonite. *Journal of Colloid and Interface Science* **217**, 19-27.

Amri, J., Gulbrandsen, E., and Nogueira, R. P. (2011). Role of acetic acid in CO2 top of the line corrosion of carbon steel. *NACE - International Corrosion Conference Series, Houston - USA*.

Anderson, R., Ratcliffe, I., Greenwell, H., Williams, P., Cliffe, S., and Coveney, P. (2010). Clay swelling—a challenge in the oilfield. *Earth-Science Reviews* **98**, 201-216.

Apostolopoulos, C. A., Demis, S., and Papadakis, V. G. (2013). Chloride-induced corrosion of steel reinforcement–Mechanical performance and pit depth analysis. *Construction and Building Materials* **38**, 139-146.

Aqui, A., and Zarrouk, S. (2011a). Permeability enhancement of conventional geothermal wells. *In* "New Zealand Geothermal Workshop", pp. 1.

Aqui, A., and Zarrouk, S. (2011b). Permeability Enhancement of Conventional Geothermal Wells. *Proceedings, the 33rd New Zealand Geothermal Workshop* **Auckland, New Zealand**, pp.1.

Archer, R. (2020). Geothermal Energy. *In* "Future Energy", pp. 431-445. Elsevier.

Audiffrin, C., Cayol, J.-L., Joulian, C., Casalot, L., Thomas, P., Garcia, J.-L., and Ollivier, B. (2003). Desulfonauticus submarinus gen. nov., sp. nov., a novel sulfate-reducing bacterium isolated from a deep-sea hydrothermal vent. *International journal of systematic and evolutionary microbiology* **53**, 1585-1590.

Badathala, V. (2015). Acid treated clays: preparation, characterization and catalytic activity for synthesis of quinoxaline derivatives. *Journal of Porous Materials* **22**, 779-786.

Bahadori, A. (2017). "Oil and gas pipelines and piping systems: design, construction, management, and inspection," Elsevier. Retrieved from https://app.knovel.com/hotlink/toc/id:kpOGPPSDC3/oil-gas-pipelines-piping/oil-gas-pipelines-piping.

Bahadori, A., Zendehboudi, S., and Zahedi, G. (2013). A review of geothermal energy resources in Australia: current status and prospects. *Renewable and Sustainable Energy Reviews, Elsevier* **21(c)**, 29-34.

Bai, Y., and Bai, Q. (2005). "Subsea Pipelines and Risers, Elsevier Ocean Engineering Book Series," Elsevier, Amsterdam.

Bao, Q., Zhang, D., Lv, D., and Wang, P. (2012). Effects of two main metabolites of sulphate-reducing bacteria on the corrosion of Q235 steels in 3.5wt.% NaCl media. *Corrosion Science* **65**, 405-413.

Bao, Q., Zhang, D., and Wan, Y. (2011). 2-Mercaptobenzothiazole doped chitosan/11-alkanethiolate acid composite coating: Dual function for copper protection. *Applied surface science* **257**, 10529-10534.

Barbier, E. (2002). Geothermal energy technology and current status: an overview. *Renewable and sustainable energy reviews* **6**, 3-65.

Barrios, M. S., de Santiago Buey, C., Romero, E. G., and Pozas, J. M. (2001). Textural and structural modifications of saponite from Cerro del Aguila by acid treatment. *Clay minerals* **36**, 483-488.

Barton, L. L., and Fauque, G. D. (2009). Biochemistry, physiology and biotechnology of sulfate-reducing bacteria. *Advances in applied microbiology* **68**, 41-98.

Batis, G., Kouloumbi, N., and Kotsakou, K. (1997). Corrosion and protection of carbon steel in low enthalpy geothermal fluids. The case of Sousaki in Greece. *Geothermics* **26**, 65-82.

Beech, I. B., and Gaylarde, C. C. (1999). Recent advances in the study of biocorrosion: an overview. *Revista de microbiologia* **30**, 117-190.

Beech, I. B., and Sunner, J. (2004). Biocorrosion: towards understanding interactions between biofilms and metals. *Current Opinion in Biotechnology* **15**, 181-6.

Beech, I. B., Zinkevich, V., Tapper, R., and Gubner, R. (1998). Direct involvement of an extracellular complex produced by a marine sulfate-reducing bacterium in deterioration of steel. *Geomicrobiology Journal* **15**, 121-134.

Belchinskaya, L., Novikova, L., Khokhlov, V., and Ly Tkhi, J. (2013). Contribution of ion-exchange and non-ion-exchange reactions to sorption of ammonium ions by natural and activated aluminosilicate sorbent. *Journal of Applied Chemistry* **2013**, 9.

Bertani, R. (2016). Geothermal power generation in the world 2010–2014 update report. *Geothermics* **60**, 31-43.

Blackwood, D. (2018). An electrochemist perspective of microbiologically influenced corrosion. *Corrosion and Materials Degradation* **1**, 59-76.

Bonis, M., and Crolet, J. (1989). Basics of the Prediction of the Risks of CO2 Corrosion in Oil and Gas Wells‖, Paper No. 466. *Corrosion/89, April*, 17-21.

Breede, K., Dzebisashvili, K., and Falcone, G. (2015). Overcoming challenges in the classification of deep geothermal potential. *Geothermal Energy Science* **3**, 19-39.

Bucheli-Witschel, M., and Egli, T. (2001). Environmental fate and microbial degradation of aminopolycarboxylic acids. *FEMS microbiology reviews* **25**, 69-106.

Cama, J., and Ganor, J. (2006). The effects of organic acids on the dissolution of silicate minerals: A case study of oxalate catalysis of kaolinite dissolution. *Geochimica et Cosmochimica Acta* **70**, 2191-2209.

Caneva, G., Nugari, M. P., and Salvadori, O. (2008). "Plant biology for cultural heritage: biodeterioration and conservation," Getty Publications.

Carbonaro, R. F., Gray, B. N., Whitehead, C. F., and Stone, A. T. (2008). Carboxylate-containing chelating agent interactions with amorphous chromium hydroxide: adsorption and dissolution. *Geochimica et Cosmochimica Acta* **72**, 3241-3257.

Chagneau, A., Claret, F., Enzmann, F., Kersten, M., Heck, S., Madé, B., and Schäfer, T. (2015). Mineral precipitation-induced porosity reduction and its effect on transport parameters in diffusion-controlled porous media. *Geochemical transactions* **16**, 1-16.

Chang, L., Burke, M. G., and Scenini, F. (2019). Understanding the effect of surface finish on stress corrosion crack initiation in warm-forged stainless steel 304L in high-temperature water. *Scripta Materialia* **164**, 1-5.

Chang, X., Chen, S., Yin, C., Cheng, S., Liu, T., and Yin, Y. (2010). Study of Fe3Al Corrosion Behavior in Simulating Marine Biofilm Environment. *Materials and Manufacturing Processes* **25**, 302-306.

Chatterjee, M., Fan, Y., Cao, F., Jones, A. A., Pilloni, G., and Zhang, X. (2021). Proteomic study of Desulfovibrio ferrophilus IS5 reveals overexpressed extracellular multi-heme cytochrome associated with severe microbiologically influenced corrosion. *Scientific reports* **11**, 1-11.

Chen, Y.-H., and Lu, D.-L. (2015). CO2 capture by kaolinite and its adsorption mechanism. *Applied Clay Science* **104**, 221-228.

Cheng, Y. F. (2013). "Stress Corrosion Cracking of Pipelines," John Wiley & Sons, Hoboken.

Chidiebere, M. A., Oguzie, E. E., Liu, L., Li, Y., and Wang, F. (2015). Ascorbic acid as corrosion inhibitor for Q235 mild steel in acidic environments. *Journal of Industrial and Engineering Chemistry* **26**, 182-192.

Civan, F. (2007). "Reservoir Formation Damage:: fundamentals, modeling, assessment,

and mitigation," 2nd ed. Gulf Professional Publishing.

Clarke, B. H., and Aguilera, A. M. (2001). Microbiologically influenced corrosion in fire sprinkler systems. *Fire Protection Engineering* **9**, 14-22.

Cody, A. D. (2007). "Geodiversity of geothermal fields in the Taupo Volcanic Zone," Science and Technical Pub., Department of Conservation.

Cord-Ruwisch, R., Kleinitz, W., and Widdel, F. (1987). Sulfate-reducing bacteria and their activities in oil production. *Journal of petroleum technology* **39**, 97-106.

Craddock, P. R., Bake, K. D., and Pomerantz, A. E. (2018). Chemical, molecular, and microstructural evolution of kerogen during thermal maturation: case study from the Woodford Shale of Oklahoma. *Energy & Fuels* **32**, 4859-4872.

Cramer, S. D., and Covino, B. S. (2003). "ASM Handbook: Corrosion: fundamentals, testing, and protection. Vol. 13 A," ASM international.

Crolet, J., and Bonis, M. (1983). pH measurements in aqueous CO2 solutions under high pressure and temperature. *Corrosion* **39**, 39-46.

Crundwell, F. (2014). The mechanism of dissolution of minerals in acidic and alkaline solutions: Part II Application of a new theory to silicates, aluminosilicates and quartz. *Hydrometallurgy* **149**, 265-275.

Cudahy, T., Caccetta, M., Thomas, M., Hewson, R., Abrams, M., Kato, M., Kashimura, O., Ninomiya, Y., Yamaguchi, Y., and Collings, S. (2016). Satellite-derived mineral mapping and monitoring of weathering, deposition and erosion. *Scientific reports* **6**, 1-12.

Curley, R. (2011). "Fossil fuels," Britannica Educational Publishing.

Dai, C., and Zhao, F. (2019). "Oilfield Chemistry," Springer, Singapore.

Dailynews (2020). Fuel wealth vast, TPDC explains. *In* "Daily News, https://www.habarileo.co.tz/habari/2020-04-095e8f51395a702.aspx". Tanzania Government, Dar es Salaam.

Daniilidis, A., Nick, H. M., and Bruhn, D. F. (2020). Interdependencies between physical, design and operational parameters for direct use geothermal heat in faulted hydrothermal reservoirs. *Geothermics* **86**, 101806.

Dariva, C. G., and Galio, A. F. (2014). Corrosion Inhibitors-Principles , Mechanisms and Applications *In* "Developments in Corrosion Protection", pp. 365-378. IntechOpen.

Davey, M. E., and O'toole, G. A. (2000). Microbial biofilms: from ecology to molecular genetics. *Microbiology and molecular biology reviews* **64**, 847-867.

Davis, K. M., and Isberg, R. R. (2016). Defining heterogeneity within bacterial populations via single cell approaches. *Bioessays* **38**, 782-790.

de Pater, C. H., and Shaoul, J. R. (2019). Stimulation for geothermal wells in the Netherlands. *Netherlands Journal of Geosciences* **98, e11**.

Dong, Z. H., Liu, T., and Liu, H. F. (2011). Influence of EPS isolated from thermophilic sulphate-reducing bacteria on carbon steel corrosion. *Biofouling* **27**, 487-495.

Dresel, P., and Rose, A. (2010). Chemistry and Origin of Oil and Gas Well Brines in western Pennsylvania, Open-File Oil and Gas Report 10-01.0. Pennsylvania geological survey.

Duckworth, O. W., and Martin, S. T. (2001). Surface complexation and dissolution of hematite by C1-C6 dicarboxylic acids at pH= 5.0. *Geochimica et Cosmochimica Acta* **65**, 4289-4301.

Dworkin, M. (2006). "The Prokaryotes: Vol. 1: Symbiotic Associations, Biotechnology, Applied Microbiology," Springer Science & Business Media.

Earle, S. (2019). "Physical geology," BCcampus Open Education.

Edenhofer, O., Pichs-Madruga, R., Sokona, Y., Seyboth, K., Matschoss, P., Kadner, S., Zwickel, T., Eickemeier, P., Hansen, G., and Schlömer, S. (2011). IPCC special report on renewable energy sources and climate change mitigation. *Prepared By Working Group III of the Intergovernmental Panel on Climate Change, Cambridge University Press, Cambridge, UK*.

El Hajj, H., Abdelouas, A., El Mendili, Y., Karakurt, G., Grambow, B., and Martin, C. (2013). Corrosion of carbon steel under sequential aerobic–anaerobic environmental conditions. *Corrosion Science* **76**, 432-440.

El Mendili, Y., Abdelouas, A., and Bardeau, J.-F. (2013). Impact of a sulphidogenic environment on the corrosion behavior of carbon steel at 90° C. *Rsc Advances* **3**, 15148-15156.

Faes, W., Lecompte, S., Van Bael, J., Salenbien, R., Bäßler, R., Bellemans, I., Cools, P., De Geyter, N., Morent, R., and Verbeken, K. (2019). Corrosion behaviour of different steel types in artificial geothermal fluids. *Geothermics* **82**, 182-189.

Fang, Q., Hong, H., Zhao, L., Kukolich, S., Yin, K., and Wang, C. (2018). Visible and near-infrared reflectance spectroscopy for investigating soil mineralogy: A review. *Journal of Spectroscopy* **2018**.

Farrell, N., Debenham, N., Wilson, L., Wilson, M., Healy, D., King, R. C., Holford, S. P., and Taylor, C. (2021). The effect of authigenic clays on fault zone permeability. *Journal of Geophysical Research: Solid Earth* **126**, e2021JB022615.

Fatah, M. C., and Ismail, M. C. (2013). Empirical equation of CO2corrosion with presence of low concentrations of acetic acid under turbulent flow conditions. *Corrosion Engineering, Science and Technology* **46**, 49-55.

Fatah, M. C., Ismail, M. C., Ari-Wahjoedi, B., and Kurnia, K. A. (2011). Effects of sulphide ion on the corrosion behaviour of X52 steel in a carbon dioxide environment at temperature 40°C. *Materials Chemistry and Physics* **127**, 347-352.

Fatah, M. C., Ismail, M. C., and Wahjoedi, B. A. (2013). Effects of sulphide ion on corrosion behaviour of X52 steel in simulated solution containing metabolic products species: a study pertaining to microbiologically influenced corrosion (MIC). *Corrosion Engineering, Science and Technology* **48**, 211-220.

Feng, L., Ma, X., and A-li, L. (2006). Influence of sulfide on corrosion of carbon steel. *Corrosion Science and Protection Technology* **18**, 180.

Feng, X., Simpson, A. J., and Simpson, M. J. (2005). Chemical and mineralogical controls on humic acid sorption to clay mineral surfaces. *Organic Geochemistry* **36**, 1553-1566.

Ferreira, E., Giacomelli, C., Giacomelli, F., and Spinelli, A. (2004). Evaluation of the inhibitor effect of L-ascorbic acid on the corrosion of mild steel. *Materials Chemistry and Physics* **83**, 129-134.

Field, B., Barton, B., Funnell, R., Higgs, K., Nicol, A., and Seebeck, H. (2018). Managing potential interactions of subsurface resources. *Proceedings of the Institution of Mechanical Engineers, Part A: Journal of Power and Energy* **232**, 6-11.

Frenier, W., Brady, M., Al-Harthy, S., Arangath, R., Chan, K. S., Flamant, N., and Samuel, M. (2004). Hot oil and gas wells can be stimulated without acids. *In* "SPE International Symposium and Exhibition on Formation Damage Control". Society of Petroleum Engineers.

Fritz, B., Jacquot, E., Jacquemont, B., Baldeyrou-Bailly, A., Rosener, M., and Vidal, O. (2010). Geochemical modelling of fluid–rock interactions in the context of the Soultz-sous-Forêts geothermal system. *Comptes Rendus Geoscience* **342**, 653-667.

Fuadi, A. (2019). Investigation of ascorbic acid as environment-friendly corrosion inhibitor of low carbon steel in marine environment. *In* "IOP Conference Series: Materials Science and Engineering", Vol. 536, pp. 012108. IOP Publishing.

Fuchs-Godec, R., Pavlović, M., and Tomić, M. V. (2013). The inhibitive effect of vitamin-C on the corrosive performance of steel in HCl solutions. *International Journal of Electrochemical Science* **8**, 1551-1519.

Fulignati, P. (2020). Clay Minerals in Hydrothermal Systems. *Minerals* **10**, 919.

Furrer, G., and Stumm, W. (1986). The coordination chemistry of weathering: I. Dissolution kinetics of δ-Al2O3 and BeO. *Geochimica et Cosmochimica Acta* **50**, 1847-1860.

Ganor, J., Cama, J., and Metz, V. (2003). Surface protonation data of kaolinite—reevaluation based on dissolution experiments. *Journal of colloid and interface science* **264**, 67-75.

Gdanski, R. (1997). Kinetics of the secondary reaction of HF on alumino-silicates. *Society of Petroleum Engineers, Production and Facilities* **14 (04)**, 260–268.

Gehringer, M., and Loksha, V. (2012). Geothermal handbook: planning and financing power generation. Energy Sector Management Assistance Program (ESMAP). *The International Bank for Reconstruction and Development, The World Bank Group, Washington DC, United States, Energy Sector Management Assistance Program technical report* **2**, 164.

Go, L. C., Depan, D., Holmes, W. E., Gallo, A., Knierim, K., Bertrand, T., and Hernandez, R. (2020). Kinetic and thermodynamic analyses of the corrosion inhibition of synthetic extracellular polymeric substances. *PeerJ Materials Science* **2**, e4.

Gray, M., Neerdael, B., and Degnan, P. (2013). Characterization of swelling clays as component of the Engineered Barrier system for Geological Repositories. *IAEA, Vienna International centre, Austria. wwwpub. iaea. org/MTCD/Publications/PDF/TE-178_web. pdf-1152 am* **10**, 2014.

Gu, S., Kang, X., Wang, L., Lichtfouse, E., and Wang, C. (2019a). Clay mineral adsorbents for heavy metal removal from wastewater: a review. *Environmental Chemistry Letters* **17**, 629-654.

Gu, T., Jia, R., Unsal, T., and Xu, D. (2019b). Toward a better understanding of microbiologically influenced corrosion caused by sulfate reducing bacteria. *Journal of materials science & technology* **35**, 631-636.

Gunderson, R., Cumming, W., Astra, D., and Harvey, C. (2000). Analysis of smectite clays in geothermal drill cuttings by the methylene blue method: for well site geothermometry and resistivity sounding correlation. *In* "Proceedings World Geothermal Congress", pp. 1175-1181.

Gunnlaugsson, E., Ármannsson, H., Thorhallsson, S., and Steingrímsson, B. (2014a). Problems in geothermal operation–scaling and corrosion. *Goethermal Training Program, United Nations University*, 1-18.

Gunnlaugsson, E., Ármannsson, H., Þórhallsson, S., and Steingrímsson, B. (2014b). Problems in geothermal operation-scaling and corrosion. *In: Short Course VI on utilization of low- and medium enthalpy geothermal resources and financial aspects of utilization, organized by UNU-GTP and LaGeo, in Santa Tecla, El Salvador*

Gupta, H. K., and Roy, S. (2006). "Geothermal energy: an alternative resource for the 21st century," Elsevier.

Hanna, H., and Somasundaran, P. (1979). Equilibration of kaolinite in aqueous inorganic and surfactant solutions. *Journal of Colloid and Interface Science* **70**, 181-191.

Hansen, B., and Davies, S. (1994). Review of potential technologies for the removal of dissolved components from produced water. *Chemical engineering research & design* **72**, 176-188.

Hao, W., Pudasainee, D., Gupta, R., Kashiwabara, T., Alessi, D. S., and Konhauser, K. O. (2019). Effect of acidic conditions on surface properties and metal binding capacity of clay minerals. *ACS Earth and Space Chemistry* **3**, 2421-2429.

Hassan, A., and Al-Hashim, H. (2016). Cost Effective Chelating Agent EOR Fluid System for Carbonate Reservoirs. *In* "SPE 182788 presented at Annual Technical Symposium and Exhibition, Dammam, Saudi Arabia", pp. 25-28.

He, J., Mohamed, I. M., and Nasr-El-Din, H. A. (2012). Mitigation of calcium sulfate scale formation when seawater is used to prepare HCl-based acids. *In* "SPE International Symposium and Exhibition on Formation Damage Control". OnePetro.

Helgeson, H. C., Murphy, W. M., and Aagaard, P. (1984). Thermodynamic and kinetic constraints on reaction rates among minerals and aqueous solutions. II. Rate constants, effective surface area, and the hydrolysis of feldspar. *Geochimica et Cosmochimica Acta* **48**, 2405-2432.

Hernandez, J., Muñoz, A., and Genesca, J. (2012). Formation of iron-carbonate scale-layer and corrosion mechanism of API X70 pipeline steel in carbon dioxide-saturated 3% sodium chloride. *Afinidad* **69**, 251-258.

Higgs, K., Haese, R., Golding, S., Schacht, U., and Watson, M. (2015). The Pretty Hill Formation as a natural analogue for CO2 storage: An investigation of mineralogical and isotopic changes associated with sandstones exposed to low, intermediate and high CO2 concentrations over geological time. *Chemical Geology* **399**, 36-64.

Hinz, N., Cumming, B., and Sussman, D. (2018). Exploration of fault-related deep-circulation geothermal resources in the western branch of the East African Rift System: examples from Uganda and Tanzania. *In* "In Proceedings, 7th African Rift Geothermal Conference, Kigali, Rwanda ".

Hodson, M. (2006). Searching for the perfect surface area normalizing term—a comparison of BET surface area-, geometric surface area-and mass-normalized dissolution rates of anorthite and biotite. *Journal of geochemical exploration* **88**, 288-291.

Hodson, M. E., Lee, M. R., and Parsons, I. (1997). Origins of the surface roughness of unweathered alkali feldspar grains. *Geochimica et Cosmochimica Acta* **61**, 3885-3896.

Hong, M.-S., Kim, S.-H., Im, S.-Y., and Kim, J.-G. (2016). Effect of ascorbic acid on the pitting resistance of 316L stainless steel in synthetic tap water. *Metals and Materials International* **22**, 621-629.

Hussain, A., Hasan, A., Javid, A., and Qazi, J. I. (2016). Exploited application of sulfate-reducing bacteria for concomitant treatment of metallic and non-metallic wastes: a mini review. *3 Biotech* **6**, 119.

Ibrahim, A., Hawboldt, K., Bottaro, C., and Khan, F. (2018). Review and analysis of microbiologically influenced corrosion: the chemical environment in oil and gas facilities. *Corrosion Engineering, Science and Technology* **53**, 549-563.

Jack, T. R., Wilmott, M. J., Sutherby, R. L., and Worthingham, R. G. (1996). External corrosion of line pipe--A summary of research activities. *Materials performance* **35**, 18-24.

Javed, M., Zahoor, S., Sabar, H., Haq, I., and Babar, M. (2012). Thermophilic bacteria from the hot springs of Gilgit (Pakistan). *J. Anim. Plant. Sci* **22**, 83-87.

Jeon, I., and Nam, K. (2019). Change in the site density and surface acidity of clay minerals by acid or alkali spills and its effect on pH buffering capacity. *Scientific reports* **9**, 1-10.

Jia, R., Tan, J. L., Jin, P., Blackwood, D. J., Xu, D., and Gu, T. (2018). Effects of biogenic H2S on the microbiologically influenced corrosion of C1018 carbon steel by sulfate reducing Desulfovibrio vulgaris biofilm. *Corrosion Science* **130**, 1-11.

Jia, R., Yang, D., Al-Mahamedh, H. H., and Gu, T. (2017). Electrochemical testing of biocide enhancement by a mixture of D-amino acids for the prevention of a corrosive biofilm consortium on carbon steel. *Industrial & Engineering Chemistry Research* **56**, 7640-7649.

Jiang, S. (2012). Clay minerals from the perspective of oil and gas exploration. *Clay Minerals in Nature-Their Characterization, Modification and Application. 1st ed. Rijeka, Croatia: InTech*, 21-38.

Junrong, L., Rongqiang, L., and Zhixue, S. (2015). Exploitation and utilization technology of geothermal resources in oil fields. *In* "Proceedings World Geothermal Congress Melbourne, Australia 2015".

Kagel, A., Bates, D., and Gawell, K. (2005). "A guide to geothermal energy and the environment," Geothermal Energy Association. Washington, DC (USA).

Kagel, A., Geothermal Energy Association., & United States (2008). "The State of Geothermal Technology: Part II: Surface Technology," Geothermal Energy Association, Washington, D.C.

Kajugus, S. I., Kabaka, K. T., and Mnjokava, T. T. (2018). Geothermal Development in Tanzania-a Country Update. *In* "The Proceedings, 7th African Rift Geothermal Conference Kigali, Rwanda 31st October–2nd November".

Kamal, M. S., Mahmoud, M., Hanfi, M., Elkatatny, S., and Hussein, I. (2019). Clay minerals damage quantification in sandstone rocks using core flooding and NMR. *Journal of Petroleum Exploration and Production Technology* **9**, 593-603.

Kang, S., and Xing, B. (2007). Adsorption of dicarboxylic acids by clay minerals as examined by in situ ATR-FTIR and ex situ DRIFT. *Langmuir* **23**, 7024-7031.

Karn, S. K., Fang, G., and Duan, J. (2017). Bacillus sp. acting as dual role for corrosion induction and corrosion inhibition with carbon steel (CS). *Frontiers in microbiology* **8**, 2038.

Karygianni, L., Ren, Z., Koo, H., and Thurnheer, T. (2020). Biofilm matrixome: extracellular components in structured microbial communities. *Trends in Microbiology* **28**, 668-681.

Kenaston, B. (2019). Malvern Panalytical's ASD TerraSpec® Halo for the Mine Geologist. [online] Materials Talks. Available at: https://www.materials-talks.com/blog/2018/04/10/malvern-panalyticals-asd-terraspec-halo-for-the-mine-geologist-an-overview-by-geometallurgist-stacey-leichliter/ [Accessed 6 Jun. 2019].

Khadom, A. A., Yaro, A. S., AlTaie, A., and Kadum, A. (2009). Electrochemical, activations and adsorption studies for the corrosion inhibition of low carbon steel in acidic media. *Portugaliae Electrochimica Acta* **27**, 699-712.

Khan, M., Hussain, M., and Djavanroodi, F. (2021). Microbiologically influenced corrosion in oil and gas industries: A review. *Int. J. Corros. Scale Inhib* **10**, 80-106.

Khanna, A., and Patwardhan, S. (2019). Integrating, Predicting and Preventing Flow Assurance Issues—A Review. *In* "Proceedings of the Fourth International Conference in Ocean Engineering (ICOE2018)", pp. 941-954. Springer.

Kiani Khouzani, M., Bahrami, A., Hosseini-Abari, A., Khandouzi, M., and Taheri, P. (2019). Microbiologically Influenced Corrosion of a Pipeline in a Petrochemical Plant. *Metals* **9**, 459.

Kim, M., Cho, A., Lim, H. S., Hong, S. G., Kim, J. H., Lee, J., Choi, T., Ahn, T. S., and Kim, O.-S. (2015). Highly heterogeneous soil bacterial communities around Terra Nova Bay of northern Victoria Land, Antarctica. *PLoS One* **10**, e0119966.

Kip, N., and Van Veen, J. A. (2015). The dual role of microbes in corrosion. *The ISME journal* **9**, 542-551.

Kisku, N. (2020). Strengthening of High-Alloy Steel through Innovative Heat Treatment Routes. *In* "Welding-Modern Topics". IntechOpen.

Kostecki, R., Ebendorff-Heidepriem, H., Davis, C., McAdam, G., Wang, T., and Monro, T. M. (2016). Fiber optic approach for detecting corrosion. Sensors and Smart Structures Technologies for Civil, Mechanical, and Aerospace Systems 2016 (Vol. 9803, p. 98031I). International Society for Optics and Photonics., Vol. 9803, pp. 98031I. International Society for Optics and Photonics.

Kristjansson, J. K. (1991). "Thermophilic bacteria," CRC press.

Kuila, U., and Prasad, M. (2013). Specific surface area and pore-size distribution in clays and shales. *Geophysical Prospecting* **61**, 341-362.

Kushkevych, I., Hýžová, B., Vítězová, M., and Rittmann, S. K.-M. (2021). Microscopic Methods for Identification of Sulfate-Reducing Bacteria from Various Habitats. *International Journal of Molecular Sciences* **22**, 4007.

Kvarekval, J., Nyborg, R., and Seiersten, M. (2002). Corrosion product films on carbon steel in semi-sour CO2/H2S environments. *In* "CORROSION 2002". NACE International.

Lagaly, G. (1984). Clay-organic interactions. *Philosophical Transactions of the Royal Society of London. Series A, Mathematical and Physical Sciences* **311**, 315-332.

Lagaly, G., Ogawa, M., and Dékány, I. (2013). Clay mineral–organic interactions. *In* "Developments in Clay Science", Vol. 5, pp. 435-505. Elsevier.

Larson, R., Hostetler, R. P., Hodgkins, A. V., and Heyd, D. E. (1996). "College algebra: Concepts and models," DC Heath.

Li, C. (2004). "Fine scale sandstone acidizing coreflood simulation," The University of Texas at Austin.

Li, H., Xu, D., Li, Y., Feng, H., Liu, Z., Li, X., Gu, T., and Yang, K. (2015a). Extracellular electron transfer is a bottleneck in the microbiologically influenced corrosion of C1018 carbon steel by the biofilm of sulfate-reducing bacterium Desulfovibrio vulgaris. *PloS one* **10**, e0136183.

Li, K., Bian, H., Liu, C., Zhang, D., and Yang, Y. (2015b). Comparison of geothermal with solar and wind power generation systems. *Renewable and Sustainable Energy Reviews* **42**, 1464-1474.

Li, K., Whitfield, M., and Van Vliet, K. J. (2013). Beating the bugs: roles of microbial biofilms in corrosion. *Corrosion Reviews* **31**, 73-84.

Li, N., Zhang, Q., Wang, Y., Liu, P., and Zhao, L. (2015c). A new multichelating acid system for high-temperature sandstone reservoirs. *Journal of Chemistry* **2015**.

Li, S.-L., Wang, Y.-J., Chen, Y.-C., Liu, S.-M., and Yu, C.-P. (2019). Chemical characteristics of electron shuttles affect extracellular electron transfer: shewanella decolorationis NTOU1 simultaneously exploiting acetate and mediators. *Frontiers in microbiology* **10**, 399.

Li, Y., and Ning, C. (2019). Latest research progress of marine microbiological corrosion and bio-fouling, and new approaches of marine anti-corrosion and anti-fouling. *Bioactive materials* **4**, 189-195.

Li, Y., Xu, D., Chen, C., Li, X., Jia, R., Zhang, D., Sand, W., Wang, F., and Gu, T. (2018). Anaerobic microbiologically influenced corrosion mechanisms interpreted using bioenergetics and bioelectrochemistry: a review. *Journal of Materials Science & Technology* **34**, 1713-1718.

Liang, R., Grizzle, R. S., Duncan, K. E., McInerney, M. J., and Suflita, J. M. (2014). Roles of thermophilic thiosulfate-reducing bacteria and methanogenic archaea in the biocorrosion of oil pipelines. *Front Microbiol* **5**, 89.

Liang, T., Gu, F., Yao, E., Zhang, L., Yang, K., Liu, G., and Zhou, F. (2017). Formation damage due to drilling and fracturing fluids and its solution for tight naturally fractured sandstone reservoirs. *Geofluids* **2017**.

Little, B., Blackwood, D., Hinks, J., Lauro, F., Marsili, E., Okamoto, A., Rice, S., Wade, S., and Flemming, H.-C. (2020). Microbially influenced corrosion–any progress? *Corrosion Science* **170**, 108641.

Little, B. J., and Lee, J. S. (2006). Diagnosing Microbiologically Influenced Corrosion. *In* "Microbiologically Influenced Corrosion", pp. 56-77. John Wiley & Sons, Inc.

Little, B. J., Lee, J. S., and Ray, R. (2006). Diagnosing microbiologically influenced corrosion: a state-of-the-art review. *Corrosion* **62**, 1006-1017.

Liu, H., Meng, G., Li, W., Liu, H., and Gu, T. (2019). Microbiologically influenced corrosion of carbon steel beneath a deposit in CO2-saturated formation water containing Desulfotomaculum nigrificans. *Frontiers in microbiology* **10**, 1298.

Liu, Q., Li, Z., Liu, Z., Li, X., and Wang, S. (2017). Effects of H 2 S/HS− on stress corrosion cracking behavior of X100 pipeline steel under simulated sulfate-reducing bacteria metabolite conditions. *Journal of Materials Engineering and Performance* **26**, 2763-2775.

Liu, W., and Ramirez, A. (2017). State of the art review of the environmental assessment and risks of underground geo-energy resources exploitation. *Renewable and Sustainable Energy Reviews* **76**, 628-644.

Lucas, Y., Ngo, V. V., Clément, A., Fritz, B., and Schäfer, G. (2020). Modelling acid stimulation in the enhanced geothermal system of Soultz-sous-Forêts (Alsace, France). *Geothermics* **85**, 101772.

Lugauskas, A., Prosycevas, I., Ramanauskas, R., Asta Griguceviciene, A., Selskiene, A., and Pakštas, V. (2009). The influence of micromycetes on the corrosion behaviour of metals (steel, al) under conditions of the environment polluted with organic substances. *Medziagotyra* **15**, 224-235.

Lund, J. W. (2008). Development and utilization of geothermal resources. *In* "Proceedings of ISES World Congress 2007 (Vol. I–Vol. V)", pp. 87-95. Springer.

Lund, J. W. (2018). Geothermal energy. *Encyclopædia Britannica. Encyclopædia Britannica, inc.*

Ma, H., Cheng, X., Li, G., Chen, S., Quan, Z., Zhao, S., and Niu, L. (2000). The influence of hydrogen sulfide on corrosion of iron under different conditions. *Corrosion science* **42**, 1669-1683.

Mackenzie, A. S., and Quigley, T. M. (1988). Principles of geochemical prospect appraisal. *AAPG bulletin* **72**, 399-415.

Madejova, J., and Komadel, P. (2001). Baseline studies of the clay minerals society source clays: infrared methods. *Clays and clay minerals* **49**, 410-432.

Madirisha, M., Hack, R., and Van der Meer, F. (2022a). The influence of chelating agents on clays in geothermal reservoir formations: Implications to reservoir acid stimulation. *Geothermics* **99**, 102305.

Madirisha, M., Hack, R., and Van der Meer, F. (2022b). The role of organic acid metabolites in geo-energy pipeline corrosion in a sulfate reducing bacteria environment. *Heliyon,* **8**, e09420.

Madirisha, M., Hack, R., and van der Meer, F. (2022c). Simulated microbial corrosion in oil, gas and non-volcanic geothermal energy installations: The role of biofilm on pipeline corrosion. *Energy Reports,* **8**, 2964-2975.

Madirisha, M., Lievens, C., Hack, R., and Van der Meer, F. (2019). The Influence of Chelating Agents on Clays of the Geothermal Cap Rock: Implications for Enhancing Geothermal Reservoir Quality: poster. *In* "International Conference on Energy, Aquatech and Sustainability 2019. https://www.researchgate.net/publication/335465557_The_Influence_of_Chelating_Agents_on_Clays_of_the_Geothermal_Cap_Rock_Implications_for_Enhancing_Geothermal_Reservoir_Quality".

Magot, M., Ollivier, B., and Patel, B. K. (2000). Microbiology of petroleum reservoirs. *Antonie van Leeuwenhoek* **77**, 103-116.

Magot, M., Tardy-Jacquenod, C., and Crolet, J.-L. (1997). An updated portrait of the sulfidogenic bacteria potentially involved in the microbial corrosion of steel. *Book-Institute of Materials* **686**, 3-10.

Mahmoud, M., Barri, A., and Elkatatny, S. (2017). Mixing chelating agents with seawater for acid stimulation treatments in carbonate reservoirs. *Journal of Petroleum Science and Engineering* **152**, 9-20.

Mahmoud, M. A., and Abdelgawad, K. Z. (2015). Chelating-Agent Enhanced Oil Recovery for Sandstone and Carbonate Reservoirs. *SPE Journal* **20**, 483-495.

Marcus, P. (2011). "Corrosion mechanisms in theory and practice," Crc Press.

Marshall, J. (1994). Origin, Diagenesis, and Petrophysics of Clay Minerals in Sandstones. Sepm Special Publication No. 47 by David W. Houseknecht and Edward D. Pitman, 1992; No. of pages: 282. Price: SEPM members 61.00;non-members 86.00. Wiley Online Library.

Mayo, A. W., and Mnzava, L. J. (2010). Geochemical investigation of geothermal power potential exploration of hot springs in South-western Tanzania. *International Journal of Water Resources and Environmental Engineering* **5(10)**, 601-611.

Metz, V., Cama, J., and Ganor, J. (1995). Toward defining the reactive surface area of dissolving smectite. *In* "GSA Abstracts", Vol. 27, pp. 184.

Metz, V., Raanan, H., Pieper, H., Bosbach, D., and Ganor, J. (2005). Towards the establishment of a reliable proxy for the reactive surface area of smectite. *Geochimica et Cosmochimica Acta* **69**, 2581-2591.

Miranda-Herrera, C., Sauceda, I., González-Sánchez, J., and Acuña, N. (2010). Corrosion degradation of pipeline carbon steels subjected to geothermal plant conditions. *Anti-Corrosion Methods and Materials* **57**, 167-172.

Miranda, E., Bethencourt, M., Botana, F., Cano, M., Sánchez-Amaya, J., Corzo, A., De Lomas, J. G., Fardeau, M.-L., and Ollivier, B. (2006). Biocorrosion of carbon steel alloys by an hydrogenotrophic sulfate-reducing bacterium Desulfovibrio capillatus isolated from a Mexican oil field separator. *Corrosion Science* **48**, 2417-2431.

Mnjokava, T. T., Kabaka, K., and Mayalla, J. (2012). Geothermal development in Tanzania–a country update. *In* "Proceedings of the 4th African Rift Geothermal Conference. Presented at the 4th African Rift Geothermal Conference, Nairobi, Kenya".

Moeck, I. S. (2014). Catalog of geothermal play types based on geologic controls. *Renewable and Sustainable Energy Reviews* **37**, 867-882.

Mokaya, R., and Jones, W. (1995). Pillared clays and pillared acid-activated clays: a comparative-study of physical, acidic, and catalytic properties. *Journal of Catalysis* **153**, 76-85.

Moore, J., and Allis, R. (2017). "Novel Geothermal Development of Deep Sedimentary Systems in the United States." Univ. of Utah and Energy & Geoscience Institute, Salt Lake City, UT (United ….

Mori, K., Tsurumaru, H., and Harayama, S. (2010). Iron corrosion activity of anaerobic hydrogen-consuming microorganisms isolated from oil facilities. *Journal of bioscience and bioengineering* **110**, 426-430.

Morozova, D., Alawi, M., Shaheed, M., Krüger, M., Kock, D., and Würdemann, H. (2011). The influence of microbial activity on rock fluid interaction: Baseline characterization of deep biosphere for Enhanced Gas Recovery in the Altmark natural gas reservoir. *Energy Procedia* **4**, 4633-4640.

Muhongo, S. (2013). Tanzania as an emerging energy producer. Africa meeting summary. Chatham house, London.

Munoz, A., Andrade, C., and Torres, A. (2007). Corrosion products pressure needed to crack the concrete cover. *Advances in Construction Materials 2007*, 359-370.

Muramatsu, Y., Komatsu, R., Sawaki, T., Sasaki, M., and Yanagiya, S. (2000). Geochemical study of fluid inclusions in anhydrite from the Kakkonda geothermal system, northeast Japan. *Geochemical Journal* **34**, 175-193.

NAM (2015). Technical evaluation of Twente water injection wells ROW3, ROW4, ROW7, ROW9, TUB7 and TUB10, 3 years after start of injection. *NAM report EP201410210164*, 45.

Naranjo, L., Pernía, B., Inojosa, Y., Rojas, D., D’Anna, L. S., González, M., and Sisto, Á. D. (2015). First Evidence of Fungal Strains Isolated and Identified from Naphtha Storage Tanks and Transporting Pipelines in Venezuelan Oil Facilities. *Advances in Microbiology* **05**, 143-154.

Nassif, L. A., Rioual, S., Farah, W., Hellio, C., Fauchon, M., Trepos, R., Abboud, M., Diler, E., Thierry, D., and Lescop, B. (2020). Reduction of potential ennoblement of stainless steel in natural seawater by an ecofriendly biopolymer. *Journal of Environmental Chemical Engineering* **8**, 103609.

Neff, J., Lee, K., and DeBlois, E. M. (2011). Produced Water: Overview of Composition, Fates, and Effects. *In* ": Lee K., Neff J. (eds) Produced Water", pp. 3-54, Springer, New York, NY.

Newman, R., Rumash, K., and Webster, B. (1992). The effect of pre-corrosion on the corrosion rate of steel in neutral solutions containing sulphide: relevance to microbially influenced corrosion. *Corrosion Science* **33**, 1877-1884.

Ngata, M. R., Yang, B., Aminu, M. D., Iddphonce, R., Omari, A., Shaame, M., Nyakilla, E. E., Mwakateba, I. A., Mwakipunda, G. C., and Yanyi-Akofur, D. (2021). Review of Developments in Nanotechnology Application for Formation Damage Control. *Energy & Fuels*.

Ngo, V. V., Lucas, Y., Clément, A., and Fritz, B. (2016). Modeling the impact of temperature on the saturation state and behavior of minerals in the Soultz-sous-Forêts geothermal system. *Geothermics* **64**, 196-208.

Nguyen, P. D., Weaver, J. D., Rickman, R. D., and Parker, M. A. (2005). Controlling formation fines at their sources to maintain well productivity. *In* "SPE International Improved Oil Recovery Conference in Asia Pacific". OnePetro.

Ngwira, C. M., and Pulkkinen, A. A. (2018). An overview of science challenges pertaining to our understanding of extreme geomagnetically induced currents. *Extreme Events in Geospace*, 187-208.

Nitters, G., Pittens, B., and Buik, N. (2016). Well Stimulation Techniques for Geothermal Projects in Sedimentary Basins. *Dutch Geothermal Research Agenda (Kennisagenda Aardwarmte), the Netherlands*.

Nogara, J., and Zarrouk, S. J. (2018a). Corrosion in geothermal environment Part 2: Metals and alloys. *Renewable and Sustainable Energy Reviews* **82**, 1347-1363.

Nogara, J., and Zarrouk, S. J. (2018b). Corrosion in geothermal environment: Part 1: Fluids and their impact. *Renewable and Sustainable Energy Reviews* **82**, 1333-1346.

Nor Asma, R., Yuli, P., and Mokhtar, C. (2011). Study on the Effect of Surface Finish on Corrosion of Carbon Steel in CO2 Environment. *Journal of Applied Sciences* **11**, 2053-2057.

Odusote, J. K., Ajiboye, T. K., and Rabiu, A. B. (2012). Evaluation of mechanical properties of medium carbon steel quenched in water and oil. *Journal of minerals and materials characterization and engineering* **11**, 859-862.

Okewale, A., and Adesina, O. (2020). Kinetics and thermodynamic study of corrosion inhibition of mild steel in 1.5 M HCl medium using cocoa leaf extract as inhibitor. *Journal of Applied Sciences and Environmental Management* **24**, 37-47.

Ouali, S., Hazmoune, M., and Bouzidi, K. (2015). Low Temperature Geothermal Energy for Rural Development. *European Conference on Renewable Energy Systems, Antalya, TURKEY*.

Owusu, P. A., and Asumadu-Sarkodie, S. (2016). A review of renewable energy sources, sustainability issues and climate change mitigation. *Cogent Engineering* **3**, 1167990.

Pan, J., Xiang, L., Chen, S., and Zhong, Y. (2017). Experimental study on electrochemical corrosion of FV520B in natural gas environment. *Results in physics* **7**, 4405-4411.

Parthipan, P., Elumalai, P., Karthikeyan, O. P., Ting, Y. P., and Rajasekar, A. (2017). A review on biodegradation of hydrocarbon and their influence on corrosion of carbon steel with special reference to petroleum industry. *Journal of Environment & Biotechnology Research* **6**, 12-33.

Pavlov, A., Shelegedin, V., Kogan, V., Pavlov, A., Vdovina, M., and Tret'iakov, A. (2007). Can microorganisms survive upon high-temperature heating during the interplanetary transfer by meteorites? *Biofizika* **52**, 1136-1140.

Pearce, J. K., Dawson, G. K., Blach, T. P., Bahadur, J., Melnichenko, Y. B., and Golding, S. D. (2018). Impure CO2 reaction of feldspar, clay, and organic matter rich cap-rocks: Decreases in the fraction of accessible mesopores measured by SANS. *International Journal of Coal Geology* **185**, 79-90.

Peksa, A., Ilangovan, N., Deon, F., Nick, M. H., and Bruhn, D. (2016). Kennisagenda Aardwarmte: A workflow for laboratory and numerical analysis of matrix acidizing in geothermal wells. *Kennisagenda Aardwarmte*

Pinto, I. S., Neto, I. F., and Soares, H. M. (2014). Biodegradable chelating agents for industrial, domestic, and agricultural applications--a review. *Environ Sci Pollut Res Int* **21**, 11893-906.

Plugge, C. M., Zhang, W., Scholten, J., and Stams, A. J. (2011). Metabolic flexibility of sulfate-reducing bacteria. *Frontiers in microbiology* **2**, 81.

Popoola, L. T., Grema, A. S., Latinwo, G. K., Gutti, B., and Balogun, A. S. (2013). Corrosion problems during oil and gas production and its mitigation. *International Journal of Industrial Chemistry* **4**, 35.

Portier, S., André, L., and Vuataz, F.-D. (2007). Review on chemical stimulation techniques in oil industry and applications to geothermal systems. *Engine, work package* **4**, 32.

Portier, S., Vuataz, F.-D., Nami, P., Sanjuan, B., and Gérard, A. (2009). Chemical stimulation techniques for geothermal wells: experiments on the three-well EGS system at Soultz-sous-Forêts, France. *Geothermics* **38**, 349-359.

Priisholm, S., Nielsen, B., and Haslund, O. (1987). Fines migration, blocking, and clay swelling of potential geothermal sandstone reservoirs, Denmark. *SPE Formation Evaluation* **2**, 168-178.

Procópio, L. (2019). The role of biofilms in the corrosion of steel in marine environments. *World Journal of Microbiology and Biotechnology* **35**, 73.

Provoost, M., Albeda, L., Godschalk, B., van der Werff, B., and Schoof, F. (2018). Geothermal energy use, country update for The Netherlands. *POLICY* **2015**, 3.1.

Rachel Angelo, S., Ehinola, O., Mtelela, C., and Edwin Ayuk, N. (2019). Intergrated Seismic Stratigraphic and Structural Analysis of the Songo Songo Gas-Field, Shallow Offshore Tanzania, Using Seismic and Well Data. *J Geol Geophys* **8**, 2.

Reinecker, J., Hochschild, T., Kraml, M., Löschan, G., and Kreuter, H. (2019). Experiences and challenges in geothermal exploration in the Upper Rhine Graben. *In* "Proceedings of European Geothermal Congress," pp. 11-12.

Revie, R., and Uhlig, H. (2008). "Corrosion and corrosion control: an introduction to corrosion science and engineering," Ed. 4/Ed. John Wiley & Sons, Hoboken New Jersey.

Riazi, M. (2005). "Characterization and properties of petroleum fractions," ASTM international.

Riskin, J., and Khentov, A. (2019). "Electrocorrosion and protection of metals," Elsevier.

Riyono, S., Siagian, U. W., Siregar, H. P. S., and Permadi, A. K. (2018). An Experimental Study of Clay Swelling Phenomenon by Carbonic Acid Injection in Clay Sandstone: Implication for CO2 Injection. *Modern Applied Science* **12**.

Roberts, E. M., O'Connor, P. M., Gottfried, M. D., Stevens, N., Kapalima, S., and Ngasala, S. (2004). Revised stratigraphy and age of the Red Sandstone Group in the Rukwa Rift Basin, Tanzania. *Cretaceous Research* **25**, 749-759.

Romanov, V. N. (2013). Evidence of irreversible CO2 intercalation in montmorillonite. *International Journal of Greenhouse Gas Control* **14**, 220-226.

Rose, P. E., Xu, T., Fayer, S., and Pruess, K. (2010). Chemical Stimulation for EGS: the use of chelating agents at high pH for the simultaneous dissolution of Calcium Carbonate, Silicas, and Silicates. *In* "Proceedings World Geothermal Congress".

Rufe, E., and Hochella, M. F. (1999). Quantitative assessment of reactive surface area of phlogopite during acid dissolution. *Science* **285**, 874-876.

Saeed, N., and Ronagh, H. R. (2015). Design of fibre-reinforced polymer overwraps for pipe pressure. *In* "Rehabilitation of pipelines using fiber-reinforced polymer (FRP) composites", pp. 211-223. Elsevier.

Saemundsson, K., Axelsson, G., and Steingrímsson, B. (2009). Geothermal systems in global perspective. Papers presented at “Short Course on Surface Exploration for Geothermal Resources”, organized by UNU-GTP and LaGeo, San Salvador, El Salvador, 16 pp.

Salvatore, M. M., and Salvatore, F. (2015). Understanding Complexometric Titrations of Metal Cations with Aminopolycarboxylic Acids (EDTA and Analogs) within the frame of the Notion of Reactions between Groups of Chemical Species. *World Journal of Chemical Education* **3**, 5-21.

Sameni, A., Pourafshary, P., Ghanbarzadeh, M., and Ayatollahi, S. (2015). Effect of nanoparticles on clay swelling and migration. *Egyptian journal of petroleum* **24**, 429-437.

Sanchez, J., Fullea, J., and Andrade, C. (2017). Corrosion-induced brittle failure in reinforcing steel. *Theoretical and Applied Fracture Mechanics* **92**, 229-232.

Sanchez Roa, C., Saldi, G., Mitchell, T., Iacoviello, F., Striolo, A., Meredith, P., Jones, A., and Oelkers, E. (2019). Experimental study of fluid-rock interaction and permeability evolution in granite: applications to geothermal energy reservoirs in Cornwall. *In* "AGU Fall Meeting Abstracts", Vol. 2019, pp. MR11C-0064.

Sand, W. (2003). Microbial life in geothermal waters. *Geothermics* **32**, 655-667.

Sand, W., and Gehrke, T. (2003). Microbially influenced corrosion of steel in aqueous environments. *Reviews in Environmental Science and Biotechnology* **2**, 169-176.

Schwantes, J. M., Marsden, O., and Pellegrini, K. L. (2017). State of practice and emerging application of analytical techniques of nuclear forensic analysis: highlights from the 4th Collaborative Materials Exercise of the Nuclear Forensics International Technical Working Group (ITWG). *Journal of Radioanalytical and Nuclear Chemistry* **311**, 1441-1452.

Sen, A., and Johnson, B. (1999). Acidophilic sulphate-reducing bacteria: candidates for bioremediation of acid mine drainage. *In* "Process metallurgy", Vol. 9, pp. 709-718. Elsevier.

Shafiq, M. U., and Mahmud, H. B. (2017). Sandstone matrix acidizing knowledge and future development. *Journal of Petroleum Exploration and Production Technology* **7**, 1205-1216.

Shafiq, M. U., Mahmud, H. K. B., and Arif, M. (2018). Mineralogy and pore topology analysis during matrix acidizing of tight sandstone and dolomite formations using chelating agents. *Journal of Petroleum Science and Engineering* **167**, 869-876.

Sherar, B., Power, I., Keech, P., Mitlin, S., Southam, G., and Shoesmith, D. (2011). Characterizing the effect of carbon steel exposure in sulfide containing solutions to microbially induced corrosion. *Corrosion Science* **53**, 955-960.

Simon, D., and Anderson, M. (1990). Stability of clay minerals in acid: Society of Petroleum Engineers. *In* "9th SPE Symposium on Formation Damage, Lafayette, Louisiana, SPE", Vol. 19413, pp. 201-212.

Singer, M. (2017). Top-of-the-line corrosion. *Trends in Oil and Gas Corrosion Research and Technologies; Elsevier*, 385-408.

Singh, M., and Gupta, A. (2000). Corrosion behavior of mild steel in acetic acid solutions. *Corrosion* **56**, 371-379.

Singh, S., and Mukherjee, A. (2010). Kinetics of mild steel corrosion in aqueous acetic acid solutions. *Journal of Materials Science & Technology* **26**, 264-269.

Sorokin, D., Chernyh, N., and Poroshina, M. (2015). Desulfonatronobacter acetoxydans sp. nov.: a first acetate-oxidizing, extremely salt-tolerant alkaliphilic SRB from a hypersaline soda lake. *Extremophiles* **19**, 899-907.

Starkey, R. L. (1985). Anaerobic Corrosion--Perspectives About Causes. *Biologically Induced Corrosion*, 3-7.

Stoch, L. (1990). Chemical reactions of clay minerals and their utilization. *In* " Proceedings of the 9th International Clay Conference, Strasbourg, 1989, V.C. FARMER and Y. TARDY (Eds), Sciences Géologiques. Mémoire", Vol. 89, pp. 111-120.

Streicher, M. (2011). Uhlig's Corrosion Handbook 3rd Edition ed RW Revie (Hoboken, NJ. John Wiley & Sons.

Stumm, W. (1992). Chemistry of the solid-water interface: processes at the mineral-water and particle-water interface in natural systems.

Stumm, W. (1997). Reactivity at the mineral-water interface: dissolution and inhibition. *Colloids and Surfaces A: Physicochemical and Engineering Aspects* **120**, 143-166.

Sumi, L. (2005). Produced Water from Oil and Gas Production: Toxics in Our Communities. *Presentation at the 2005 People's Oil and Gas Summit. Farmington, New Mexico*

Tariq, A., Hong, J. N., and Nasr-El-Din, H. (2017a). "Chelating Agents in Productivity Enhancement: A Review. SPE Oklahoma City Oil and Gas Symposium, Oklahoma City, Oklahoma, USA, 27-31 March." SPE-185097-MS. https://doi. org/10.2118/185097-MS.

Tariq, A., Hong, J. N., and Nasr-El-Din, H. (2017b). Oilfield scale removal by chelating agents: An aminopolycarboxylic acids review. *In* "SPE Western Regional Meeting". Society of Petroleum Engineers.

Theyab, M. A. (2018). Fluid flow assurance issues: literature review. *SciFed Journal of Petroleum* **2**, 1-11.

Thomas, R., Nasr-El-Din, H., Mehta, S., Hilab, V., and Lynn, J. (2002). The impact of HCl to HF ratio on hydrated silica formation during the acidizing of a high temperature sandstone gas reservoir in Saudi Arabia. *In* "SPE Annual Technical Conference and Exhibition". Society of Petroleum Engineers.

Toth, A., and Bobok, E. (2016). "Flow and Heat Transfer in Geothermal Systems: Basic Equations for Describing and Modeling Geothermal Phenomena and Technologies," Elsevier.

Tournassat, C., Bourg, I. C., Steefel, C. I., and Bergaya, F. (2015). Surface properties of clay minerals. *In* "Developments in clay science", Vol. 6, pp. 5-31. Elsevier.

Tran, T. T. T., Kannoorpatti, K., Padovan, A., and Thennadil, S. (2021). Sulphate-Reducing Bacteria's Response to Extreme pH Environments and the Effect of Their Activities on Microbial Corrosion. *Applied Sciences* **11**, 2201.

Treiman, A., Robinson, K., Blake, D., and Bish, D. (2010). Mineralogy determinations by CheMin Xrd, tested on ultramafic rocks (mantle xenoliths). *LPICo* **1538**, 5351.

Tripathi, M. K., Govil, H., and Chattoraj, S. (2020). Identification of hydrothermal altered/weathered and clay minerals through airborne AVIRIS-NG hyperspectral data in Jahajpur, India. *Heliyon* **6**, e03487.

TU-Delft (2018). Geo-energy.https://www.tudelft.nl/en/energy/research/geo-energy. Vol. 2021.

Van der Meer, F. D., Van der Werff, H. M., Van Ruitenbeek, F. J., Hecker, C. A., Bakker, W. H., Noomen, M. F., Van Der Meijde, M., Carranza, E. J. M., De Smeth, J. B., and Woldai, T. (2012). Multi-and hyperspectral geologic remote sensing: A review. *International Journal of Applied Earth Observation and Geoinformation* **14**, 112-128.

Vandenbroucke, M. (2003). Kerogen: from types to models of chemical structure. *Oil & gas science and technology* **58**, 243-269.

Veldkamp, J. G., Boxem, T. T., Waldmann, S. S., Candela, T. T., Nepveu, M. M., & van der Gijp, S. S (2015). Sector Outlook: Geothermal power increase in the Netherlands by enhancing the capacity (TNO 2015 R11618 | Final report). *Energy/Geological Survey of the Netherlands, TNO, Utrecht, Netherlands Utrecht*.

Veldkamp, J. G., Goldberg, T.V., Bressers, P.M.M.C and Wilschut, F (2016). Corrosion in Dutch geothermal systems (TNO 2015 R10160 | Final report). *Energy/Geological Survey of the Netherlands, TNO, Utrecht, Netherlands*, 105.

Videla, H., and Herrera, L. (2004). Biocorrosion. *In* "Studies in Surface Science and Catalysis", Vol. 151, pp. 193-218. Elsevier.

Videla, H. A., and Characklis, W. G. (1992). Biofouling and microbially influenced corrosion. *International Biodeterioration & Biodegradation* **29**, 195-212.

Videla, H. A., and Herrera, L. K. (2005). Microbiologically influenced corrosion: looking to the future. *International microbiology* **8**, 169.

Videla, H. A., and Herrera, L. K. (2009). Understanding microbial inhibition of corrosion. A comprehensive overview. *International Biodeterioration & Biodegradation* **63**, 896-900.

Vigneron, A., Head, I. M., and Tsesmetzis, N. (2018). Damage to offshore production facilities by corrosive microbial biofilms. *Applied microbiology and biotechnology* **102**, 2525-2533.

Vilarrasa, V., Makhnenko, R. Y., and Parisio, F. (2020). Geomechanics and Fluid Flow in Geothermal Systems. *Geofluids* **2020**, 6085738.

Vitaller, A. V., Angst, U. M., and Elsener, B. (2020). Laboratory tests simulating corrosion in geothermal power plants: influence of service conditions. *Geothermal Energy* **8**, 1-17.

von Bloh, W., Jørgensen, S., and Fath, B. (2008). Climate change 2: long-term dynamics. *In* "Encyclopedia of Ecology (Vol. 1)", pp. 592-598. Elsevier.

Wang, D., Liu, J., Jia, R., Dou, W., Kumseranee, S., Punpruk, S., Li, X., and Gu, T. (2020). Distinguishing two different microbiologically influenced corrosion (MIC) mechanisms using an electron mediator and hydrogen evolution detection. *Corrosion Science* **177**, 108993.

Wang, J., Meng, L., Fan, Z., Liu, Q., and Tong, Z. (2019). Mechanism and modelling of CO2 corrosion on downhole tools. *Royal Society Open Science* **6**, 181899.

Wang, S., Yan, J., Li, F., Hu, J., and Li, K. (2016a). Exploitation and Utilization of Oilfield Geothermal Resources in China. *Energies* **9**.

Wang, S., Yan, J., Li, F., Hu, J., and Li, K. (2016b). Exploitation and utilization of oilfield geothermal resources in China. *Energies* **9**, 798.

Wang, Z. (2018). The Effect of Temperature on the Hydrogen Permeation of Pipeline Steel in Wet Hydrogen Sulfide Environments. *International Journal of Electrochemical Science* **13**, 915-924.

Welte, D., and Tissot, P. (1984). "Petroleum formation and occurrence," Springer.

Widdel, F. (1988). Microbiology and ecology of sulfate-and sulfur-reducing bacteria. *Biology of anaerobic microorganisms.*, 469-585.

Wilson, M., Wilson, L., and Patey, I. (2014). The influence of individual clay minerals on formation damage of reservoir sandstones: a critical review with some new insights. *Clay Minerals* **49**, 147-164.

Wolf, P. G., Biswas, A., Morales, S. E., Greening, C., and Gaskins, H. R. (2016). H2 metabolism is widespread and diverse among human colonic microbes. *Gut Microbes* **7**, 235-245.

Wong, G. C., Antani, J. D., Lele, P. P., Chen, J., Nan, B., Kühn, M. J., Persat, A., Bru, J.-L., Høyland-Kroghsbo, N. M., and Siryaporn, A. (2021). Roadmap on emerging concepts in the physical biology of bacterial biofilms: from surface sensing to community formation. *Physical biology* **18**, 051501.

Xiao, J., Wang, J., and Sun, X. (2017). Fines migration: problems and treatments. *Oil & Gas Research* **3**, 123.

Xiao, M., Sun, S.-S., Zhang, Z.-Z., Wang, J.-M., Qiu, L.-W., Sun, H.-Y., Song, Z.-Z., Zhang, B.-Y., Gao, D.-L., and Zhang, G.-Q. (2016a). Analysis of bacterial diversity in two oil blocks from two low-permeability reservoirs with high salinities. *Scientific reports* **6**, 1-10.

Xiao, M., Sun, S. S., Zhang, Z. Z., Wang, J. M., Qiu, L. W., Sun, H. Y., Song, Z. Z., Zhang, B. Y., Gao, D. L., Zhang, G. Q., and Wu, W. M. (2016b). Analysis of bacterial diversity in two oil blocks from two low-permeability reservoirs with high salinities. *Sci Rep* **6**, 19600.

Xiong, H., and Holditch, S. A. (1995). A comprehensive approach to formation damage diagnosis and corresponding stimulation type and fluid selection. *In* "SPE Production Operations Symposium". Society of Petroleum Engineers.

Xu, D., Li, Y., and Gu, T. (2016). Mechanistic modeling of biocorrosion caused by biofilms of sulfate reducing bacteria and acid producing bacteria. *Bioelectrochemistry* **110**, 52-58.

Yang, M. (2011). Measurement of oil in produced water. *In* "Produced water", pp. 57-88. Springer.

Yariv, S., and Cross, H. (1979). Colloid geochemistry of clay minerals. *In* "Geochemistry of Colloid Systems", pp. 287-333. Springer.

Yuan, S., Liang, B., Zhao, Y., and Pehkonen, S. (2013). Surface chemistry and corrosion behaviour of 304 stainless steel in simulated seawater containing inorganic sulphide and sulphate-reducing bacteria. *Corrosion Science* **74**, 353-366.

Zarrouk, A., Hammouti, B., Zarrok, H., Al-Deyab, S., and Messali, M. (2011). Temperature effect, activation energies and thermodynamic adsorption studies of L-cysteine methyl ester hydrochloride as copper corrosion inhibitor in nitric acid 2M. *Int. J. Electrochem. Sci* **6**, 6261-6274.

Zhang, L., Yan, M., Zhang, S., Zhu, L., Umoh, A., Ma, A., Zheng, Y., and Wang, J. (2020). Significantly enhanced resistance to SRB corrosion via Fe-based amorphous coating designed with high dose corrosion-resistant and antibacterial elements. *Corrosion Science* **164**, 108305.

Zhang, Y., Du, M., Zhang, J., and Du, J. (2015). Corrosion behavior of X65 carbon steel in simulated oilfield produced water. *Materials and Corrosion* **66**, 366-374.

Zhao, L., Hong, H., Liu, J., Fang, Q., Yao, Y., Tan, W., Yin, K., Wang, C., Chen, M., and Algeo, T. J. (2018). Assessing the utility of visible-to-shortwave infrared reflectance spectroscopy for analysis of soil weathering intensity and paleoclimate reconstruction. *Palaeogeography, Palaeoclimatology, Palaeoecology* **512**, 80-94.

Ziabakhsh-Ganji, Z., Nick, H. M., Donselaar, M. E., and Bruhn, D. F. (2018). Synergy potential for oil and geothermal energy exploitation. *Applied energy* **212**, 1433-1447.

Zuo, R. (2007). Biofilms: strategies for metal corrosion inhibition employing microorganisms. *Applied microbiology and biotechnology* **76**, 1245-1253.

Papers published/submitted

Journal publication

1. Madirisha, M., Hack, R., & Van der Meer, F. (2022). The influence of chelating agents on clays in geothermal reservoir formations: Implications to reservoir acid stimulation. Geothermics, 99, 102305.
2. Madirisha, M., Hack, R., & Van der Meer, F. (2022). Simulated microbial corrosion in oil, gas and non-volcanic geothermal energy installations: The role of biofilm on pipeline corrosion. Status: Accepted and it is the production section. Energy Reports, 8, 2964-2975
3. Madirisha, M., Hack, R., & Van der Meer, F. (2022). The role of organic acid metabolites in geo-energy pipeline corrosion in a sulfate reducing bacteria environment. Heliyon, 8, e09420

Conference proceedings

1. Madirisha, M. M., Lievens, C., Hack, H. R. G. K., & van der Meer, F. D. (2020, March). Bio-corrosion and acid stimulation in geothermal operations: abstract+ presentation. In 3rd International Tanzania Energy Platform Conference 2020: Energy Transition in Sub-Saharan Africa.

2. Madirisha, M. M., Lievens, C., Hack, H. R. G. K., & van der Meer, F. D. (2019, August). The Influence of Chelating Agents on Clays of the Geothermal Cap Rock: Implications for Enhancing Geothermal Reservoir Quality: poster. In International Conference on Energy, Aquatech and Sustainability 2019.

Appendix: Copyright statements

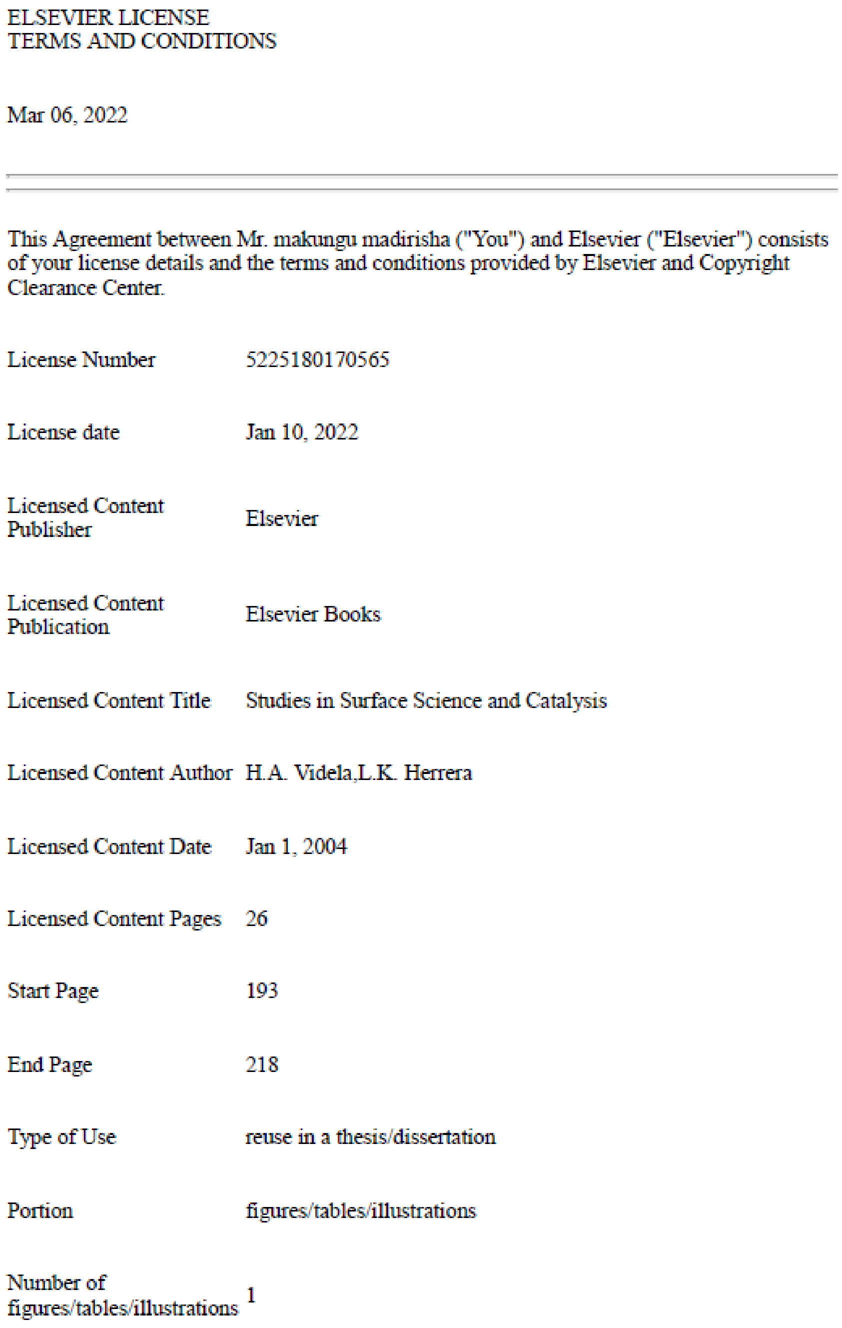

ELSEVIER LICENSE
TERMS AND CONDITIONS

Mar 06, 2022

This Agreement between Mr. makungu madirisha ("You") and Elsevier ("Elsevier") consists of your license details and the terms and conditions provided by Elsevier and Copyright Clearance Center.

License Number	5225180170565
License date	Jan 10, 2022
Licensed Content Publisher	Elsevier
Licensed Content Publication	Elsevier Books
Licensed Content Title	Studies in Surface Science and Catalysis
Licensed Content Author	H.A. Videla,L.K. Herrera
Licensed Content Date	Jan 1, 2004
Licensed Content Pages	26
Start Page	193
End Page	218
Type of Use	reuse in a thesis/dissertation
Portion	figures/tables/illustrations
Number of figures/tables/illustrations	1

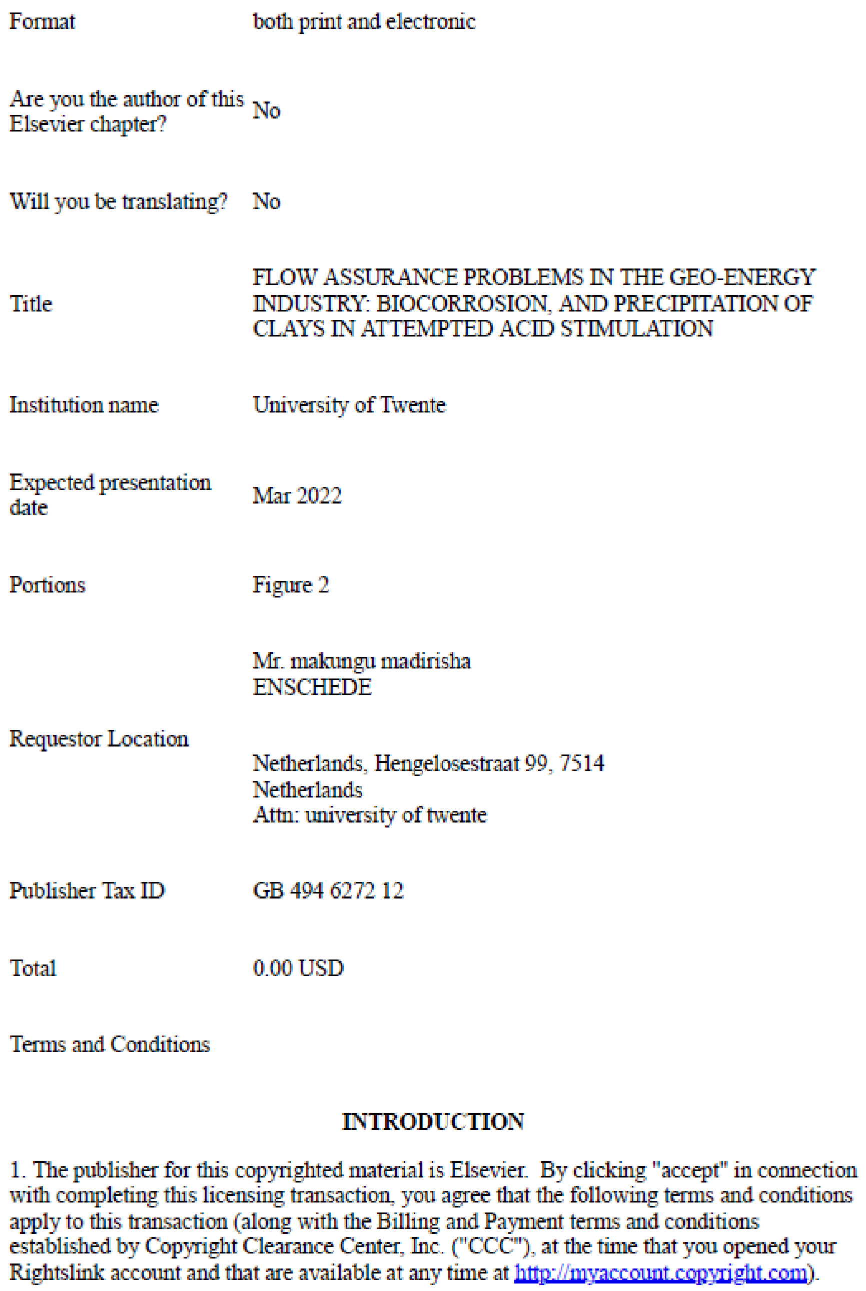

Format	both print and electronic
Are you the author of this Elsevier chapter?	No
Will you be translating?	No
Title	FLOW ASSURANCE PROBLEMS IN THE GEO-ENERGY INDUSTRY: BIOCORROSION, AND PRECIPITATION OF CLAYS IN ATTEMPTED ACID STIMULATION
Institution name	University of Twente
Expected presentation date	Mar 2022
Portions	Figure 2
Requestor Location	Mr. makungu madirisha ENSCHEDE Netherlands, Hengelosestraat 99, 7514 Netherlands Attn: university of twente
Publisher Tax ID	GB 494 6272 12
Total	0.00 USD
Terms and Conditions	

INTRODUCTION

1. The publisher for this copyrighted material is Elsevier. By clicking "accept" in connection with completing this licensing transaction, you agree that the following terms and conditions apply to this transaction (along with the Billing and Payment terms and conditions established by Copyright Clearance Center, Inc. ("CCC"), at the time that you opened your Rightslink account and that are available at any time at http://myaccount.copyright.com).

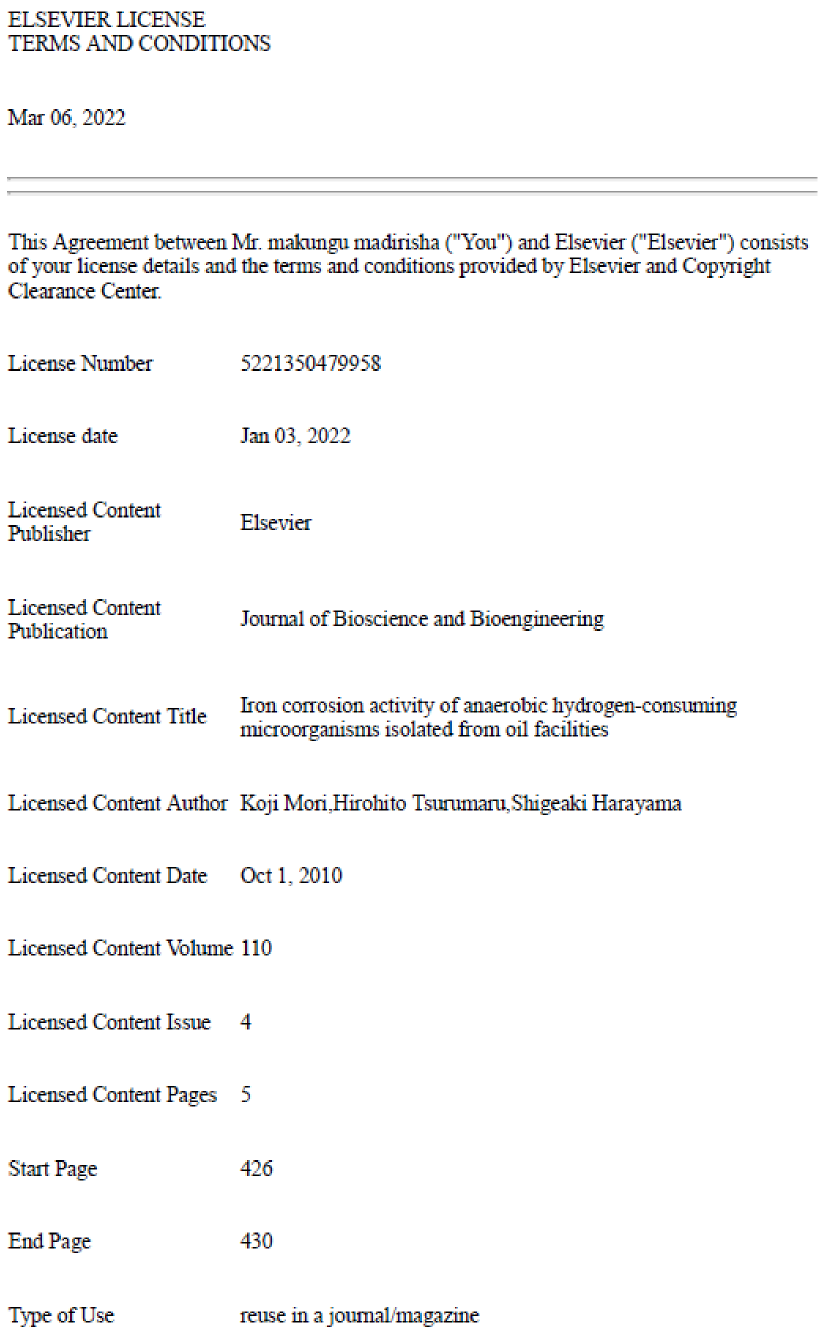

ELSEVIER LICENSE
TERMS AND CONDITIONS

Mar 06, 2022

This Agreement between Mr. makungu madirisha ("You") and Elsevier ("Elsevier") consists of your license details and the terms and conditions provided by Elsevier and Copyright Clearance Center.

License Number	5221350479958
License date	Jan 03, 2022
Licensed Content Publisher	Elsevier
Licensed Content Publication	Journal of Bioscience and Bioengineering
Licensed Content Title	Iron corrosion activity of anaerobic hydrogen-consuming microorganisms isolated from oil facilities
Licensed Content Author	Koji Mori,Hirohito Tsurumaru,Shigeaki Harayama
Licensed Content Date	Oct 1, 2010
Licensed Content Volume	110
Licensed Content Issue	4
Licensed Content Pages	5
Start Page	426
End Page	430
Type of Use	reuse in a journal/magazine

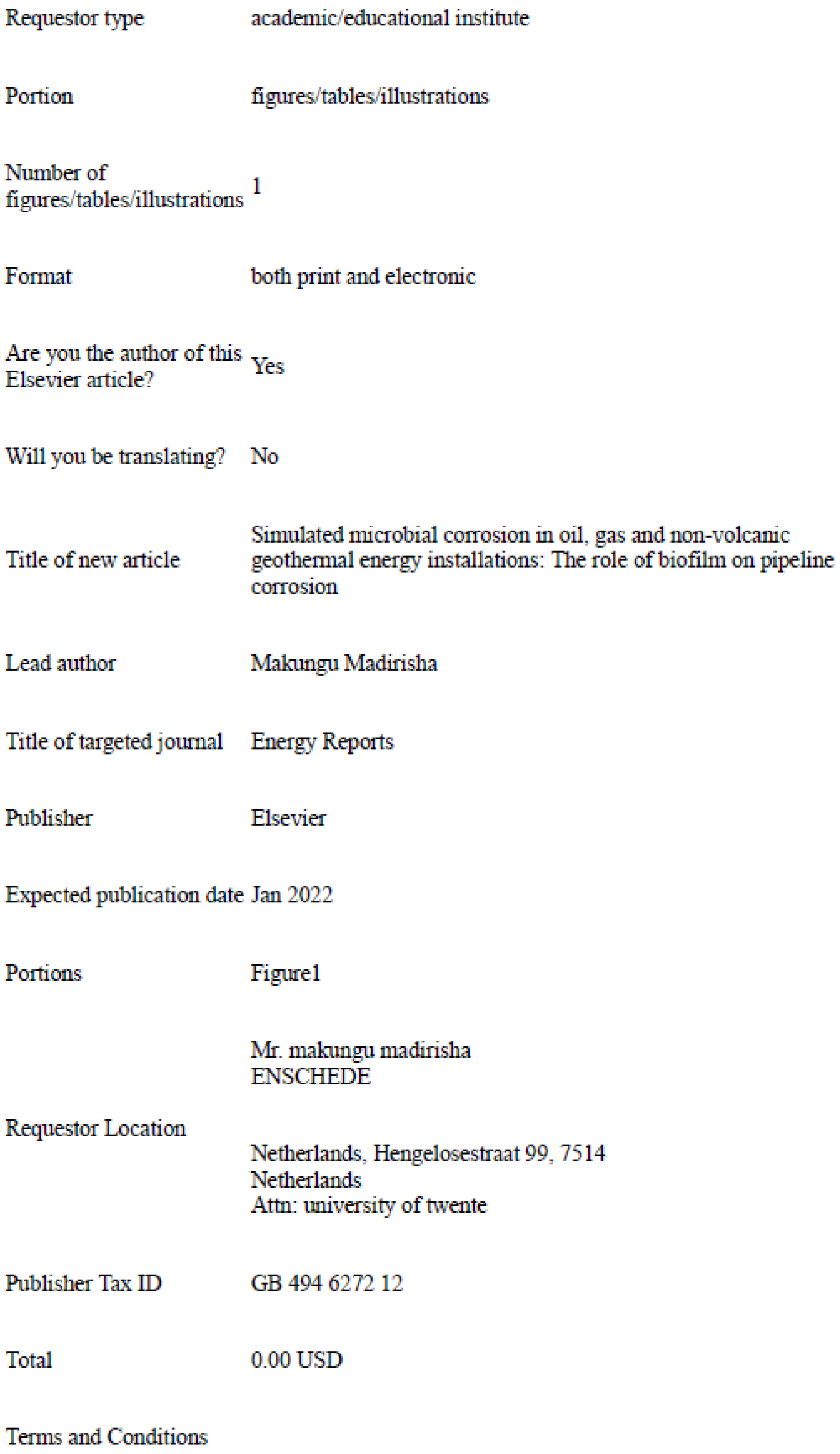

Requestor type	academic/educational institute
Portion	figures/tables/illustrations
Number of figures/tables/illustrations	1
Format	both print and electronic
Are you the author of this Elsevier article?	Yes
Will you be translating?	No
Title of new article	Simulated microbial corrosion in oil, gas and non-volcanic geothermal energy installations: The role of biofilm on pipeline corrosion
Lead author	Makungu Madirisha
Title of targeted journal	Energy Reports
Publisher	Elsevier
Expected publication date	Jan 2022
Portions	Figure1
Requestor Location	Mr. makungu madirisha ENSCHEDE Netherlands, Hengelosestraat 99, 7514 Netherlands Attn: university of twente
Publisher Tax ID	GB 494 6272 12
Total	0.00 USD
Terms and Conditions	

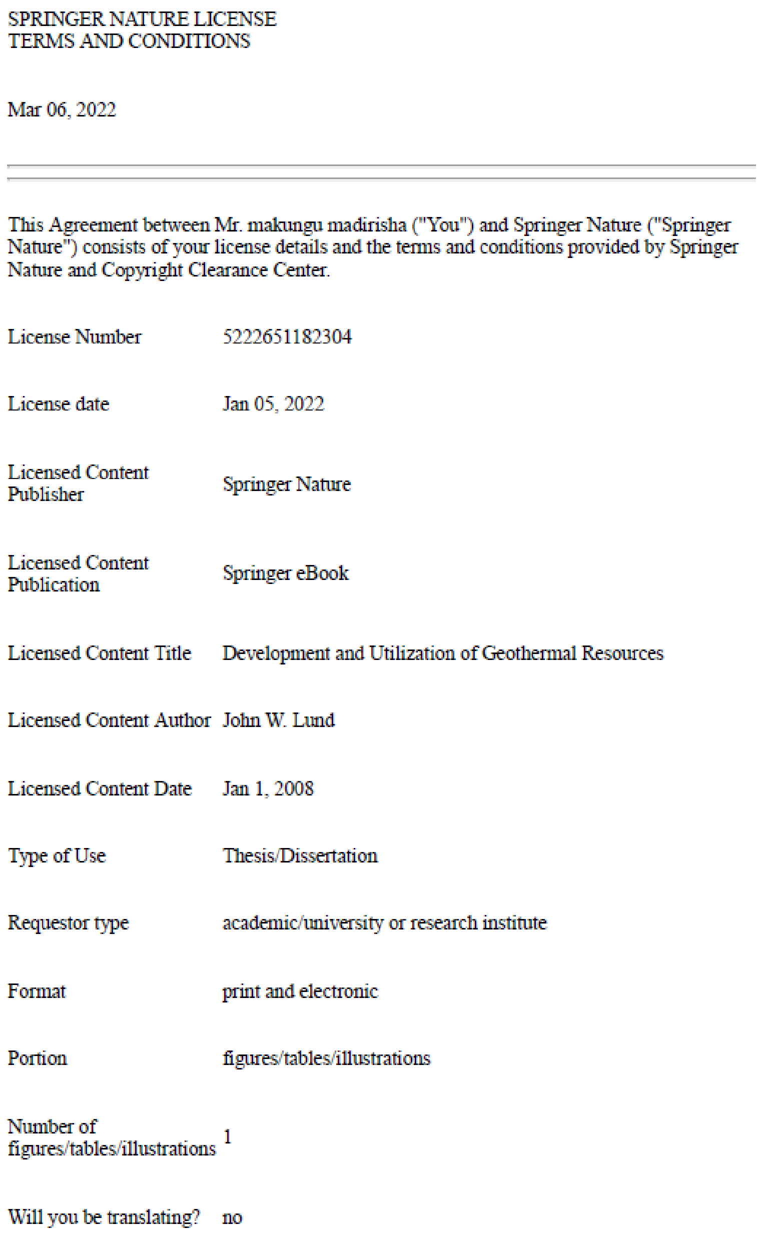

SPRINGER NATURE LICENSE
TERMS AND CONDITIONS

Mar 06, 2022

This Agreement between Mr. makungu madirisha ("You") and Springer Nature ("Springer Nature") consists of your license details and the terms and conditions provided by Springer Nature and Copyright Clearance Center.

License Number	5222651182304
License date	Jan 05, 2022
Licensed Content Publisher	Springer Nature
Licensed Content Publication	Springer eBook
Licensed Content Title	Development and Utilization of Geothermal Resources
Licensed Content Author	John W. Lund
Licensed Content Date	Jan 1, 2008
Type of Use	Thesis/Dissertation
Requestor type	academic/university or research institute
Format	print and electronic
Portion	figures/tables/illustrations
Number of figures/tables/illustrations	1
Will you be translating?	no

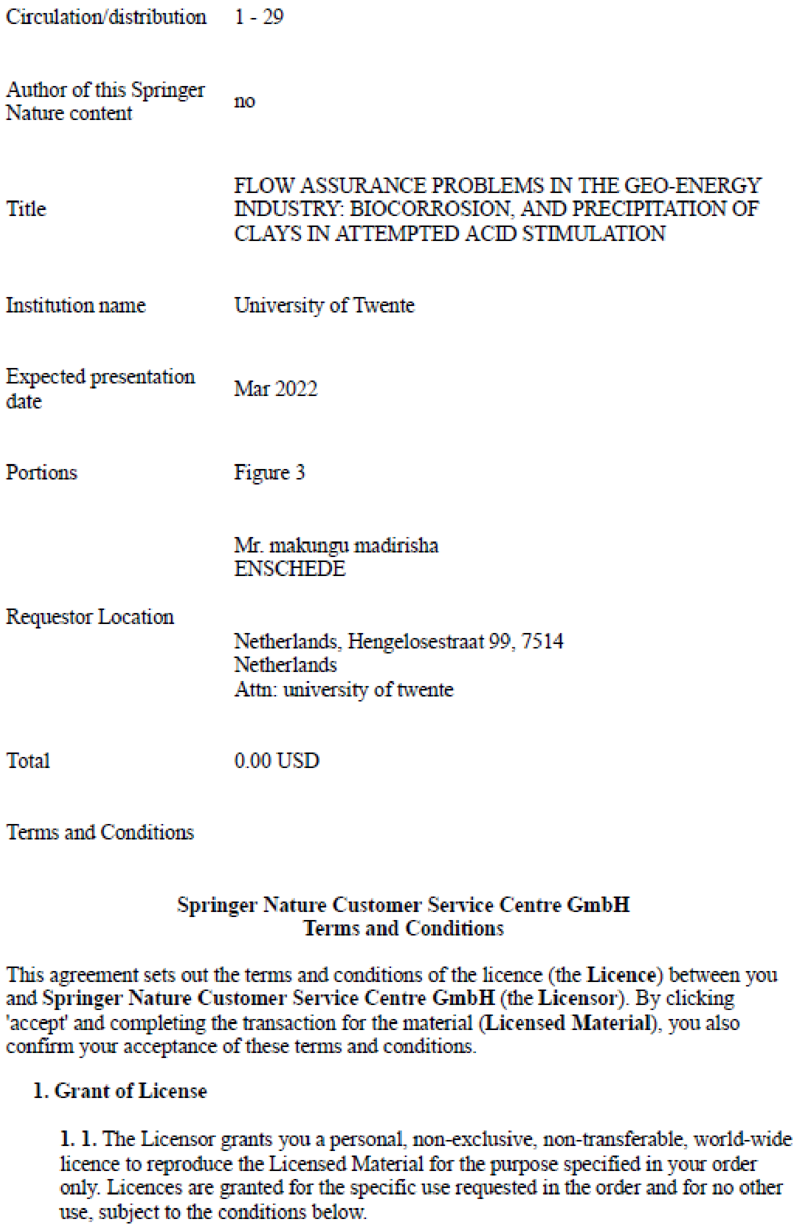

Circulation/distribution	1 - 29
Author of this Springer Nature content	no
Title	FLOW ASSURANCE PROBLEMS IN THE GEO-ENERGY INDUSTRY: BIOCORROSION, AND PRECIPITATION OF CLAYS IN ATTEMPTED ACID STIMULATION
Institution name	University of Twente
Expected presentation date	Mar 2022
Portions	Figure 3
Requestor Location	Mr. makungu madirisha ENSCHEDE Netherlands, Hengelosestraat 99, 7514 Netherlands Attn: university of twente
Total	0.00 USD
Terms and Conditions	

Springer Nature Customer Service Centre GmbH
Terms and Conditions

This agreement sets out the terms and conditions of the licence (the **Licence**) between you and **Springer Nature Customer Service Centre GmbH** (the **Licensor**). By clicking 'accept' and completing the transaction for the material (**Licensed Material**), you also confirm your acceptance of these terms and conditions.

1. **Grant of License**

   1. 1. The Licensor grants you a personal, non-exclusive, non-transferable, world-wide licence to reproduce the Licensed Material for the purpose specified in your order only. Licences are granted for the specific use requested in the order and for no other use, subject to the conditions below.

Appendix: Supplemental figures and tables

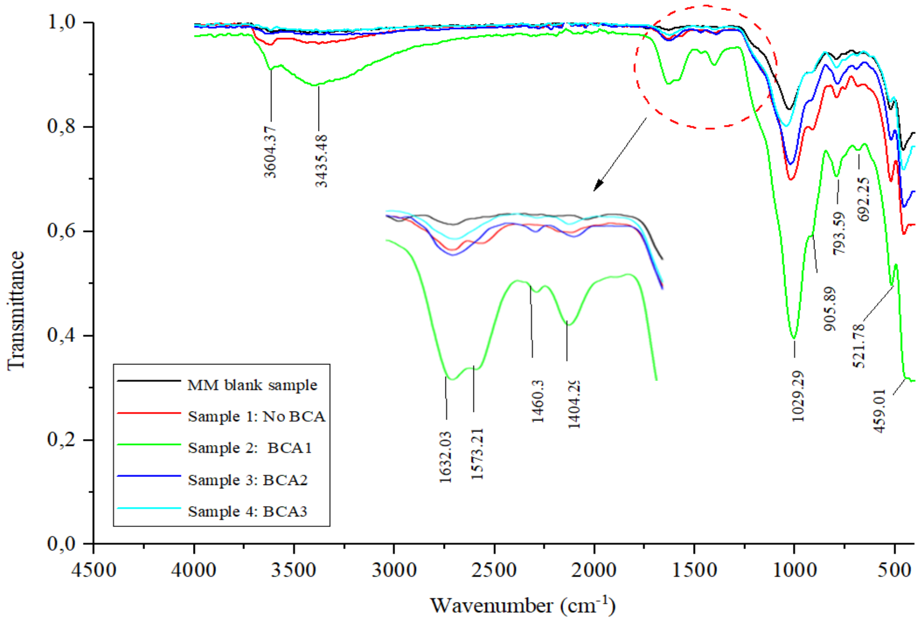

Fig. S5.1: Transmittance vs wavenumber for the MM blank sample and MM sediments of experiments non-dozed and dozed with BCAs in distilled water under CO_2 environment

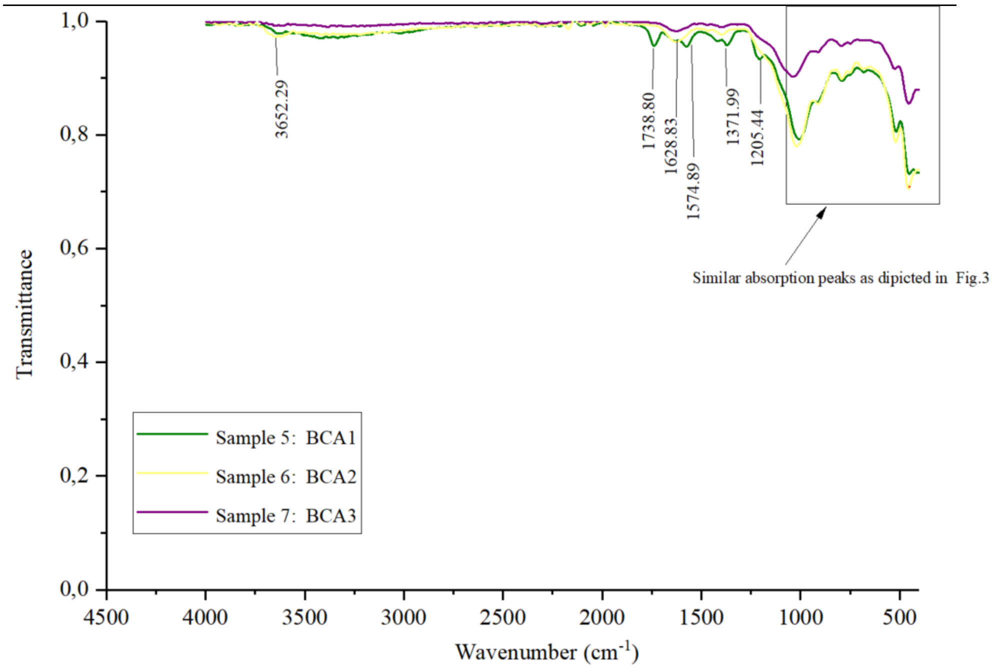

Fig.S5.2: Transmittance vs wavenumber for MM sediments of experiments dozed with BCAs in brine in CO_2 environment

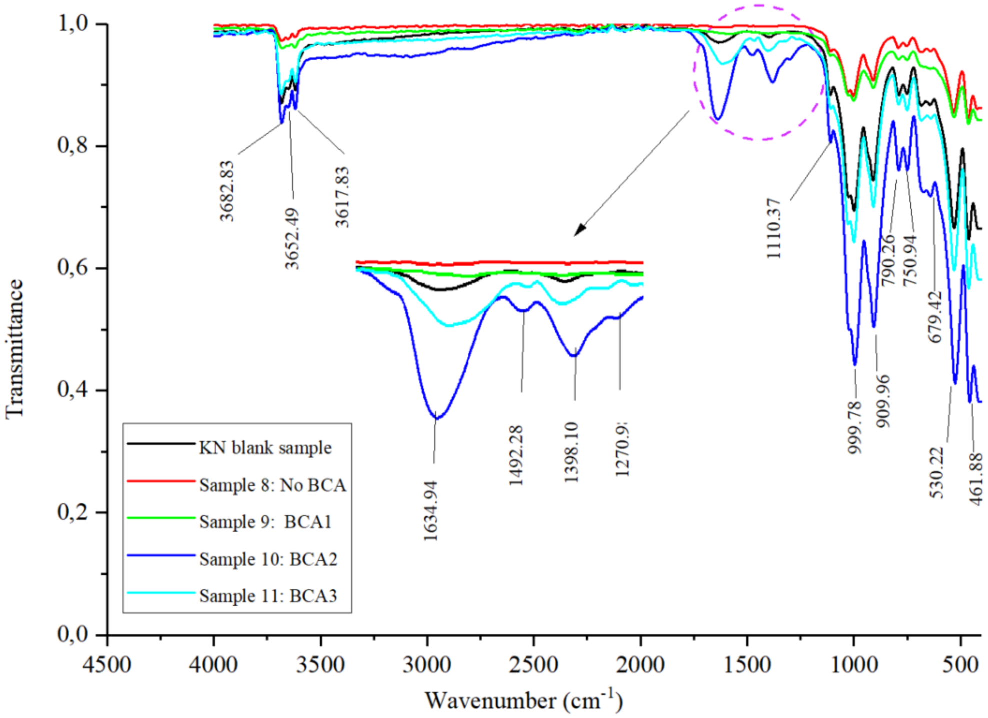

Fig. S5.3: Transmittance vs wavenumber for the KN blank sample and KN sediments of experiments non-dozed and dozed with BCAs in distilled water under CO_2 environment

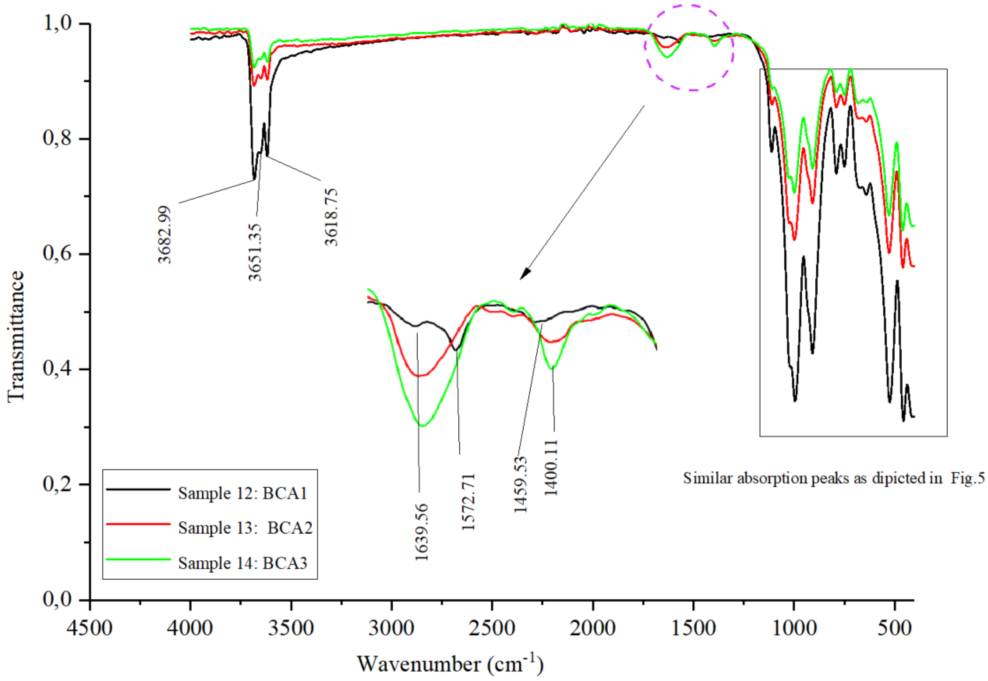

Fig. S5.4: Transmittance vs wavenumber for KN sediments of experiments dozed with BCAs in brine in CO_2 environment

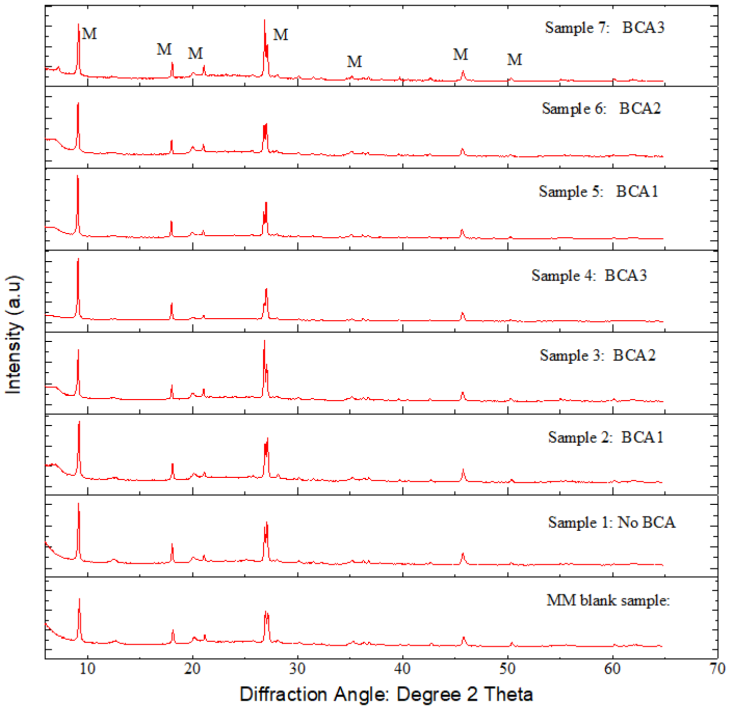

Fig. S5.5: Diffractograms of the MM blank sample and MM sediments of experiments non-dozed and dozed with BCAs in distilled water and brine under CO_2 environment

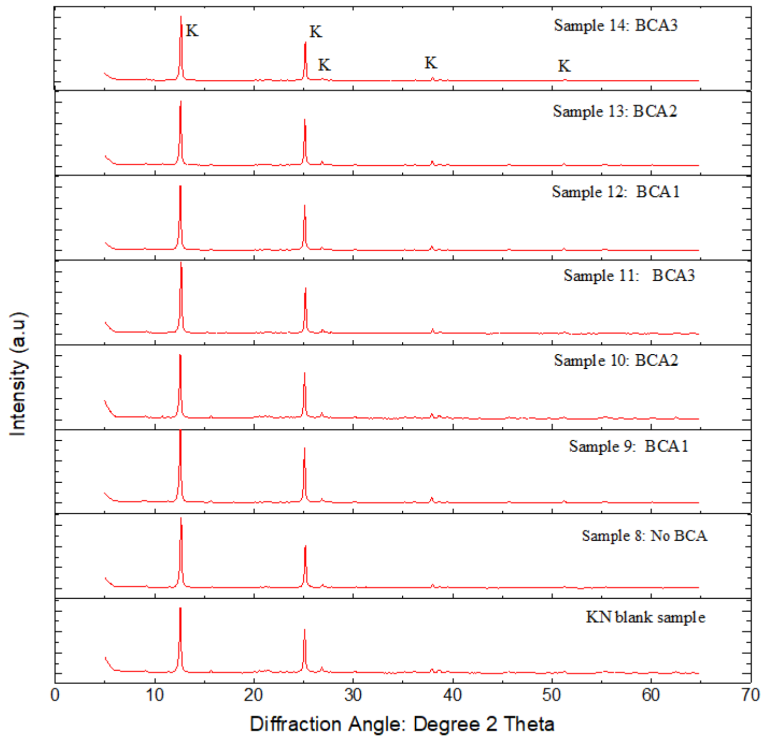

Fig. S5.6: Diffractograms of the KN blank sample and KN sediments of experiments non-dozed and dozed with BCAs in distilled water and brine under CO_2 environment

Table S5.1: Concentrations of metal ions in blank samples of distilled water and brine and supernatants of MM experiments non-dozed and dozed with BCAs in distilled water and brine under CO_2 environment

Experiment/Test	BCAs	Samples	Concentration of metal ions (ppm)					
			Al	Si	Ca	Na	Mg	$[C_{total}]$
DW	No BCA	Blank	< 0.01	< 0.01	< 0.01	0.17	0.03	0.20
Brine	No BCA	Blank	< 0.01	< 0.01	< 0.01	7.76	0.15	7.91
Supernatant from MM + DW + CO_2	No BCA	1	0.00	0.00	0.00	0.23	0.03	0.26
	BCA-1	2	0.23	18.80	0.13	0.23	0.00	19.39
	BCA-2	3	0.13	0.25	0.49	0.00	0.11	0.98
	BCA-3	4	8.67	2.20	0.63	0.32	0.72	12.54
Supernatant from MM + Brine + CO_2	BCA-1	5	0.00	25.5	0.31	6.18	0.00	31.99
	BCA-2	6	0.14	0.74	0.80	0.04	0.23	1.95
	BCA-3	7	11.68	9.00	1.03	0.38	1.13	23.22

Notes: Detection limit of the ICP-OES used is 0.01 ppm; $[C_{total}]$ is the concentration of all metal ions

Table S5.2: Concentrations of metal ions in supernatants of KN experiments non-dozed and dozed with BCAs in distilled water and brine under CO_2 environment

Test	BCA	Sample	Concentration of metal ions (ppm)					
			Al	Si	Ca	Na	Mg	$[C_{total}]$
Supernatant from -KN + DW + CO_2	No BCA	8	0.21	0.00	0.00	0.00	1.01	1.22
	BCA1	9	0.05	30.60	0.43	0.00	0.06	31.14
	BCA2	10	1.31	2.70	0.54	2.04	0.12	6.71
	BCA3	11	18.64	1.10	0.32	0.00	0.19	20.25
Supernatant from- KN + Brine + CO_2	BCA1	12	0.03	21.4	0.21	0.51	0.00	22.15
	BCA2	13	0.37	1.05	0.90	0.00	0.02	2.34
	BCA3	14	8.40	1.91	0.38	0.00	0.02	10.71

Notes: Detection limit of the ICP-OES used is 0.01 ppm; $[C_{total}]$ is the concentration of all metal ions

Biography

Makungu Marco Madirisha is born on 5th February 1979 in Magu district, Mwanza region in Tanzania. His high education study started with education in teaching majoring in physics and chemistry at Dar es Salaam University College of Education (DUCE), a constituent of the University of Dar es Salaam. In 2011, he completed a Bachelor of Science degree with education (Hons). In 2013, he was transferred to the University of Dar es Salaam where he began to work as a Tutorial assistant in chemistry. Before transfer, he worked as a teacher/tutor in various primary and secondary schools and one primary teachers' college (Mkidoma) since the year 2001. In the year 2015, he continued his studies at the University of Nairobi, Kenya where he completed the Master of Science degree in chemistry. In the year 2016, he was promoted to the position of assistant lecturer in chemistry. In the year 2017, he joined the Faculty of Geo-Information Science and Earth Observation (ITC), the University of Twente to carry out PhD research on flow assurance problems in the geo-energy industry: microbial influenced corrosion, and precipitation of clays in acid stimulation. Specifically, his research aimed at understanding the role of biofilm in corrosion due to SRB and the role of organic acid metabolites in SRB corrosion. Further, his research aimed at understanding the influence of biodegradable chelating agents on the precipitation of clay minerals in the geothermal reservoir formation.

During his PhD research, he attended various professional and generic courses and was awarded certificates. The courses which he attended included corrosion science and corrosion for infrastructure, reservoir geomechanics, geological remote sensing I and II, introduction to ground mechanics, introduction to geology, academic integrity, technical and editing, scientific editing, and academic publishing. He was involved in the supervision of MSc students; 01 from Utrecht University and 03 from the University of Dar es Salaam. Moreover, he attended international conferences to promote his work. His research has contributed to three peer-reviewed papers, and this thesis is the output of his research.

Summary

In the geo-energy industry, bio-corrosion of wells and surface installation, and precipitation of clays in reservoirs during acid stimulation cause several problems such as reduction of mechanical properties of the casing and pipe materials and flow path blockages. These types of problems are commonly denoted as “flow assurance problems”. The dominant factors in bio-corrosion are hard to determine because normally several species of micro-organisms and their metabolites are involved and interact. Moreover, different metabolites may cause opposing effects. The role of individual metabolites can be determined only if the influence of one metabolite is isolated from the influence of other metabolites. Moreover, the knowledge on the interaction between clays and the agents used in acid stimulation in a reservoir such as biodegradable chelating agents is paramount to avoid problems such as precipitation of clay minerals that can hamper the smooth flow of fluids and gases from the reservoir. Proper knowledge of these processes and mechanisms is a priory requirement for optimal production and avoiding flow assurance problems.

The purpose of this research is to improve understanding of bio-corrosion and understanding of precipitation of clay during acid stimulation as these both hamper flow assurance problems in the geo-energy industry. This research is formulated in the following research questions:

i. What is the role of biofilm in corrosion due to Sulfate Reducing Bacteria (SRB)?
ii. What is the role of organic acid metabolites in SRB corrosion?

iii. What is the influence of biodegradable chelating agents in the precipitation of clay minerals responsible for decreasing reservoir permeability?

The methodology for answering the research questions is as follows. To better understand the role of simulated biofilm and organic acid metabolites (acetic or L-ascorbic acid) in SRB corrosion, the research investigated the influence of temperature (30, 45, and 60 ^{o}C) and exposure time (60 and 120 min) in the presence of simulated H_2S, depleted O_2 environment (CO_2), brine and smooth test coupons. The influence is determined by electrochemical (PDP and EIS) and pH measurements, the chemical composition of the surface material of the test coupons using XRD and SEM-EDS, and quantities of dissolved metal ions in solution using ICP-OES. To better understand the influence of biodegradable chelating agents (BCA1, BCA2, and BCA3) in the precipitation of clays (kaolinite-natural (KN) and montmorillonite-K10 (MM)), the research investigated the influence of functional groups of biodegradable chelating agents and brine (pH, salinity and conductivity) in a depleted O_2 environment with constant temperature and pressure. The influence is determined by changes in surface properties of the clay minerals using porosimetry, ATR-FTIR, XRD, and infrared reflectance spectroscopy, and quantities of dissolved metal ions in solution using ICP-OES. Reference experiments are done for all investigations. Furthermore, multiple linear regression and t-tests are used to analyze the data obtained.

The results show that the simulated biofilm in the reference experiments at 60 min exposure time has a very small inhibiting effect on corrosion while at 120 min exposure time and in brine experiments neither inhibits nor accelerates corrosion. Furthermore, the obtained corrosion rates (0.25 to 1.6 mm/year) in a simulated SRB environment are comparable to published corrosion rates obtained in SRB experiments (0.20 to 1.2 mm/year). Results on the role of organic acid metabolites show that simulated organic acid metabolites accelerate corrosion in a simulated SRB environment. However, a comparison of these results with those for a simulated SRB environment without acetic or L-ascorbic acid under similar experimental conditions shows that the addition of acetic results in an inhibitory effect while the addition of L-ascorbic acid results in acceleration of corrosion. The results to understand the influence of biodegradable chelating agents show changes in surface properties and structure of KN and MM which in turn suggest chemical interaction to take place. The ICP-OES, pH, conductivity, and salinity results strongly support that chemical interactions (dissolution reactions) take place. BCAs' functional groups have more influence than pH on the dissolution. BCA1 and BCA3 cause greater dissolution with lower precipitation as compared to BCA2 and no-BCA.

The results on the role of biofilm contradict the existing literature. This discrepancy is likely due to differences in experimental conditions as the majority of MIC literature and laboratory investigations are focused on H_2S as the only SRB product. Such studies ignore the presence of metabolic heterogeneity in SRB and the presence of biofilm and CO_2 that are likely to have their kinetics/influence on corrosion. Despite the discrepancy in the role of biofilm in SRB simulated studies, the obtained corrosion rates in a simulated SRB environment in this study are comparable to published corrosion rates obtained in SRB experiments implying that simulated H_2S, CO_2, and biofilm are representative of the SRB media for corrosion studies. Moreover, the results on the role of simulated organic acid metabolites highlight that H_2S has the key role in corrosion in the presence of acetic or L-ascorbic acid. The results are important new and novel information on the role of acetic and L-ascorbic acids in corrosion of geo-energy pipelines in the SRB environment. The results have a direct impact on the role of other microbial metabolites in the corrosion of carbon steel. In acid stimulation using BCAs, the results reveal that BCA1 and BCA3 could be useful acids for reservoir stimulation for improving permeability, especially in geothermal reservoir formations that contain clay minerals.

Samenvatting

In de geo-energie industrie veroorzaken biocorrosie van putten en oppervlakte-installaties en neerslag van klei in reservoirs tijdens zuurstimulatie verschillende problemen, zoals vermindering van de mechanische eigenschappen van materialen van pijpleidingen en verbuizing in boorgaten, en blokkades van stroompaden. Dit soort problemen wordt gewoonlijk aangeduid als "stroomzekerheidsproblemen" ("flow assurance problems"). De dominante factoren in biocorrosie zijn moeilijk te bepalen omdat normaal gesproken verschillende soorten micro-organismen en hun metabolieten betrokken zijn en een wisselwerking hebben. Bovendien kunnen verschillende metabolieten tegengestelde effecten veroorzaken. De rol van individuele metabolieten kan alleen worden bepaald als de invloed van één metaboliet wordt geïsoleerd van de invloed van andere metabolieten. De kennis over de interactie tussen kleisoorten en de middelen die worden gebruikt bij zuurstimulatie in een reservoir, zoals biologisch afbreekbare chelaatvormers ("chelating agents"), zijn van het grootste belang om problemen te voorkomen zoals het neerslaan van kleimineralen die een vlotte stroming van vloeistoffen en gassen uit het reservoir kunnen belemmeren. Een goede kennis van bovenstaande processen en mechanismen is een vereiste voor een optimale productie en het vermijden van problemen met de stroomzekerheid. Het doel van dit onderzoek is om de kennis omtrent biocorrosie en de kennis omtrent de neerslag van klei tijdens zuurstimulatie te verbeteren, aangezien deze beide problemen met de stromingsgarantie in de geo-energie industrie veroorzaken. Dit onderzoek is geformuleerd in de volgende onderzoeksvragen:

i. Wat is de rol van biofilm bij corrosie door sulfaatreducerende bacteriën (SRB) ("Sulfate Reducing Bacteria")?

ii. Wat is de rol van metabolieten van organisch zuur bij SRB-corrosie?

iii. Wat is de invloed van biologisch afbreekbare chelaatvormers ("chelating agents") bij het neerslaan van kleimineralen verantwoordelijk voor een afname van de doorlaatbaarheid van een reservoir?

De methodologie voor het beantwoorden van de onderzoeksvragen is als volgt. Om de rol van gesimuleerde biofilm en metabolieten van organisch zuur (azijnzuur of L-ascorbinezuur) bij SRB-corrosie beter te begrijpen, is de invloed van temperatuur (30, 45 en 60 °C) en blootstellingstijd (60 en 120 min) in aanwezigheid van gesimuleerde H_2S, een verarmde O_2-omgeving (CO2), pekel en gladde testcoupons onderzocht. De invloed is bepaald aan de hand van elektrochemische (PDP en EIS) en pH-metingen, de chemische samenstelling van het oppervlaktemateriaal van de testcoupons met XRD en SEM-EDS en de hoeveelheden opgeloste metaalionen in oplossing met ICP-OES. Om de invloed van biologisch afbreekbare chelaatvormers (BCA1, BCA2 en BCA3) in de precipitatie van klei (kaoliniet-natuurlijk (KN) en montmorilloniet-K10 (MM)) beter te begrijpen, is de invloed van functionele groepen van biologisch afbreekbare chelaatvormers en pekel (pH, zoutgehalte en geleidbaarheid) in een verarmde O2-omgeving en constante temperatuur en druk onderzocht. De invloed wordt bepaald door veranderingen in oppervlakte-eigenschappen van de kleimineralen en is bepaald met behulp van porosimetrie, ATR-FTIR, XRD en infrarood reflectie-spectroscopie, en de hoeveelheden opgeloste metaalionen in oplossing bepaalt met ICP-OES. Voor alle onderzoeken worden referentie-experimenten gedaan. Verder worden meervoudig lineaire regressie en t-tests gebruikt om de verkregen gegevens te analyseren.

De resultaten laten zien dat de gesimuleerde biofilm in de referentie-experimenten bij 60 min blootstellingstijd een zeer klein remmend effect heeft op corrosie, terwijl bij 120 min blootstellingstijd en in pekelexperimenten de corrosie niet wordt geremd of versnelt. Bovendien zijn de verkregen corrosiesnelheden (0,25 tot 1,6 mm/jaar) in de gesimuleerde SRB-omgeving vergelijkbaar met de gepubliceerde corrosiesnelheden verkregen in SRB-experimenten (0,20 tot 1,2 mm/jaar). De resultaten laten zien dat gesimuleerde metabolieten van organisch zuur de corrosie versnellen in een gesimuleerde SRB-omgeving. Vergelijking van deze resultaten met die voor een gesimuleerde SRB-omgeving zonder azijn- of L-ascorbinezuur onder vergelijkbare experimentele omstandigheden laat echter zien dat de toevoeging van azijn resulteert in een remmend effect terwijl de toevoeging van L-ascorbinezuur resulteert in versnelling van corrosie. De biologisch afbreekbare chelaatvormers geven waarschijnlijk veranderingen in oppervlakte-eigenschappen en structuur van KN en MM, die op hun beurt suggereren dat er chemische interactie plaatsvindt. De ICP-OES-, pH-, geleidbaarheids- en zoutgehalte-resultaten ondersteunen sterk dat er chemische interacties (oplosreacties) plaatsvinden. De functionele groepen van BCA's hebben meer invloed dan de pH op het oplossen. BCA1 en BCA3 veroorzaken een grotere oplossing met lagere precipitatie in vergelijking met BCA2 en zonder-BCA.

De resultaten betreffende de rol van biofilm spreken de bestaande literatuur tegen. Deze discrepantie is waarschijnlijk te wijten aan verschillen in experimentele omstandigheden, aangezien de meeste MIC-literatuur en laboratoriumonderzoeken gericht zijn op H_2S als het enige SRB-product. Dergelijke studies negeren de aanwezigheid van metabole heterogeniteit in SRB, en de aanwezigheid van biofilm en CO_2 die waarschijnlijk hun kinetiek/invloed op corrosie hebben. Ondanks de discrepantie in de rol van biofilm in SRB-gesimuleerde studies zijn de verkregen corrosiesnelheden vergelijkbaar met de gepubliceerde corrosiesnelheden van SRB-experimenten. Dit houdt in dat de gesimuleerde H_2S, CO_2, en de biofilm representatief zijn voor de SRB-media in de corrosie studies. Bovendien benadrukken de resultaten dat H_2S een sleutelrol heeft in corrosie in de aanwezigheid van azijnzuur of L-ascorbinezuur. Deze resultaten zijn nieuw en zijn belangrijke nieuwe informatie over de rol van azijnzuur en L-ascorbinezuur in de corrosie van geo-energie pijpleidingen in een SRB-omgeving. De resultaten hebben een directe invloed op de rol van andere microbiële metabolieten bij de corrosie van koolstofstaal. Bij zuurstimulatie met behulp van BCA's laten de resultaten zien dat BCA1 en BCA3 bruikbare zuren kunnen zijn voor reservoirstimulatie voor het verbeteren van de permeabiliteit, vooral in geothermische reservoirformaties die kleimineralen bevatten.